Universitat Autònoma de Barcelona

Biocompatibility of new biomaterials for orthopaedic applications

Andreu Blanquer Jerez

Universitat Autònoma de Barcelona

Biocompatibility of new biomaterials for orthopaedic applications

Andreu Blanquer Jerez

Memòria presentada per Andreu Blanquer Jerez per optar al grau de Doctor amb Menció Internacional per la Universitat Autònoma de Barcelona dins el Programa de Doctorat en Biologia Cel·lular

Directors:

Dr. Leonardo Barrios Sanromà

Dra. Elena Ibáñez de Sans

Dra. Carme Nogués Sanmiquel

Bellaterra, 26 d'abril de 2016

Universitat Autònoma de Barcelona

El **Dr. Leonardo Barrios Sanromà**, catedràtic del Departament de Biologia Cel·lular, Fisiologia i Immunologia de la Universitat Autònoma de Barcelona,

La **Dra. Elena Ibáñez de Sans**, professora agregada del Departament de Biologia Cel·lular, Fisiologia i Immunologia de la Universitat Autònoma de Barcelona,

I la **Dra, Carme Nogués Sanmiquel**, professora titular del Departament de Biologia Cel·lular, Fisiologia i Immunologia de la Universitat Autònoma de Barcelona,

CERTIFIQUEN:

Que **Andreu Blanquer Jerez** ha realitzat sota la seva direcció el treball d'investigació que s'exposa en la memòria titulada "Biocompatibility of new biomaterials for orthopaedic Applications" per optar al grau de **Doctor per la Universitat Autònoma de Barcelona**.

Que aquest treball s'ha dut a terme a la Unitat de Biologia Cel·lular del Departament de Biologia Cel·lular, Fisiologia i Immunologia de la Universitat Autònoma de Barcelona, dins el Programa de Doctorat en Biologia Cel·lular.

I perquè així consti, signen el present certificat,

Dr. Leonardo Barrios Sanromà **Dra. Elena Ibáñez de Sans** **Dra. Carme Nogués Sanmiquel**

Bellaterra, 26 d'abril de 2016

Aquesta tesi s'ha realitzat amb el finançament del Ministerio de Ciencia e Innovación (TEC2011-29140-C03-03 i MAT2014-57960-C03-3-R) i la Generalitat de Catalunya (2014-SGR-254). Andreu Blanquer Jerez ha gaudit d'una beca predoctoral de personal investigador en formació (PIF), concedida per la Universitat Autònoma de Barcelona.

Als meus pares,

al meu germà,

a la Blanca,

per ser els meus pilars.

Table of contents

Abbreviations and Acronyms

ALP	Alkaline phosphatase
BMG	Bulk metallic glass
CSF	Colony-stimulating factor
ECM	Extracellular matrix
IL	Interleukine
MTT	3-(4, 5-dimethylthiazolyl-2)-2, 5-diphenyltetrazolium bromide
NG	Nanogenerator
NITINOL	Nikel-Titanium alloy
NS	Nanosheet
PMMA	Polymethyl methacrylate
PTV	Peak-to-valley
PZT	Lead zirconate titanate
qPCR	Quantitative PCR
Ra	Roughness amplitude value
RANKL	Receptor activator for nuclear factor K B ligand
RMS	Root mean square
SACC	Stretch-activated cation channel
TNF-(alpha)	Tumor necrosis factor (alpha)
VGCC	Voltage-gated calcium channel

Abstract

The use of biocompatible materials has attained an increasing importance for medical surgery and orthopaedics due to population aging. Metallic alloys currently used in bone implants have physical and mechanical properties different from those of the bone, which increases the probability of implant loosening. For this reason, new metallic alloys with better properties are being developed. In this regard, the present thesis aims to analyse the biocompatibility of new biomaterials for orthopaedic applications. First, we demonstrated the biocompatibility of TiZrCuPd bulk metallic glass in terms of cytotoxicity, and osteoblast adhesion and differentiation. Second, we assessed the effect of surface modification of TiZrCuPd and Ti-6Al-4V alloys by electrochemical anodization and physical modification on osteoblast behaviour. Differences in topography did not cause changes on osteoblasts adhesion, proliferation and differentiation. Third, we demonstrated that TiZrPdSi and TiZrPdSiNb alloys are also biocompatible and enhance osteoblasts adhesion, spreading, proliferation and differentiation. Fourth, we evaluated the electrostimulation effect of two new ZnO piezoelectric nanogenerators using two cell lines involved in bone regeneration (osteoblasts and macrophages). We observed that both nanogenerators are biocompatible and that their interaction with cells produces a local electric field that stimulate macrophages motility and the increase in intracellular Ca^{2+} concentration in osteoblasts. Thus, these new smart materials have interesting properties for their use in biomedical devices. Collectively, the results obtained in our studies contribute to the progress in the development of better materials for bone repair and regeneration.

Resum

L'ús de materials biocompatibles ha assolit una importància creixent en aplicacions ortopèdiques i quirúrgiques, degut a l'envelliment de la població. Els aliatges metàl·lics que s'empren actualment en medicina presenten propietats físiques i mecàniques diferents a les de l'os humà, incrementant la probabilitat de pèrdua de l'implant. Per aquesta raó, s'estan desenvolupant nous aliatges metàl·lics amb millors propietats. En aquest sentit, la present tesi té com objectiu l'anàlisi de la biocompatibilitat de nous aliatges pel seu ús en implants ortopèdics. En primer lloc, s'ha demostrat la biocompatibilitat del vidre metàl·lic massís TiZrCuPd en termes de citotoxicitat, i d'adhesió i de diferenciació d'osteoblasts. En segon lloc, s'ha avaluat l'efecte de dues modificacions de superfície, anodització electroquímica i modificació física, dels aliatges TiZrCuPd i Ti-6Al-4V sobre el comportament dels osteoblasts. En aquest cas, no hem observat cap efecte de la topografia en la proliferació, l'adhesió i la diferenciació. En tercer lloc, hem demostrat que els aliatges TiZrPdSi i TiZrPdSiNb són biocompatibles i afavoreixen l'adhesió, la proliferació i la diferenciació d'osteoblasts. Finalment, hem avaluat l'efecte electroestimulador de dos nous nanogeneradors piezoelèctrics, basats en ZnO, emprant dues línies cel·lulars implicades en la regeneració òssia (osteoblasts i macròfags). Els resultats observats indiquen que els nanogeneradors són biocompatibles i que la seva interacció amb les cèl·lules produeix un camp elèctric local que estimula la motilitat dels macròfags i l'augment de la concentració intracel·lular de Ca^{2+} en osteoblasts. Aquests nous materials intel·ligents presenten propietats força interessants pel seu ús en aplicacions biomèdiques. En conjunt, els resultats obtinguts en els nostres estudis contribueixen en el desenvolupament de materials per millorar la reparació i la regeneració òssia.

1. Introduction

1.1. Bone structure and physiology

Bones are vascularized and innervated organs composed of different mesodermal tissues, such as bone, hematopoietic and adipose tissue. The bone tissue is a specialized connective tissue formed by different cell types and an extracellular matrix (ECM), which is mineralized and contains inorganic calcium phosphate structured as hydroxyapatite crystals. This ECM is composed mainly of collagen, representing 90% of the ECM proteins, and other non-collagenous proteins, such as proteoglycans, adhesive glycoproteins and growth factors, which are necessary for the development and mineralization of the bone. In addition, bone tissue is formed by 4 different cell types, which interact to maintain the homeostasis of the tissue: osteoblasts, osteocytes, bone lining cells and osteoclasts.

Osteoblasts are located on bone surfaces and contribute to bone formation and mineralization. Their precursors are the mesenchymal stem cells, which differentiate into the osteoblast lineage by the activation of the Wnt/β-catenin pathway (Clarke 2008). The osteoblast lineage includes several cell types that can be divided into subpopulations of cells depending on their response to different hormonal, mechanical or cytokine signals. For example, osteocytes and bone lining cells, described below, are osteoblast-lineage cells.

Osteocytes are mature bone cells located within the bone matrix, constituting more than 90% of the cells in the bone. Osteocytes maintain connections with each other, and with osteoblasts and bone lining cells, via their multiple filopodial processes that lie within the canaliculi in the mineralized bone. Their most important function is mechanotransduction through the extensive filopodial processes, which respond to external mechanical forces (Clarke 2008).

Bone lining cells are quiescent osteoblasts that are involved in the regulation of influx and efflux of mineral ions, mainly calcium, into and out of the bone extracellular fluid. Their main function is to act as a blood-bone barrier, but they also have the ability to re-differentiate into osteoblasts when exposed to specific factors (Dobnig & Turner 1995).

Finally, osteoclasts are multinucleated cells derived from monocyte lineage cells, and they play an important role in bone remodelling. Osteoclasts main function is bone matrix resorption and they are located in cavities named Howship lacunae. Mature osteoclasts are the result of the fusion of different osteoclast progenitor cells, which need the presence of two cytokines (RANKL and macrophage CSF) to proliferate, survive and differentiate (Clarke 2008). Bones are in constant remodelling through osteoclastic resorption and osteoblastic bone formation. Therefore, balanced cell type activity is crucial to maintain the homeostasis of the bone tissue (Imai et al. 2013; Ross & Pawlina 2004) (Figure 1).

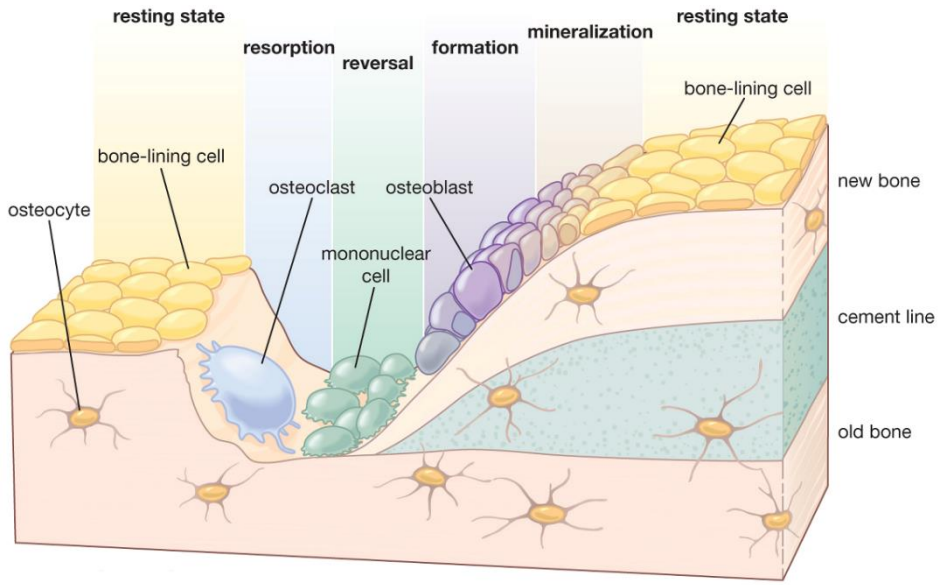

Figure 1. Bone remodelling process and cellular composition. Four major types of cells constitute bone tissue: osteoclasts, bone resorbing cells derived from a monocyte lineage of the hematopoietic stem cells; osteoblasts, bone forming cells derived from the mesenchymal stem cells; osteocytes, bone matrix embedded cells originated from osteoblasts; and bone lining cells, mature quiescent osteoblasts on the bone surfaces (Encyclopaedia Britannica, 2013).

Overall, the adult human skeleton is composed of 80% cortical bone and 20% trabecular bone. Whereas cortical bone is dense and solid, trabecular bone is formed by a network of trabecular plates and rods interspersed in the bone marrow compartment. Bones contain osteons, named Haversian systems in the cortical bone and packets in the

trabecular bone. Each osteon is the end result of a bone remodelling cycle. To prevent accumulation of microdamages and to maintain their strength and mineral homeostasis, bones are in constant remodelling resorbing old bone and forming new bone. Each remodelling cycle can be divided in four sequential phases (Figure 1). First, mononuclear monocyte osteoclast precursors are recruited from circulation and activated by RANKL and macrophage CSF cytokines. Second, resorption of the bone takes place by differentiated osteoclasts, which are regulated by multiple factors. Third, a reversal phase occurs, consisting in the transition from bone resorption to bone formation. In this phase, resorption cavities contain monocytes, osteocytes and preosteoblasts recruited to begin new bone formation. Finally, bone formation is the longer phase, which can take from 4 to 6 months (Clarke 2008). Osteoblasts synthetize new organic matrix and mineralize the ECM by secreting calcium and phosphate. Osteoblasts surrounded by calcified matrix become osteocytes with extensive connections to bone surface lining cells, osteoblasts, and other osteocytes, maintained by gap junctions between the cytoplasmic processes extending from the osteocytes (Burger et al. 2003) (Figure 2).

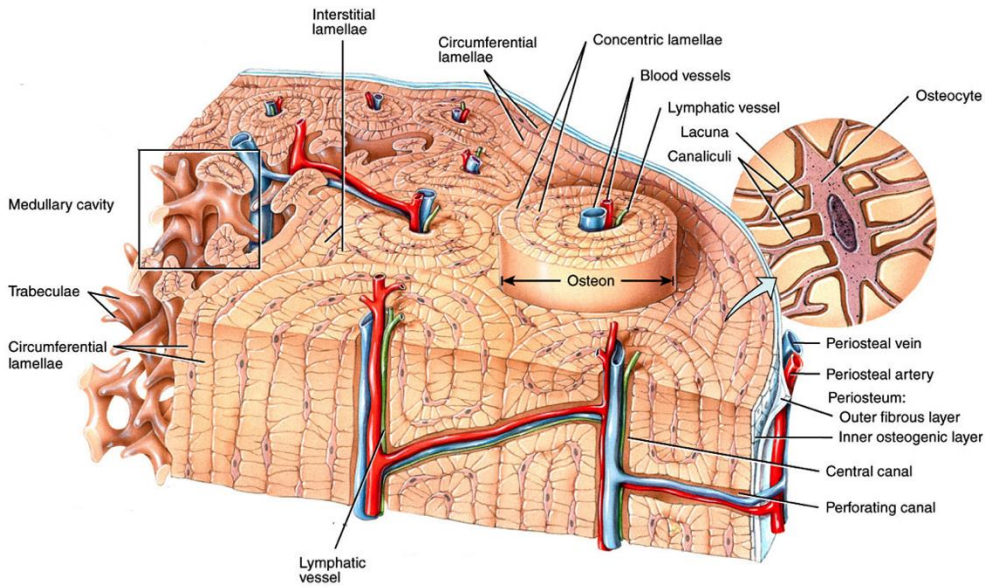

Figure 2. Bone structure. The two parts of the bone identified as cortical and trabecular bone, and osteons are represented.

Constant bone remodelling requires osteoblast differentiation into mature osteoblasts to synthesize ECM components continuously. Differentiation occurs in three different phases. First, active proliferation takes place, with the expression of cell cycle progression, procollagen I and fibronectin genes. Second, cell proliferation decreases and the expression of specific genes needed for ECM synthesis and maturation begins. In this phase, collagen I is secreted and alkaline phosphatase (ALP) enzyme reaches the maximal activity. Third, the ECM mineralizes, with up-regulation of specific genes such as osteopontin, osteocalcin and bone sialoprotein, and calcium phosphate accumulation (Postiglione et al. 2004; Goriainov et al. 2014). In general, ALP, bone sialoprotein and collagen I are considered early markers of osteoblast differentiation, whereas osteocalcin and osteopontin appear later and are thus considered late markers.

1.2. Biomaterials for orthopaedic applications

Orthopaedic implants can be defined as medical devices used to replace or provide fixation of bone, or to replace articulating surfaces of a joint (Orthopedicimplants Wordpress, 2009). Orthopaedic implants are placed into the human body in direct contact with the surrounding tissues, generally bones, and body fluids. Because of this, the aim of orthopaedic implant research is to develop new materials with improved properties and better osseointegration. In this regard, biomaterials are defined as natural or artificial materials that are used in biological systems to supply or replace the lost or diseased biological structure and to restore the function of living tissues (Viteri & Fuentes 2013).

The field of biomaterials is increasing due to population aging and the need for suitable materials for medical surgery. Medical care is extending the human life span, and some kinds of tissues succumb to wear due to aging. For instance, human joints suffer from degenerative diseases, such as arthritis, leading to pain or loss in function (Geetha et al. 2009). For this reason, bone and joint degenerative and inflammatory problems affect millions of people worldwide, and have become one of the most common chronic diseases. In fact, among all implants used in medicine, the great majority are related to orthopaedic diseases like spinal, hip and knee replacement (Viteri & Fuentes 2013). It has been estimated that 90% of the population over the age of 40 suffers from these

degenerative diseases, and it is predicted that by the end of 2030 the number of total hip replacements will rise by 174% and total knee arthroplasties will grow by 673% (Geetha et al. 2009). In relation to the orthopaedic industry, a London-based business information provider estimated that the global market for orthobiologic products generated sales of $4.8bn in 2010, and predicted that the market will be worth $15.3bn by 2022 (Visiongain, 2012). For all of this, biomaterial research for orthopaedic applications has become a hot topic in recent years.

Currently, different kinds of biomaterials are being used in the orthopaedic field, depending on the application. The main compositions of these biomaterials are ceramics, natural and artificial polymers and metals.

Ceramics were introduced 20 years ago because of their high wear resistance, reduced elastic modulus and hardness (Geetha et al. 2009). They are still widely used for total hip and knee arthropasties, femoral heads, ossicular bone substitutes and bone screws (Navarro et al. 2008; Mantripragada et al. 2013). They can be classified into inert ceramics and bioactive ceramics. Alumina and zirconia are the two most widely used inert ceramics. Alumina presents low friction and wear coefficients, although its elastic modulus is high (380 GPa) compared with that of the bone (10-30 GPa). For this reason, alumina is combined with other materials to be used in femoral head implants (Navarro et al. 2008). Zirconia is one the most used ceramics for hip replacements, showing the highest strength among ceramics and an extremely low wear. On the other hand, bioactive ceramics include calcium phosphate, glass, glass-ceramic, and composites. These bioactive materials have the capability to interact with the biological environment to improve the host response. Calcium phosphate is an important component of the bone, and different types of this ceramic can be used in orthopaedic implants. For example, hydroxyapatite and β-tricalcium phosphate are commonly used because of their physical and osteogenic properties. Whereas hydroxyapatite has good bioactive properties, β-tricalcium phosphate has the ability to be resorbed by bone tissue. Furthermore, several bioglasses and glass-ceramics have been described in the literature with a wide range of applications. Silicon, one of the glass components, has been found to promote osteoblast differentiation and neovascularization in in vitro studies, improving bone repair (Yuan et al. 2001; Rokkanen et al. 2000).

Natural and artificial polymers are also used for orthopaedic applications because their offer the possibility to design a unique composition and structure for every specific use. In addition, the main advantage of using polymers is that they can be injected into the defect site, reducing costs and pain. Currently used polymers are acrylics, polyamides, silicones, polyurethanes, polypropylene and others (Navarro et al. 2008). Polymethyl methacrylate (PMMA) is used as a bone cement and plays an important role in the anchorage of prosthesis due to an elastic modulus akin to that of the bone (Mantripragada et al. 2013). Polypropylene is used as acetabular cups in total hip arthroplasties, knee arthroplasties and intervertebral disc replacement. It presents high strength and low density, although its wear resistance is low (Navarro et al. 2008). Other polymers like silicone, for replacement of small joints, and biodegradable polymers, for bone repair, are being used in medicine.

Finally, the most widely used materials in the orthopaedic field are metallic alloys, which are the focus of the present thesis and will be described in more detail in the next section.

1.3.Metallic alloys

Metallic alloys present excellent mechanical properties compared with other biomaterials like ceramics and polymers. The alloys currently used for permanent skeleton implants can be divided into three main groups: stainless steels, cobalt-chromium alloys and titanium alloys (Hermawan et al. 2011).

Stainless steel materials are frequently used in clinical applications, because of a relatively good combination of mechanical properties, biocompatibility, corrosion resistance and cost effectiveness (Disegi 2000). Type 316L stainless steels (16-18% Cr, 12-15% Ni, 2-3% Mo, balance Fe) are austenitic stainless steels and are the most employed for implant purposes (Navarro et al. 2008). They are extensively used for fracture repairs like bone plates, screws and pins. In general, stainless steel alloys show poor resistance to corrosion and, when in contact with body fluid, they release Fe, Cr or Ni ions (Sivakumar et al. 1994). Different types of 316L alloys have been developed to improve corrosion resistance and reduce Ni content, by partially or totally substituting Ni with other elements such as Mn (Navarro et al. 2008), because Ni ions are considered especially toxic, and can cause allergy and cancer (Beyersmann & Hartwig 2008).

Cobalt-chromium alloys, specifically Co-Cr-Mo, are frequently used for joint replacements (knee and hip joints) and fracture repairs. Co-Cr-Mo was firstly used in orthopaedics in the 1940s, and in the 1950s it was introduced in hip prosthesis (McKee & Watson-Farrar 1966). Co-Cr alloys exhibit an good corrosion and wear resistances, even though wear debris can still be released from the alloy, increasing the probability of implant loosening due to an inflammatory response in the tissue near the implant (Mantripragada et al. 2013). Moreover, Co is also considered a cytotoxic element and its use should be avoided (Abdel-Hady Gepreel & Niinomi 2013).

Titanium and its alloys are the most extensively used in bone replacement implants. The range of applications is wide and includes different types of implantable devices, such as craniofacial and dental implants, joint replacement, and bone fixation nails, screws and plates. Moreover, other types of implants like prosthetic heart valves, pacemakers, artificial hearts and circulatory devices are made with Ti alloys. These alloys have good mechanical properties, improved corrosion resistance and good biocompatibility, compared with stainless steel and Co-Cr alloys. Among Ti and its alloys, the most used are pure Ti and Ti-6Al-4V, with excellent mechanical properties for hard tissue replacements (Viteri & Fuentes 2013). In addition, Ti-based materials spontaneously form an extremely thin and protective titanium oxide film (TiO_2). The presence of this oxide film increases the biocompatibility and corrosion resistance of the alloy, becoming a good choice for bone replacement (Viteri & Fuentes 2013). On the other hand, NiTi alloy (NITINOL) is one of the most commonly used shape memory alloys for orthopaedic implants (Niinomi & Boehlert 2015). NiTi alloy has unique fatigue resistance and ductile properties. However, as previously mentioned, Ni is considered toxic and various studies try to develop Ni-free shape memory alloys (Wang et al. 2010; Ikeda et al. 2004).

In the following sections, the main properties of metallic alloys are reviewed.

1.3.1. Structure

According to their structure, metallic alloys can be classified as metallic glasses and crystalline materials. A metallic glass is a vitrified liquid obtained from the melt upon rapid cooling, when the melt does not have enough time to crystallize upon cooling.

Metallic glasses are considered amorphous solids that do not possess long-range crystallographic order, i.e. their constituent atoms are not three-dimensionally arranged in an orderly manner. Metallic glasses exhibit unique physical, chemical and mechanical properties, because of their disordered atomic arrangement. To design bulk metallic glasses (BMGs), it is important to know the minimum cooling rate that allows the melt to be kept in amorphous state without any crystal precipitates. Moreover, Inoue defined three empirical rules according to which an alloy tends to become amorphous: (i) the alloy should contain at least three different elements, (ii) the difference in atomic size ratios should be higher than 12% among the three main constituent elements, and (iii) the heat of mixing among constituent elements should be negative (Inoue 2000).

On the other hand, a crystalline material exhibits a long-range order structure, with atoms arranged in a regular or periodic order. Crystallization consists of two processes: nucleation and growth. Nucleation is the initial stage of crystallization and relies on the formation of a primary phase, made of new small-size nuclei entirely from the liquid. Growth involves the aggregation of atoms onto the surface of these nuclei, leading to the disappearance of the primary phase and causing an increase in crystal size. Among crystalline materials, nanocrystalline ones are single or multiphase polycrystalline solids with characteristic grain size of a few nanometers (typically 1 – 100 nm). Due to their extremely small crystalline dimensions, the structure presents a large volume fraction of interphases, improving some properties, such as increased hardness and reduced elastic modulus compared with conventional coarse-grained materials (Hynowska 2014). Furthermore, crystalline materials can be divided into α-, (α+β)-, and β-type alloys according to their primary constitutional phases (Niinomi & Boehlert 2015).

1.3.2. Mechanical properties

The mechanical properties are crucial for selecting the best type of material for each application, as different parts of the body require specific properties of the implant to ensure a long term success. In the case of orthopaedic implants, it is expected that the biomaterial used to replace the bone has similar mechanical properties to those of the bone. If the mechanical properties are very different, a biomechanical incompatibility occurs and the implant could fracture.

Some of the most important mechanical properties are hardness, yield strength, Young's modulus and elongation:

- Hardness is the measure of how resistant a solid material is to various kinds of permanent shape changes when a force is applied.

- Yield strength is the stress at which a material begins to deform plastically. Prior to the yield point the material will deform elastically and will return to its original shape when the applied stress is removed. Once the yield point is passed, some fraction of the deformation will be permanent and non-reversible.

- Young's modulus, also called tensile modulus or elastic modulus, is a measure of the stiffness of a material in the elastic regime.

- Elongation is the increase in the gauge length, measured after fracture of the specimen within the gauge length, usually expressed as a percentage of the original gauge length.

The Young's modulus of the cortical bone ranges from 10 to 30 GPa (Hermawan et al. 2011). Among metallic alloys, Ti-based alloys have lower Young's moduli (55-110 GPa) than 316L stainless steel (210 GPa) and Co-Cr alloys (240 GPa). One of the causes of implant loosening or fracture is the difference between the elasticity of the implant and that of the bone. This biomechanical incompatibility is known as stress shielding effect, and results in increased cell death, bone resorption around the implant, and reduced bone density.

Besides a low Young's modulus, the implant should have high values of hardness. Unfortunately, as seen in figure 3, materials with high elasticity present low hardness. For this reason, it is essential to establish an equilibrium between these two properties.

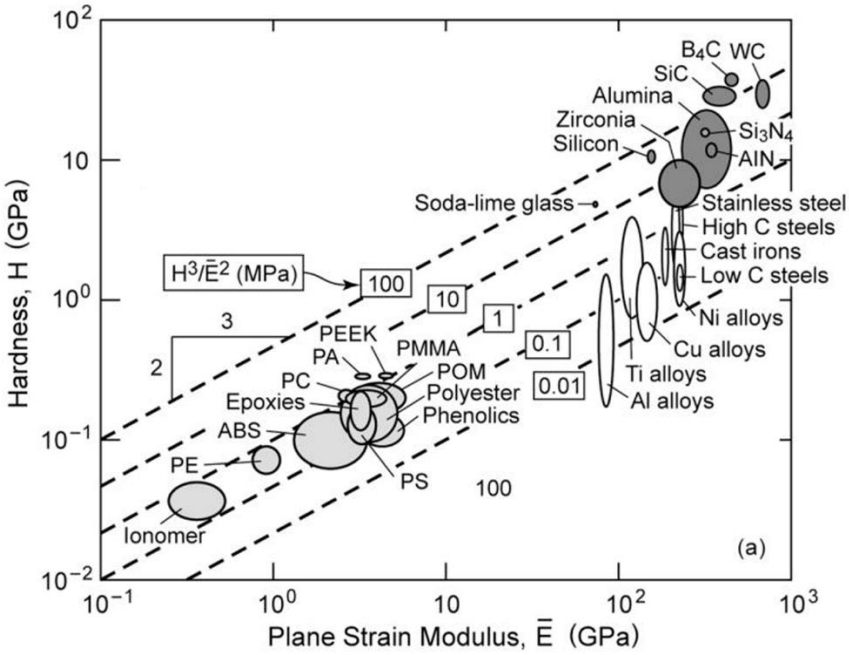

Figure 3. Relationship between hardness and elastic modulus (plain strain modulus) of several common biomaterials (Modified from Zok & Miserez 2007).

1.3.3. Corrosion

Corrosion is one of the major problems affecting the biocompatibility of orthopaedic implants made of metals and alloys (Niinomi & Boehlert 2015). Corrosion refers to the gradual degradation of the materials by electrochemical attack, when placed in a hostile electrolytic environment (Geetha et al. 2010). When a metallic implant is inserted into the body it comes in contact with an aqueous environment rich in ions such as chloride, phosphate, Na^+, K^+, Ca^{2+}, etc., and the difference in potential between the implant and this body fluid causes corrosion (Figure 4). In general, all metallic implants present some degree of corrosion, but metal composition and the type of body fluid can influence the corrosion process. For instance, pH of the body fluids is an important factor that may affect the corrosion process. The pH of the human fluids is normally maintained around 7, but can change due to several causes such as accidents and infections (Geetha et al. 2010). In addition, corrosion changes the chemical environment around the implant, changing the pH, which in turn increases the corrosion process (Aksakal et al. 2004).

Additional factors, such as mechanical factors and cell concentration around the implant can also induce corrosion.

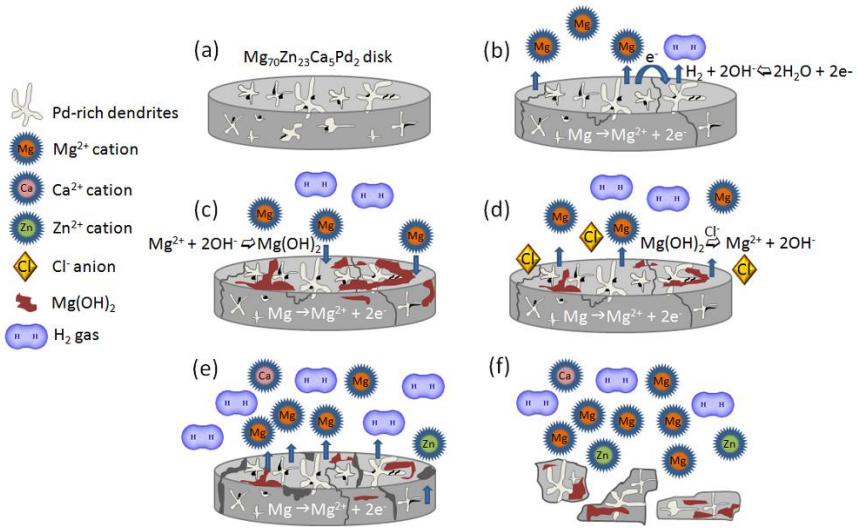

Figure 4. Illustration of the corrosion process for $Mg_{70}Zn_{23}Ca_5Pd_2$ sample (a) upon immersion in HBSS: (b) anodic dissolution of the less noble regions takes place accompanied by hydrogen gas release; (c) the Mg^{2+} ions precipitate onto the sample surface as $Mg(OH)_2$ passive layer; (d) the chloride anions destroy the hydroxide layer; (e) anodic dissolution unavoidably proceeds so that more and more Mg^{2+} (and Zn^{2+} and Ca^{2+}) ions are released into the HBSS; (f) sample disintegration occurs leaving the noble Pd-containing sample pieces undissolved (Modified from Pellicer et al. 2013).

The corrosion of metallic materials can produce adverse biological effects. When a material starts to corrode, its erosion can lead to the fracture of the implant. The metal ions and debris released form the implant may produce inflammation of the surrounding tissues and cell toxicity, which eventually can lead to dermatitis, ulcers, anaemia and Alzheimer's disease (Geetha et al. 2010).

In general, metallic biomaterials are physiologically inert and have high corrosion resistance compared with other biomaterials, due to the formation of a passive film on their surfaces. This surface oxide film plays an important role as an inhibitor of metallic ions release. Accordingly, stainless steel, Co-Cr alloys and Ti alloys are protected by an oxide layer and their rate of corrosion is very low (Geetha et al. 2009). In water, titanium is a reactive material and spontaneously covers with a thin and hard titanium oxide layer. This layer is continuously regenerating and providing a protection against chemical

attacks. In the case of titanium alloys, the oxide film is thicker than on pure Ti (Patrascu et al. 2014). In addition, Ti oxide layer is biocompatible, so it plays an important role in tissue response (Vandrovcova et al. 2012; Patel et al. 2014; Yang & Huang 2010). Therefore, improvement of corrosion resistance of biomaterials is crucial to increase the success of permanent implants.

1.3.4. Surface properties

The implantation of an orthopaedic device results in a direct contact between the alloy surface and the surrounding tissue, including biological fluids and cells. For this reason, biomaterial surfaces are specially important for alloy integration. Branemark et al. (Branemark et al. 1964) used the term osseointegration to describe the phenomenon of Ti and its alloys integration into the bone. Since then, osseointegration is defined as the process by which an orthopaedic implant develops stable fixation through direct bone-to-implant contact (Branemark 1983). This property improves the long term behaviour and reduces the risk of implant loosening (Navarro et al. 2008). Wettability, surface charge and topography are the main parameters that can modulate cell response and, consequently, osseointegration.

Wettability measures the hydrophobicity of the surface. It can be assessed by measuring the contact angle of a water droplet onto the material surface. Low contact angles (aprox. $< 90°$) are related with hydrophilic surfaces, whereas high contact angles ($> 90°$) are associated with hydrophobic ones (Figure 5). When a material is exposed to body fluid, protein adsorption plays an important role in initial cell attachment facilitating the contact with the cell adhesion receptors (Wei et al. 2009). In general, cell adhesion increases with surface hydrophilicity and it is mediated through the recognition and adhesion to the ECM molecules. If the material surface is hydrophobic, proteins are adsorbed in a denatured and rigid state that is inappropriate for cells attachment, because the specific recognition sites are less accessible to cell adhesion receptors (Bacakova et al. 2011a).

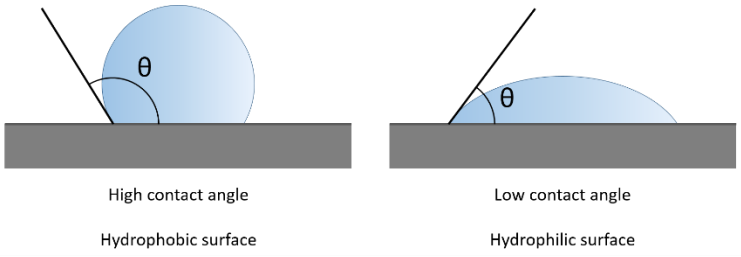

Figure 5. Contact angle measurements to test wettability.

Surface charge is another factor that influences cell adhesion. It can be estimated measuring the zeta-potential, which is caused by the net electrical charges dispersed on the material surface. Cell adhesion is better on positively charged surfaces than on negatively charged ones (Bacakova et al. 2011a; Finke et al. 2007). However, this rule cannot be generalized as it has also been reported that negatively charged hydrogel scaffolds support better adhesion and differentiation of chondrocytes than neutral or positively charged surfaces (Chang & Wang 2011).

Implant topography also seems to play an important role in osseointegration (Zareidoost et al. 2012) and can be classified by the scale of the irregularities and by their distribution. The irregularities are measured by roughness and different parameters of roughness can be determined, being the most important the roughness amplitude value (Ra), the root mean square (RMS) and the peak-to-valley value (PTV). Depending on the scale, roughness has been classified as macroroughness (> 100 μm), microroughness (100 μm – 1 μm), submicroroughness (1 μm – 100 nm), and nanoroughness (<100 nm) (Bacakova et al. 2011a). In contrast, there is no well-defined classification according to the distribution of irregularities. However, it has been reported that cells respond in different ways to different surface morphologies, like grooves (Zhou et al. 2009), tubes (Minagar et al. 2013), meshes (Yang & Huang 2010) or columns (Dalby et al. 2004). Topography usually does not have any effect on cell adhesion when roughness is higher than the cell dimension or much smaller than it. However, several authors have described that nanorough surfaces allow better osseointegration and it is believed that irregularities smaller than 100 nm can mimic the nanoarchitecture of bone (Vandrovcová & Bačáková 2011; Deng et al. 2014).

1.4. Smart materials

In recent years, the development of smart materials that are able to interact with cells or stimulate a cellular response has become a hot topic in regenerative medicine. In general, smart materials can be defined as materials that have one or more properties that can be changed in a controlled fashion by external stimuli, such as stress, temperature, moisture, pH, and electric, magnetic or ultrasonic fields (Marino et al. 2015; Badami & Ahuja 2014; Ribeiro et al. 2015). The use of the terms "smart" and "intelligent" to describe materials started in the 1980s and the first application was based on magnetostrictive technologies. Among applications, the first use in biomedicine was for dental implants with Ni-Ti alloy, due to their shape memory and superelastic properties (Walia et al. 1988).

Smart materials are typically classified according to the output response. In this regard, the classification includes piezoelectric materials, which develop a voltage when mechanical stress is applied and vice-versa; shape memory materials, in which a large deformation can be induced and recovered; and others like temperature responsive polymers, magnetostrictive materials, pH sensitive materials, self-healing materials, thermo-electric materials and conductive polymers (Reviwed by Ribeiro et al. 2015).

Among smart materials, piezoelectric ones are used in biomedical applications for the delivery of an electric stimulus without the need for an external power source (Rajabi et al. 2015). The scavenging of ambient mechanical energy for its posterior utilization has attracted scientific attention in different fields (Harb 2011). Energy harvesting relies on transduction forces that convert ambient mechanical energy, such as vibrations, random motions or noise, into electricity. One of the most common transduction methods is piezoelectricity. A piezoelectric material is a crystal, ceramic, semiconductor or other solid material, with the peculiarity of creating an inherent electric field when it is strained. Some examples of piezoelectric materials are AlN, lead zirconate titanate (PZT), ZnO and quartz. Piezoelectric materials are widely used in different fields as transducers, sensors and actuators. In particular, piezoelectricity and novel electroactive materials are being used to enhance cellular processes (Rajabi et al. 2015). Endogenous electric fields are present in living tissues and, in consequence, numerous investigations try to use electricity to mimic or change the biological responses. Exogenous electrical stimulation

has been used in medicine to repair damaged tissues and for wound healing. Moreover, devices that modulate neuronal activity are used as implants directly in contact with the tissue. During the last years, some authors have described devices to treat neurological disorders and brain injuries, to mitigate inflammation and to reduce chronic pain (Eisenstein 2013).

Because bone tissues respond to electrical stimulation, some orthopaedic research is focused on piezoelectric materials in order to improve bone remodelling. Bone was reported to be a piezoelectric tissue in 1955, with electrical fields generated by mechanical stress. Afterward, it was demonstrated that electric signals similar to those generated by mechanical stress could enhance fracture-healing (Fukada & Yasuda 1957). Several studies have analysed the roles of these electrical signals in bone growth and development using in vitro and in vivo methods (Kim et al. 2006; Shafer et al. 1995). At the cellular level, electrical stimulation was able to promote osteoblast adhesion and proliferation, and it upregulated the expression of osteoblast differentiation markers, suggesting that it promotes bone regeneration (Meng et al. 2011). In addition, it has also been reported that electrical stimulation can alter the intracellular calcium levels, which is relevant because calcium is involved in maintaining cell physiology and is crucial in many cell pathways (Özkucur et al. 2009).

Among materials with piezoelectric properties, ZnO has become popular in material science because of its wide capability to form a variety of nanostructures and its dual property of being both a semiconductive and piezoelectric material. Regarding nanostructures, nanoparticles, films, rods and flowers have been developed and their biocompatibility has been assessed to determine the behaviour of cells in the presence of the biomaterial (Park et al. 2010; Petrochenko et al. 2014). In general, results indicated that ZnO can be a good candidate to be used as an implant.

1.5. Study of biocompatibility

It is essential that the materials used in implants do not present undesirable effects when implanted in the body. They are expected to be non toxic, not to cause inflammatory response or allergies and not to be mutagenic and carcinogenic. These biological parameters should be taken into account to avoid adverse reactions such as tissue damage or necrosis. However, some of these negative effects are difficult to determine because they can appear only in the long term.

Depending on the interaction between the implant and the surrounding tissue, orthopaedic implant materials have been classified as biotolerant, bioinert and bioactive. Biotolerant materials refer to any implant to which the body reacts by the formation of a fibrous capsule around it, and the bone tissue formation is in indirect contact with the implant. Bioinert materials refer to implants that allow bone formation in direct contact with it, although do not actually interact with the surrounding tissue. And, bioactive materials interact with the bone tissue and stimulate biological responses, leading the formation of bone tissue (Viteri & Fuentes 2013; Häfeli et al. 2007). Moreover, following this classification, three different generations of biomaterials have been established, being bioinert materials considered as first generation, bioactive materials as the second generation and materials that stimulate a molecular response as the third generation (Viteri & Fuentes 2013; Navarro et al. 2008).

Regardless of these classifications, Williams et al. (Williams 2008) defined the term biocompatibility as the "ability of a biomaterial to perform its desired function with respect to a medical therapy, without eliciting any undesirable local or systemic effects in the recipient or beneficiary of that therapy, but generating the most appropriate beneficial cellular or tissue response to that specific situation, and optimising the clinically relevant performance of that therapy."

In order to assess biocompatibility, international organizations such as the U.S. Food and Drug Administration subscribed a stepwise paradigm with the description of different tests that should be performed. A new material must first be tested in in vitro assays, then in animal models, and, finally, it must reach the stage of clinical tests (Wataha 2012).

1.5.1. Selection of in vitro models

Animal models have been widely used to test materials before their use in humans. Despite their cost and controversy, animal tests are critical for assessing the biological response, as many clinically relevant biological responses cannot be currently modelled by in vitro tests. Such responses include blood interactions, wound healing, infection, carcinogenesis or chronic inflammation (Wataha 2012). However, the use of animals should be limited, and in vitro tests should instead be used for an initial evaluation.

In vitro analyses require cell culture systems to assess the interactions between cells and materials. There are different types of cell models: primary cultures, after cell isolation from the tissue; finite cultures, in which the cells have the ability to proliferate, but become senescent after a few passages; immortalized cultures, in which the cells can proliferate indefinitely; and tumour derived cultures.

Obviously, bone cells are the most used to test new materials for orthopaedic implants. The use of human cells is recommended because it has been described that there are noticeable differences regarding bone composition among different species (Aerssens et al. 1998) and significant differences in terms of viability or proteins synthesis in cell cultures from different origins (interspecies differences) (Torricelli et al. 2003; Czekanska et al. 2012). However, as only primary cell cultures or tumour cell lines are available in humans, in some cases authors prefer the use of animal cells. Indeed, the MC3T3-E1 mouse preosteoblast cell line is frequently used to study osteoblast response and differentiation on biomaterials (Hua et al. 2014; St-Pierre et al. 2005). It is an immortalized cell line that is at an early stage of differentiation. Regarding human cells, tumour cell lines have the advantage of rapid proliferation, unlimited number of cells and reproducibility. Their main disadvantage is that they present an altered behaviour when compared with normal cells. For instance, contact inhibition is disrupted in malignant cell lines, but not in immortalized ones. On the other hand, the behaviour of primary cells is closer to that of the cells in the original tissue and, therefore, the results obtained with their use are more relevant for clinical applications. However, they have the disadvantages of having to be isolated from a patient, and of their low proliferation rate.

In addition, primary cells can present differences depending on the age and physical condition of the donor.

The human cell lines most commonly used for biocompatibility studies are MG-63 cells and Saos-2 cells, both from osteosarcoma. MG-63 cells show a similar integrin expression profile to human osteoblasts and are suitable for testing initial cell attachment on materials. On the other hand, Saos-2 cells show similarities with primary osteoblasts, including mineralization potential, ALP activity and gene regulation upon differentiation (Czekanska et al. 2012).

1.5.2. Cytotoxicity and proliferation

The first parameter to analyse when studying the biocompatibility of new materials is their cytotoxicity. Materials can be cytotoxic because they kill the cells, usually detectable at 24 h, or because they slow down or even block cell proliferation. The main causes of toxicity are the amount of ions or debris released from the material and the surface properties of the material.

Some elements are known to cause adverse effects in biological environments. However, the individual elements used to synthesize an alloy cannot determine by themselves the final alloy biocompatibility, as different factors are involved in the biological response to the implant. For instance, depending on the localisation of the implant in the body and its role, biocompatibility may change. In addition, each element can be released from the alloy with different ion valence, and every ion can present different cytotoxicity. Finally, ions released from the implant can combine with other ions to form salt compounds. In this case, the same ion but forming different salts will show different cytotoxicity.

Biesiekierski et al. (Biesiekierski et al. 2012) published an extensive review on the biocompatibility, carcinogenicity, genotoxicity, mutagenicity, cytotoxicity, allergenicity and the proneness to corrosion of 27 transition metals. In table 1, a summary of the biocompatibility characteristics of the most currently used elements in orthopaedic implants is presented, modified from Biesiekierski et al. (Biesiekierski et al. 2012). The authors concluded that the most biocompatible elements were Ti, Au, Sn, Ta, Nb, Ru and Zr. Other elements, such as Hf and Re, present good biocompatibility and

osteocompatibility, without the induction of inflammatory response (Matsuno et al. 2001), but more biological experiments should be performed to confirm their safety.

Table 1. Biological impact of transition metals with potential use in orthopaedic implants (Modified from Biesiekierski et al. 2012).

Periodic position	*Element*	*Biocompatible*	*Carcinogenic*	*Genotoxic*	*Mutagenic*	*Cytotoxic*	*Allergenic*
3d	Ti	Yes	No	No	No	Low	No
	V	No	Yes	Yes	Yes	High	Disputed
	Cr	No	Disputed	Yes	Yes	Disputed	Yes
	Mn	No	No	Yes	No	High	No
	Fe	No	No	Yes	Disputed	Med	No
	Co	No	Yes	Yes	Yes	High	Yes
	Ni	No	Yes	Yes	Yes	High	Yes
	Cu	No	No	Yes	Yes	High	Yes
4d	Zr	Yes	No	No	No	Low	No
	Nb	Yes	No	No	No	Low	No
	Mo	No	Disputed	Yes	Yes	Low	Yes
	Ru	Yes	No	No	No	Med	No
	Rh	No	Yes	Yes	Yes	High	Unknown
	Pd	Disputed	Disputed	No	Disputed	Low	Yes
	Ag	No	No	No	No	Disputed	Yes
5d	Hf	Yes	Unknown	Unknown	Unknown	Med	No
	Ta	Yes	No	No	No	Low	No
	W	No	Yes	Yes	No	Med	No
	Re	Yes	Unknown	Unknown	Unknown	Unknown	No
	Os	No	Unknown	Yes	Yes	High	No
	Ir	No	No	No	Yes	High	No
	Pt	No	Yes	Yes	Yes	High	Yes
	Au	Yes	No	No	No	Disputed	No
Other	Al	No	No	Yes	No	Disputed	No
	Zn	No	No	No	No	High	No
	Sn	Yes	No	No	No	Low	No

In general, most authors agree that some of the elements used to synthetize orthopaedic implants are not biocompatible. For example, Ti-6Al-4V was the most used metallic alloy for implants during the last decade, and it is composed of Al and V, which are considered toxic and not biocompatible (Okazaki et al. 1998; Sabbioni et al. 1993). Al, for instance, is known to have adverse effects on neurons when it accumulates in the brain and has been reported to play a role in the neurodegeneration process and Alzheimer's disease (El-Rahman 2003). Other elements commonly used are Cr, Co and Ni, all of them considered cytotoxic (Biesiekierski et al. 2012). However, Cr cytotoxicity is controversial, as some authors instead suggest its low toxicity (Hallab et al. 2005).

As mentioned above, the ions valence and the salts formed when they release from the alloy can change the biological response to an element. Yamamoto et al. (Yamamoto et al. 1998) tested 43 metal salts and concluded that salts of soft acids such as Ag^{+} and Cd^{2+} were highly toxic salts, whereas salts of alkali metals showed low cytotoxicity. They also observed that Cr^{3+} presented low cytotoxicity, in contrast with the previous mentioned studies that considered Cr as cytotoxic (Biesiekierski et al. 2012). Therefore, some elements that are known to be toxic can behave differently when alloyed with other elements. For example, Zn and Cu presented high cytotoxicity when studied individually, but when alloyed, like in Mg-Zn-Ca (Zberg et al. 2009) and Ti-Cu (Zhang et al. 2015) alloys, no effect on cell toxicity was observed.

Cytotoxicity can be measured indirectly, culturing cells in the presence of a medium that has been in contact with a specific material, or directly, growing the cells on top of the specific material. An interesting approach is to perform both direct and indirect cytotoxicity assays at the same time by culturing cells in a dish that contains a small alloy disk. In this case, cells that grow on top of the alloy disk are used for direct studies whereas cells that grow on the dish surface and that are therefore exposed to ions released from the alloy but not in contact with it can be used for indirect studies (Pellicer et al. 2013).

Quantification of cytotoxicity in direct studies is hampered by the opacity of most materials, which prevents the use of light microscopy. For this reason, cytotoxicity is usually quantified by measuring the activity of certain cellular enzymes, through the use

of products that can be reduced by these enzymes. Two different approaches are commonly used: colourimetric assays (e.g. MTT assay) or fluorescent signal assays (live/dead kits). In the first case, cells must be destroyed to obtain a coloured product that is quantified in a colourimetric reader. In the second case, live cells, with enzymatic activity, reduce a specific product which emits fluorescence that can be visualized under a fluorescence microscope. To detect dead cells, a fluorescent agent specific for DNA and that can only penetrate into cells with a damaged membrane is used.

Cell proliferation can also be altered by the presence of an implant. Proliferation can be evaluated using the same methods described above, but in a time-course experiment. These experiments are costly and time consuming, and require the use of many samples of the materials, one for each time-point to be measured. To avoid this, alternative assays have been developed, like the alamar blue assay. Alamar blue is a non-toxic cell permeable compound that emits fluorescence when is reduced. This reduced form compound can exit the cell, and its fluorescence can be analysed directly in the culture medium without cell lysis, allowing the re-evaluation of the same culture over time.

1.5.3. Cell adhesion and morphology

Intracellular adhesion or adhesion between cells and the ECM, is involved in embryogenesis, maintenance of tissue integrity, would healing, immunological response and biomaterial tissue integration. Anchorage-dependent cells, like osteoblasts, need to be adhered to proliferate, and differentiate (Bacakova et al. 2011). When cell adhesion is prevented, cells can activate anoikis, a type of programmed cell death induced by the loss of cell anchorage (Grossmann et al. 2001).

Cell adhesion can be divided in different phases. First, proteins from biological fluids or cell culture medium are adsorbed on the biomaterial surface. Then, cells respond to the adsorbed proteins, rather than to the surface itself, involving ionic or van der Waals forces. Cells attached on the surface express cytoskeleton proteins and integrins. After that, there is a clustering of integrin receptors and active spreading of the cells onto the material surface. Finally, the cells synthesize ECM proteins at their interface with the material (Anselme et al. 2010).

Cell adhesion to the ECM or to a material is a complex process mediated by integrins. Integrins constitute a family of transmembrane receptors that interact with the ECM through their extracellular domains and with the cytoskeleton, specifically with actin filaments, through their intracellular domains. In the sites of adhesion, clusters of integrins form focal contacts, focal adhesions or adhesion plaques together with other cytosolic proteins such as paxillin, talin, vinculin and tensin (Anselme et al. 2010; Alberts et al. 2002) (Figure 6). The interactions between ECM proteins and their specific membrane receptors induce signal transduction processes (Keselowsky et al. 2004). The cytosolic proteins involved in focal contacts, once activated, induce actin polymerization to form stress fibres and consequently influence cell growth and differentiation (Bacakova et al. 2011b; Pellegrin & Mellor 2007).

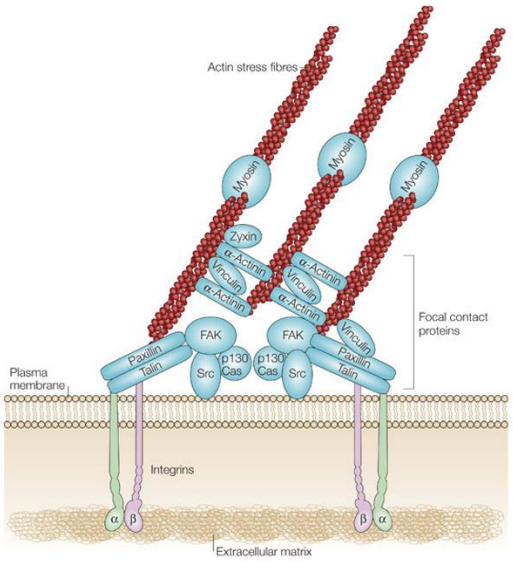

Figure 6. Main structural components of a focal contact. Transmembrane integrins link the ECM with the cytosolic component. Vinculin, talin and paxillin are some of the cytosolic proteins associated with the focal contact and actin cytoskeleton (Mitra et al. 2005).

The adsorption of proteins is influenced by the physical and mechanical properties of the material surface (Bacakova et al. 2004). Materials can adsorb adhesion-promoting proteins (fibronectin) and adhesion-inhibiting proteins (albumin) onto their surface, and the efficiency of cell adhesion and growth depends on the balance between these two types of proteins (Wei et al. 2009). As mentioned above, wettability of the material surface

is a key factor for protein adsorption, which results in different cell adhesion response. Cells adhere better on hydrophilic surfaces because in these surfaces proteins are adsorbed in a geometrical conformation appropriate to be recognized by cell adhesion receptors (Bacakova et al. 2011b). Surface charge has also an important effect on protein adsorption and, consequently, on cell adhesion. In most cases, positively charged surfaces show better cell adhesion than negatively charged ones, due to a preferential adsorption of ECM proteins (Bacakova et al. 2011b; Minagar et al. 2013). Regarding the topography, roughness usually does not interfere with cell adhesion when the Ra value is higher than the cell dimension or much smaller than it (Anselme & Bigerelle 2014) (See section 1.3.4). Roughness can be modulated by some mechanical, chemical and physical techniques, and the results of these modifications are not only changes in the topography, but also in wettability and surface chemistry. In whole, cell adhesion depends on all surface properties, so surface wettability, charge and topography should be taken into account because they can modulate cell response.

It has been described that the extent of focal contacts depends on the force applied by actin stress fibres on the substrate. For example, in smooth surfaces the distribution of ECM proteins is homogenous and cells can spread forming parallel stress fibres. However, on rough surfaces the distribution of extracellular proteins is related to the topography, and stress fibres are distributed along the direction of the adhesion force, with cells presenting irregular shapes (Passeri et al. 2010). The presence and the extent of focal contacts is usually evaluated through the detection of one of the cytosolic proteins involved in the focal adhesions, simultaneously with the detection of the actin filaments that compose the stress fibres. Furthermore, osteoblast adhesion can also be analysed by quantifying integrin gene expression. It is known that integrin expression has an important effect on cell adhesion, cell migration and cell differentiation, because integrins play an important role in signal transduction (Keselowsky et al. 2004; Yang et al. 2013).

Finally, cell morphology is related to cell adhesion and, subsequently, cell spreading. When a material surface does not allow cell adhesion, there is a high number of round cells, and some of them present membrane protrusions characteristic of apoptotic cells, due to the induction of anoikis. By contrast, well spread cells usually show a polygonal shape, although this depends on the cell type (Vandrovcová & Bačáková 2011).

Morphology can be evaluated using scanning electron microscopy and immunofluorescence techniques, which also allow assessing cell adhesion and cell spreading.

1.5.4. Osteoblast differentiation

In the case of bone repair, the implant should not interfere with the remodelling cycle, allowing osteogenic differentiation. As explained in section 1.1 osteoblast differentiation is carried out in three different phases and these phases can be assessed in vitro by culturing osteoblasts in the presence of the implant. Various osteoblast cell lines are able to differentiate in vitro, usually when cultured with specific cell culture medium (supplemented with dexamethasone, ascorbic acid and β-glycerophosphate). There are several techniques to assess osteoblast differentiation, including histological, molecular and analytical techniques.

Mineralization of the ECM is an indicator of successful in vitro osteoblast differentiation. Mineralization can be detected as calcium deposits as early as 7 or 14 days in culture, depending on the cell line. Calcium deposits appear as dispersed small spots that increase in size up to 35 days in culture (Lian & Stein 1995). These spots can be specifically detected using different histological stains (Alizarin Red S and Von Kossa), allowing to quantify ECM mineralization by counting the nodules and measuring the absorbance (Pan et al. 2012).

Another indicator of osteoblast differentiation is the expression of osteogenic markers, which can be quantified by reverse transcription and quantitative PCR (qPCR). Osteocalcin is one of the genes most frequently analysed, but other genes such as osteopontin, type I collagen, ALP and bone sialoprotein have also been studied by several authors (Popp et al. 2011; Saldaña et al. 2011; Liskova et al. 2015). As mentioned in section 1.1 some of these genes are considered early markers whereas others are considered late differentiation markers. The expression of these genes can be quantified at different time points to trace the effect of the implant on osteoblast differentiation over time.

The product of some of the aforementioned genes can also be measured or detected by western blot or immunofluorescence, depending on the quantity of cells available. In western blot quantification, large amounts of proteins are needed. When such amounts are not available, protein markers of osteoblast differentiation can be labelled with specific antibodies and the intensity of the fluorescent signal quantified using specific softwares (Novotna et al. 2013; Liskova et al. 2015).

Finally, another technique widely used to determine osteoblast differentiation is the quantification of ALP activity. ALP content increases with osteoblast differentiation and its activity can be quantified by spectrophotometry (Lee et al. 2006; Huang et al. 2011).

1.5.5. Immunogenicity

The implantation of a prosthetic material can produce tissue damage and inflammation in some cases. One of the most common responses of the human body to a foreign material is the formation of a non-adherent fibrous capsule surrounding the implant, which can promote chronic inflammation (Wang & Poh 2013). Moreover, the wear debris from the alloys or the corrosion and released ions can also initiate the inflammatory cascade, which could end in implant loosening and cause instability and pain to the patient (Wang & Poh 2013; Pizzoferrato et al. 2002). When implant loosening occurs, the surrounding tissue presents high levels of certain cytokines known to stimulate bone resorption, such as interleukin 1B, interleukin 6 or tumour necrosis factor alpha (Vallés et al. 2006). The monocyte/macrophage lineage is the main cell type involved in the inflammatory response, due to their phagocytic role and their ability to orchestrate and amplify the response. Material debris and ions released from the alloy can activate an inflammatory response in macrophages by different pathways. It has been described that to activate the inflammatory response, macrophages phagocyte material debris, but other authors have suggested that phagocytosis of metal debris is not necessary (Bitar 2015; Nakashima et al. 1999). On the other hand, low concentrations of metal ions can also induce inflammatory processes (Wataha et al. 2004; Pizzoferrato et al. 2002). For example, soluble Co, Cr, Mo and Ni ions induced NADPH/ROS-, active caspase-1, Nalp3-, and IL-1B secretion in human macrophages (Caicedo et al. 2009).

Metallic alloy topography seems to have a potential effect on macrophage function, although there is no consensus on the type of effect. Whilst some authors have described that roughness increases the production of proinflammatory cytokines (Refai et al. 2004), others have demonstrated the decrease in their expression (Hamlet & Ivanovski 2011).

The inflammatory response can be assessed by different techniques, which can be classified as in vivo and in vitro assays. The main in vivo assay is the study of histological sections of the tissue surrounding the implant. The relative number of inflammatory cells, the activity of an hydrolytic enzyme and the presence and thickness of the fibrous capsule near the implant allow to determine the host reaction to a foreign material (Rajzer et al. 2010; Geurtsen 2002). On the other hand, the most used in vitro assay is the quantification of inflammatory cytokines secreted by macrophages, using ELISA techniques (Huang et al. 2013; Bordignon et al. 2008). Other techniques of analysis of the inflammatory response include qPCR (Hamlet & Ivanovski 2011), BioplexMultiplexSystem (Ullm et al. 2014) and flow cytometry using a cytometric bead array (Young et al. 2008). Otherwise, cytokine secretion analysis can be performed using cocultures of macrophages and osteoblasts, instead of macrophages monocultures. The use of cocultures allows to determine the effect of osteoblasts on macrophage cytokine secretion (Horowitz & Gonzales 1996; Vallés et al. 2013).

The possible allergenic response that material elements might induce in the patient is another important factor to be considered. Therefore, the use of allergy-free elements is recommended. One of the elements that is known to cause an allergic effect is Ni (Bordignon et al. 2008; Faurschou et al. 2011). It is estimated that more than 17% of women and 3% of men are Ni allergic. On the other hand, between 1 and 3% of the population is allergic to Co and Cr (Hermawan et al. 2011; Thyssen & Menne 2010).

In summary, before a material is used for implant fabrication, all aforementioned issues must be taken into account, that is, the material should not be cytotoxic, should allow proliferation and differentiation, and should not induce an immunological response.

2. Objectives

The present thesis is part of an interdisciplinary research project that aims to develop new biomaterials for orthopaedic applications. The group of Física dels Materials de la Universitat Autònoma de Barcelona is working on the generation of new metallic alloys with better physical and mechanical properties than those of the currently used. Researchers from the Centro Nacional de Microelectrónica del CSIC are developing piezoelectric nanogenerators for medical purposes. Finally, our group at the Unitat de Biologia Cel·lular is responsible for assessing the biocompatibility of all these newly developed biomaterials.

The main objective of the thesis has been to study the biocompatibility of new biomaterials for orthopaedic implants. In this sense, the following specific objectives can be defined:

1. To evaluate the biocompatibility of three new Ti-based metallic alloys in terms of cytotoxicity, adhesion and osteoblast differentiation.

2. To investigate the effect of Ti-based alloys surface modifications on osteoblast behaviour.

3. To evaluate the biocompatibility of two new ZnO piezoelectric nanogenerators and to analyse the effect of electric stimulation on osteoblasts and macrophages.

3. Results

3.1. In vitro biocompatibility assessment of $Ti_{40}Cu_{38}Zr_{10}Pd_{12}$ bulk metallic glass

In vitro biocompatibility assessment of $Ti_{40}Cu_{38}Zr_{10}Pd_{12}$ bulk metallic glass

A. Blanquer[1], E. Pellicer[2*], A. Hynowska[2], L. Barrios[1], E. Ibáñez[1], M.D. Baró[2], J. Sort[2,3], C. Nogués[1]

[1] Departament de Biologia Cel·lular, Fisiologia i Immunologia, Universitat Autònoma de Barcelona, E-08193 Bellaterra, Spain.

[2] Departament de Física, Universitat Autònoma de Barcelona, E-08193 Bellaterra, Spain.

[3] Institució Catalana de Recerca i Estudis Avançats (ICREA) and Departament de Física, Universitat Autònoma de Barcelona, E-08193 Bellaterra, Spain.

Abstract

The use of biocompatible materials has attained an increasing importance for tissue regeneration and transplantation. The excellent mechanical and corrosion properties of $Ti_{40}Cu_{38}Zr_{10}Pd_{12}$ bulk metallic glass turn it into a potential candidate for its use in orthopaedic implants. Before being considered as a biomaterial, some biological parameters must be taken into account. In this study, mouse preosteoblasts were cultured in the presence or absence of the alloy at different times (24 h, 7 and 21 days) and no differences in cell viability were detected. Moreover, cells were able to adhere to the alloy surface by establishing focal contacts, and displayed a flattened polygonal morphology. After 14 days in culture, differentiation into osteoblasts was observed. Besides, the amount of Cu ions released and their potential toxic effects were analyzed, showing that the amount of Cu released did not increase cell death. Finally, the low levels of inflammatory cytokines secreted by THP-1 differentiated macrophages exposed to the alloy suggest the absence of an immunogenic response to the alloy. In conclusion, in vitro studies indicate that the $Ti_{40}Cu_{38}Zr_{10}Pd_{12}$ bulk metallic glass could be considered as a biomaterial to be used in orthopaedic implants.

Introduction

Biocompatible materials have attained an increasing importance for tissue regeneration and transplantation. Among the different materials that have been described for these purposes, metallic ones are currently being used for biomedical applications such as in orthopaedic and dental implants or in artificial heart valves. Two physical characteristics to be considered for a material used in orthopaedic implants are hardness and stiffness. Hardness is related to the resistance of a solid material against plastic deformation when a force is applied, whereas stiffness is correlated with the elastic properties when the solid it is subjected to tension or compression in a single direction and it is measured by the Young's modulus. The Young's modulus (E) of cortical bone ranges from 4 to 30 GPa. The more similar the Young's modulus of a material is to that of the bone, the most suitable is the material to be used in the orthopaedic field, reducing the possibility of loosening of the implant, a biomechanical incompatibility known as "stress shielding effect".

Nowadays, commercial Ti-6Al-4V alloy is one the material used for implants because it has good mechanical properties, but its Young's modulus is still too high (110 GPa vs 4-30 GPa of bone) [1]. For this reason, new materials have been produced during the last decade with the aim of decreasing the Young's modulus. Among these, biocompatible bulk metallic glasses (BMGs) have been widely studied. Due to absence of long range atomic order, BMGs present unique mechanical properties such as superior strength, high elastic strain limit, relatively low Young's modulus (typically between 30 and 200 GPa), excellent corrosion resistance, and good wear resistance [2].

In fact, at present, these are the bulk metallic alloys with Young's moduli closer to that of the bone. Among the different BMGs families, the ones based on Ti and Zr have attracted much attention because of their suitable mechanical characteristics to be used as biomaterials.

In addition to the physical characteristics, some biological parameters related to the biomaterial must be taken into account, as it has been described that surface hydrophobicity, roughness and topography play a major role in the osseointegration of the implant [1]. Thus, biomaterials have to allow cell adhesion, cell proliferation and cell

differentiation, and the formation of an extracellular matrix (ECM) [3]. Another concern is the possible toxicity of the material or the toxicity derived from elements released during osseointegration. Many studies have shown toxicity for elements like mercury, beryllium, nickel, cobalt or chrome [4,5]; long-term exposure to aluminium has been linked to Alzheimer disease development due to the induction of reactive oxygen species [6]. Nevertheless, the toxic effect of the majority of elements depends on their relative amount in the alloy and, more importantly, on their capability of being released from the alloy. The threshold between toxicity and physiological dose is not clear-cut, because an essential element could become toxic with a minimal increase in its concentration [7]. Copper, for instance, is an essential bioelement for cells but has been considered cytotoxic by several authors [5,8]. When cells are cultured onto pure copper, most of them fail to adhere to the metal surface and die by non-apoptotic cell death [9]. Another important factor to be considered is the possibility that a single or the combined alloy elements might induce an allergenic response in the patient. It is estimated that up to 17% of women and 3% of men are nickel allergic, whereas 1-3% of the population are allergic to cobalt and chromium [10].

The biocompatibility of a material is usually evaluated in cell culture assays. Initially, cell viability and proliferation is analysed by culturing cells in the presence of medium that has been previously in contact with a specific alloy (indirect studies). If toxicity is not observed, the cells are then seeded onto the material to evaluate their ability to adhere and proliferate on the material surface (direct studies). Cell adhesion to the ECM or to the material surface is a complex process mediated by a family of transmembrane proteins called integrins, which cluster together to form focal contacts with other cytosolic proteins such as paxillin, talin, vinculin and tensin. The characteristics of the material surface are important for cell adhesion because if ECM adhesion-mediating proteins from the cell culture cannot be adsorbed to the material, integrin clustering and the formation of the focal contacts is prevented [11]. In this situation cells can activate anoikis, a form of programmed cell death induced by the loss of cell anchorage.

In addition, cell culture assays allow to test whether cells can differentiate correctly in contact with the material. Mouse preosteoblasts differentiate into osteoblasts in three stages: proliferation (rapid increase in cell number), ECM synthesis and maturation, and

ECM mineralization (accumulation of mineral deposits of calcium phosphate called nodules) [12]. Thus, cell culture mineralization provides evidence for osteoblast differentiation.

Finally, in relation to a possible immunogenic response induced by the biomaterial, *in vitro* studies of inflammatory cytokine secretion may also be performed. An implant can produce an inflammatory reaction when it is placed inside the body, and the reaction could become chronic if the implant is not removed. At the implant site, where the concentration of released ions is high, inflammatory reactions can take place and macrophages play an important role in these reactions because of their ability to orchestrate and amplify the inflammatory response. In this sense, several studies have tested the ability of macrophages and other immunologic cells to secrete inflammatory cytokines in front of wear debris of several materials [13,14], and in front of metal ions [15-17].

The biocompatibility of different BMGs has been tested *in vitro* following some of the analyses mentioned above. According to these analyses, alloys based on Zr [18,19], on Mg [20-22] or on Ti [23,24] have shown to be appropriate for cell growth or differentiation.

The material presented here, $Ti_{40}Cu_{38}Zr_{10}Pd_{12}$ (at%), is a bulk glassy alloy that exhibits high hardness (H = 7.5 GPa), relatively low Young's modulus (E = 100 GPa), good wear resistance and excellent corrosion behaviour in simulated body fluid (E_{corr} = -0.031 V vs. Ag/AgCl and $j_{corr} = 4.36 \cdot 10^{-7}$ A/cm^2). Because of these characteristics, this BMG could constitute a new generation of metallic materials for orthopaedic implants [25]. However, this alloy contains 38 at% of copper, an element that has been considered potentially toxic in some studies, as mentioned above.

In this study, we attempt to demonstrate the *in vitro* biocompatibility of $Ti_{40}Cu_{38}Zr_{10}Pd_{12}$ bulk metallic glass. We have evaluated indirect and direct cytotoxicity, cell morphology, cell adhesion and cell differentiation using the mouse preosteoblasts cell line MC3T3. In addition, we have studied the capacity of the alloy to trigger immunogenicity response using macrophages differentiated *in vitro* (THP-1 cell line). Finally, copper release from

the alloy in presence and absence of the preosteoblasts has been quantified at different culture times (24 h, 3, 7 and 21 days).

Material and Methods

Cell lines

Mouse preosteoblasts MC3T3-E1 (ATCC) were cultured in α-minimum essential medium (MEMα, Invitrogen) with 10% foetal bovine serum (FBS, Gibco) at 37°C and 5% CO_2.

THP-1 monocyte cells were grown in RPMI 1640 medium (Gibco) supplemented with 10% FBS at 37°C and 5% CO_2. To differentiate monocytes into macrophages, 60,000 cells were seeded into 96-well plates and treated with 0.16 μM phorbol-12-myristate-13-acetate (PMA, Sigma) for 72 h. Then, cells were washed and incubated in fresh medium for 24 h before carrying out the experiments.

Material synthesis

$Ti_{40}Cu_{38}Zr_{10}Pd_{12}$ (at. %) BMG alloy was prepared by levitation melting mixtures of the high purity elements in an Ar atmosphere [Ref X]. Rods of 3 mm in diameter were obtained from the arc-melt by copper mold casting. Disks of approximately 500 μm thickness were cut from the rod and carefully grinded with SiC paper (up to 4000 grit), degreased with acetone and finally cleaned with distilled water. After the treatment, the root mean square (rms) value of the surface was found to be 34 nm as determined by Dual Core 3D Profiler (Leica DCM 3D).

Cell viability assay

Alloy disks were glued individually onto a glass coverslip with silicone (Bayer), introduced into a 4-multiwell culture plate and sterilized by UV light for at least 2 h. Once sterilized, 50,000 preosteoblasts were seeded into each well and cultured in standard conditions for 24 h. In parallel, control cells were seeded directly onto a glass coverslip in the absence of the alloy.

Cytotoxicity was evaluated by detecting the activity of intracellular esterases using the Live/Dead Viability/Cytotoxicity Kit for mammalian cells (Invitrogen), according to the manufacturer's protocol. Live cells show green colour because their esterase activity

converts nonfluorescent calcein AM into fluorescent, whereas dead cells show red colour because of the permeability of their damaged plasma membrane to propidium iodide.

Samples were observed with an Olympus IX71 inverted microscope equipped with epifluorescence. Images from different regions (alloy disk and coverslip) of each culture sample were captured. A minimum of 300 cells were analyzed and experiments were performed in triplicate.

Cell morphology analysis

After the cell viability assay, the samples were processed to be analyzed by scanning electron microscopy (SEM). Cells were rinsed twice in phosphate buffered saline (PBS), fixed in 4% paraformaldehyde in PBS for 45 min at room temperature (RT) and rinsed again twice in PBS. Cell dehydratation was performed in a series of ethanol washes (50, 70, 90 and twice 100%), 8 min each. Finally, samples were dried using 50% hexamethyl disilazane (HMDS; Electron Microscope Science) in absolute ethanol, followed by 10 min of 100% HMDS. Samples were mounted on special stubs and analyzed using a SEM (Zeiss Merlin) equipped with energy-dispersive X-ray spectroscopy (EDX) analysis.

Contact angle measurements

To assess the wettability of the alloy surfaces, the contact angle of an aqueous drop (1.5 μl of culture medium MEMα) deposited onto the surface of the alloy was measured using a contact Angle Measuring System DSA 100 (Krüss) at RT (i.e., sessile drop technique).

Cell adhesion analysis

Cell adhesion onto the alloy surface was determined by the presence of focal contacts. Phalloidin was used to visualize actin filaments whereas an antibody against vinculin was used to detect the focal contacts. Following the same protocol described for viability studies, 50,000 preosteoblasts were seeded into a well containing an alloy disk glued onto a coverslip. After 24 h of culture, cells were fixed in 4% paraformaldehyde (Sigma) in PBS for 45 min at RT, permeabilized with 0.1% Triton X-100 (Sigma) in PBS for 15 min and blocked for 25 min with 1% PBS-bovine serum albumin (BSA; Sigma) at RT. Samples were then incubated with a mouse anti-vinculin primary antibody (Chemicon)

for 60 min at RT and washed with 1% PBS-BSA. Then, samples were incubated with a mixture of Alexa fluor 594-conjugated phalloidin (Invitrogen), Alexa fluor 488 goat anti-mouse IgG1 and Hoechst 33258 (both from Sigma) for 60 min at RT. Finally, samples were washed in 1% PBS-BSA, air dried and mounted on specific bottom glass dishes (MatTek) using Fluoroprep mounting solution (Biomerieux). Control analyses were performed in absence of the alloy. All experiments were done in triplicate.

Sample evaluation was done in a confocal laser scanning microscope (CLSM, Leica SP5). Series of horizontal optical sections were collected at 400 nm intervals and projections were generated with Imaris software (Bitplane).

Cell differentiation assay

Preosteoblasts differentiation in the presence of the alloy was studied through the detection of calcium deposits, a sign of ECM mineralization. For this purpose, 500,000 preosteoblasts were seeded into 35 mm culture dishes containing an alloy disk glued to a coverslip with silicone. After 24 h in culture, MEMα medium was removed and differentiation medium, consisting in MEMα supplemented with 10^{-8} M dexamethasone, 50 μg/ml ascorbic acid and 8 mM β-glycerophosphate (all from Sigma), was added. Cells were cultured during 14 or 21 days in presence of the differentiation medium, which was replaced every 3-4 days. Control analyses were performed in absence of the alloy. All experiments were done in triplicate.

Secreted calcium deposits were detected using Alizarin Red S staining. After 14 or 21 days in culture, cells were rinsed in PBS and fixed in 4% paraformaldehyde in PBS for 45 min at RT. Then, cells were washed twice with PBS and incubated with 2% Alizarin Red S (Sigma) for 30 min at RT. Finally, samples were washed with milliQ water and visualized using Olympus IX71 inverted microscope.

Copper ions release and assessment of cytotoxicity

In order to quantify the amount of copper ions released from the alloy into the medium (V = 2 mL), three parallel experiments were conducted: (1) cells were seeded in the presence of the disk, (2) cells were seeded without the disk (control experiment) and (3) no cells were seeded but the disk was incubated in the culture medium (MEMα).

In experiments (1) and (2) 500,000 preosteoblasts were seeded into 35 mm culture dishes. In experiments (1) and (3) the dishes contained the disk glued to the coverslip with silicone. For each experiment, two replicas were done in order to analyse the amount of copper released at different time points. The culture medium was withdrawn after 24 h and after 3, 7 and 21 days, and the copper concentration was analysed by inductively coupled plasma mass spectrometry (ICP-MS) on an Agilent ICP-MS 7500ce equipment (Agilent Technologies).

In addition to the experiments described, another preosteoblast cell culture (4) was established in the absence of the alloy disk but using the culture medium where the alloy disk had been incubated for 21 days. The cells were incubated in this medium for 3 days.

In all experiments containing cells, cytotoxicity was evaluated using Live/Dead Viability/Cytotoxicity Kit for mammalian cells (Invitrogen).

Quantification of inflammatory cytokines secretion

To conduct these experiments, THP-1 cells differentiated into macrophages were used. One alloy disk, previously sterilized by UV light, was placed over a culture of macrophages and maintained in contact with the cells for 5 or 24 h to analyze the secretion of inflammatory cytokines. As a positive control, 1 μg/ml of lipopolysaccharide (LPS; Sigma) was added to the macrophages culture. As a negative control, macrophages cultured in the absence of the disk or LPS were used. After 5 and 24 h, supernatants were removed and used to quantify cytokine secretion. Inflammatory cytokines TNFα, IL-1β and IL-6 were evaluated by flow cytometry using cytometric bead array (CBA, Becton-Dickinson). Cytokine concentrations in the supernatant were analyzed according to the manufacturer's protocol. Negative control was considered as basal level secretion with a 0 value. Experiments were performed in triplicate.

Statistical analysis

Cell viability data and cytokine secretion data were analyzed using the Fisher's exact test and the Kruskal-Wallis test, respectively, using SPSS software (IBM). Statistical significance was considered when $p < 0.05$.

Results

Cell viability in the presence of the $Ti_{40}Cu_{38}Zr_{10}Pd_{12}$ alloy

The potential effect of the $Ti_{40}Cu_{38}Zr_{10}Pd_{12}$ metallic glass on preosteoblast cultures was analyzed using direct and indirect studies at the same time. Gluing the alloy disk to a coverslip allowed us to study the cells that were adhered to the surface of the disk (direct studies) and the cells that were adhered to the coverslip, which, although were not in close contact with the disk, were exposed to alloy corrosion and thus to ions released from the alloy to the culture medium (indirect studies). Preliminary results indicated that the silicone used to glue the alloy disks to the coverslips did not affect cell viability (data not shown).

The number of cells with esterase activity (live cells) was superior to 94 % in all cases (Fig. 1) and no significant differences were found when comparing direct cultures, indirect cultures and control cultures (in absence of the alloy).

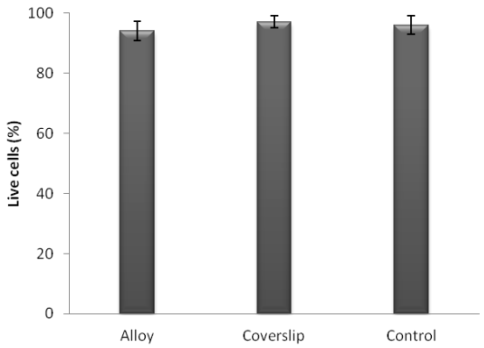

Fig. 1 Mean percentage of live cells (with esterase activity) adhered on the surface of the $Ti_{40}Cu_{38}Zr_{10}Pd_{12}$ alloy, on the coverslip and in the control culture.

Cell morphology and adhesion to the $Ti_{40}Cu_{38}Zr_{10}Pd_{12}$ alloy

SEM analysis of preosteoblasts grown in the presence or absence of the alloy showed that, in all cases, cells presented a flattened polygonal morphology with cytoplasmic extensions in different directions (Fig. 2). Moreover, cells established contacts with

nearby cells through membrane prolongations, and most of the cells presented several nucleoli in their nucleus (Fig. 2b). Cells were randomly distributed on the alloy surface.

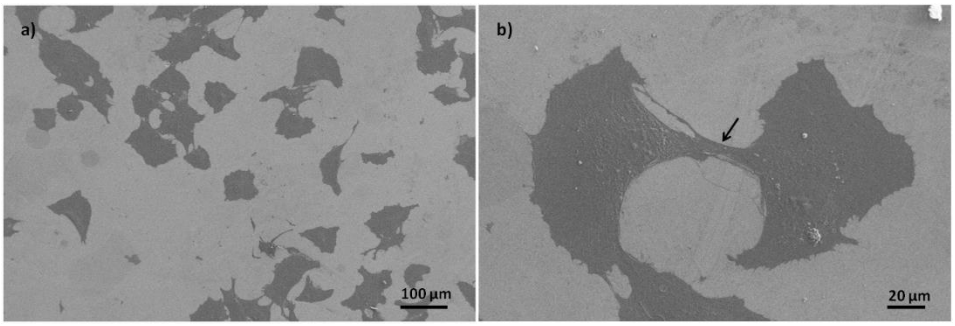

Fig. 2 SEM images of preosteoblasts adhered to the surface of the alloy disk (a, b). Different polygonal morphologies can be seen (a); contact between cells (arrow) can be observed (b).

Immunofluorescence analysis of focal contacts and stress fibres showed that preosteoblasts were completely adhered to the alloy surface or to the coverslip (Fig. 3) and were able to establish focal contacts with both surfaces. Stress fibres were well defined, some of them crossing the totality of the cell and some of them ending clearly in a focal contact. Stress fibres were found either in a parallel orientation (Fig. 3b) or without a defined orientation.

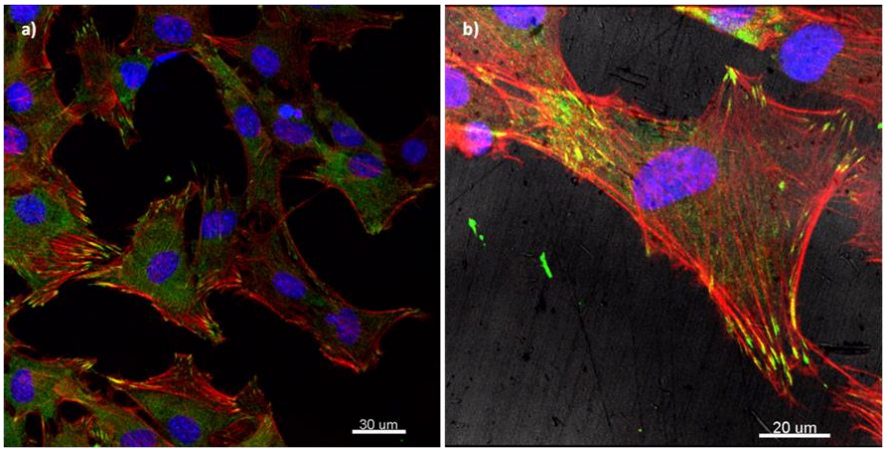

Fig. 3 Cells adhered to the surface of the alloy (a,b). Stress fibres (actin; red), focal contacts (vinculin; green) and nuclei (DNA; blue) can be observed. Stress fibres are capped by the focal contacts.

Wettability of the $Ti_{40}Cu_{38}Zr_{10}Pd_{12}$ alloy surface

The value of the contact angle of a MEMα drop with the surface of the alloy before preosteoblast culture was 78°.

Cell differentiation in the presence of the $Ti_{40}Cu_{38}Zr_{10}Pd_{12}$ alloy

To demonstrate that preosteoblasts can differentiate into osteoblasts in the presence of the alloy, the capacity to mineralize the ECM was analyzed both on the surface of the alloy and of the coverslip. After 7 days in culture, cell proliferation was evident and, in addition, a tendency of cells to orientate in a parallel disposition was observed. After 14 days, the first calcium phosphate nodules were detected (Fig. 4). These nodules progressively grew in size and number, and after 21 days a large number of nodules were observed in the culture dish. A similar ECM mineralization pattern was observed between cultures in the presence or absence of the alloy (Fig. 4).

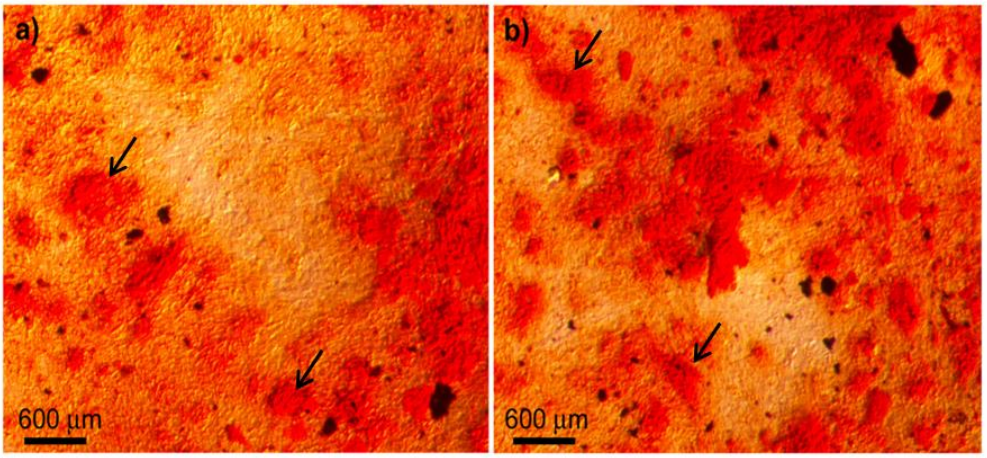

Fig. 4 Mineralization of the ECM by differentiated osteoblasts after 14 days in culture in the presence of the alloy (a), and without the alloy (b). Calcium nodules can be observed using Alizarin Red S staining (red) and some of them are indicated as an arrow.

Release of copper ions from the alloy into the culture medium

Quantification of copper ions released from the bulk metallic glass, using ICP-MS, indicated a time-dependent dissolution, with a progressive increase of copper concentration in the culture medium over time, but especially during the first 24 h. Thus, in the presence of cultured cells, the concentration of copper increased from 12 μg/L (t=0 h) to 32 μg/L (t= 24 h), and slowed down thereafter. After 7 days of culture in the presence of the alloy, copper concentration in the culture medium increased to 44 μg/L. It is important to note that no differences were observed in the concentration of copper ions in the presence or absence of cells (Fig. 5).

Quantification of ions released from the alloy at day 21 was done only in the absence of cells, because cells cannot be kept in culture for 21 days without medium replacement or without adding fresh medium. At this time point, the concentration of copper ions in the medium was 36 μg/L (Fig. 5).

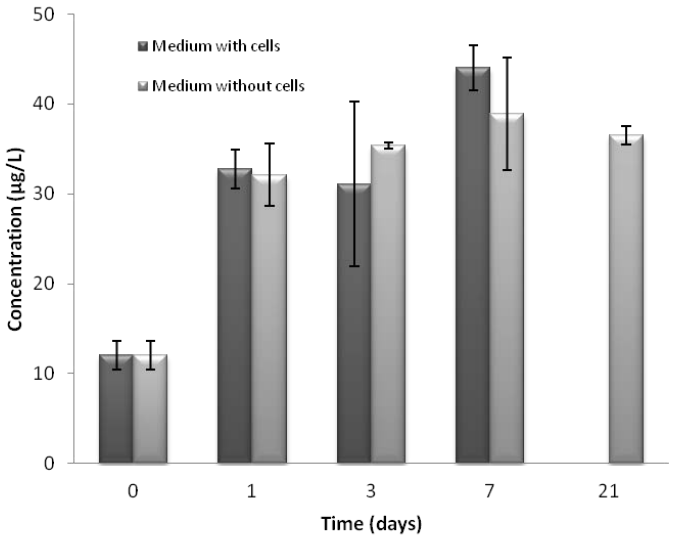

Fig. 5 Concentration of copper ions released from the alloy over time in culture medium with cells and without cells.

Cytotoxic effect of released copper ions

To analyze if copper ions released from the alloy into the culture medium could have a cytotoxic effect, we analyzed the viability of preosteoblasts cultured during 7 days in the presence of the alloy without changing the medium. Preosteoblast proliferated in culture, reaching a confluent monolayer where more than 94 % of the cells were alive. No differences were detected between preosteoblasts grown on top of the alloy (direct study) or onto coverslip (indirect study).

Further, preosteoblasts were cultured during 3 days without the alloy disk, but using culture medium that had been incubated with an alloy disk during 21 days. Cells were seeded in a 35 mm culture dish using this medium and adding fresh medium up to 2 mL. After 3 days, the maximum concentration of copper in the cell culture medium was 68 μg/L and 97 % of the cells were alive.

Induction of inflammatory cytokine secretion by macrophages in contact with the alloy

To find out whether the metallic alloy activates the secretion of inflammatory cytokines, alloy disks were added to macrophage cultures. Results of CBA showed that the presence of the alloy did not activate the secretion of TNFα, IL-6 or IL-1β in macrophages. However, when macrophages were exposed to LPS (positive control), an increase in the concentration of the three cytokines was detected in the culture medium. At 24 h the concentration of the three cytokines analyzed was significantly higher in the medium of the positive control when compared to that of the alloy (Fig. 6).

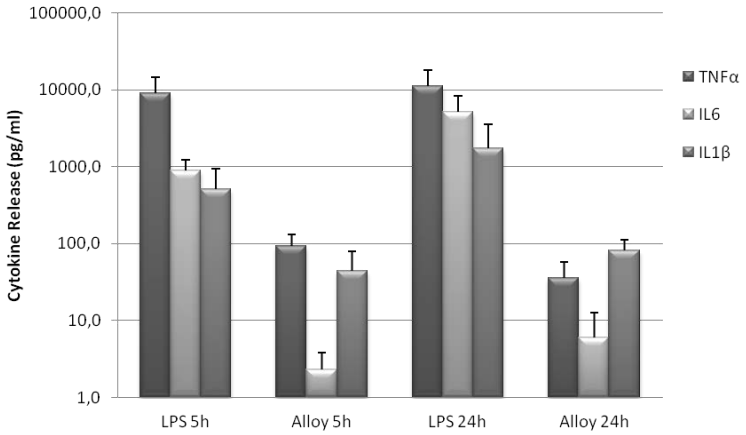

Fig. 6 Logarithmic representation of cytokine release. Secretion was analyzed by the CBA test at 5 and 24 h of culture. LPS = positive control, Alloy = $Ti_{40}Cu_{38}Zr_{10}Pd_{12}$ metallic glass. Error bars indicate the standard deviation of the three replicas.

Discussion

The $Ti_{40}Cu_{38}Zr_{10}Pd_{12}$ BMG alloy is a promising candidate for orthopaedic implants because of its mechanical and other physicochemical properties, such as high hardness (compared to commercial Ti-6Al-4V), relatively low Young's modulus, and excellent corrosion behaviour in bodily fluids [25]. However, before being considered as a biomaterial it is necessary to demonstrate its safeness in biological conditions.

Cytotoxicity was evaluated by indirect and direct studies, in which mouse preosteoblasts were cultured in the presence of the alloy during 24 h. Interestingly, despite the 38 at% copper content in the alloy, no toxic effects were observed.

Moreover, cell morphology and cell adhesion capacity were not modified by the presence of the alloy or in cells growing onto it. SEM images showed flattened preosteoblasts adhered to the alloy and immunofluorescence analysis confirmed that adhesion occurred through focal contacts connected between them by stress fibers. Focal contacts are cell structures where integrins present in the plasma membrane interact with proteins of the ECM and with cytosolic proteins. The cytosolic proteins involved in focal contacts, once activated, induce actin polymerization to form stress fibers and activation of the signalling pathways related to proliferation or differentiation. In particular, the establishment of focal contacts activates signalling pathways through the focal adhesion kinase, which subsequently triggers mitogen-activated protein kinases pathways involved in cell proliferation or differentiation [11]. Thus, focal contacts are necessary for cell adhesion but also for cell proliferation and differentiation. Our results are in agreement with different studies regarding cell adhesion, via focal contacts, on different surfaces such as chemically modified pure titanium surfaces [26] or Zr-based BMG surfaces [18].

The topography and wettability of the material surface are also critical issues for cell adhesion. In general, cell adhesion increases as the surface wettability increases, because materials in contact with body fluid or culture media adsorb proteins of the ECM that play an important role in the initiation of cell attachment [27]. Contact angle analysis showed that the surface of the $Ti_{40}Cu_{38}Zr_{10}Pd_{12}$ alloy is wettable, though slightly less than for conventional Ti6Al4V (around 60º for simulated body fluids [Ref Y]) and, hence, compatible with preosteoblasts adhesion. Besides, it has been described that micro- or

nano-roughness can modulate the biological response of cells in contact with the implant, and consequently cell adhesion [11]. In the present study, preosteoblasts adhered completely onto the mirror-like surface of the $Ti_{40}Cu_{38}Zr_{10}Pd_{12}$ alloy disks, which is in consonance with studies reporting that the same preosteoblast cell line prefer mirror-like rather than rough topographies to adhere [28]. As mentioned before, cell adhesion plays a decisive role in cell proliferation and differentiation. Cells must adhere to resume their cellular cycle but, when cells are strongly adhered with numerous and large focal adhesion plaques, they are more active in the expression of differentiation markers than in proliferation [29]. The accumulation of calcium carbonate nodules in the ECM of the preosteoblast cultures grown onto the $Ti_{40}Cu_{38}Zr_{10}Pd_{12}$ alloy in fact indicates that cells have not only attached and proliferate, but that they are also able to differentiate, as demonstrated by the mineralization of the ECM, a characteristic behaviour of osteoblast cells.

One significant concern regarding the $Ti_{40}Cu_{38}Zr_{10}Pd_{12}$ alloy was its copper content (38%). Previous studies have considered copper as a toxic element that has to be avoided in biomedical applications [5,8]. It has been demonstrated that cells cannot live adhered onto pure copper disk or plates. Some authors have reported that cells undergo lysis or adopt a rounded appearance when exposed to pure copper materials [8], whilst others have reported that cells die after 3 h in culture by a non-apoptotic way [9]. Thus, according to these authors, the cytotoxic effect of copper is very fast. In the case of the $Ti_{40}Cu_{38}Zr_{10}Pd_{12}$ alloy presented here, cell viability studies clearly demonstrated that this alloy is not cytotoxic, as cells are viable even after 24 h in contact with the alloy. Further, when cells are cultured for up to 21 days in the presence of the alloy, they do not only remain viable but they are also able to differentiate into osteoblasts.

Nevertheless, the release of metal ions from an alloy can still induce toxicity and immunogenic reactions. Several studies have analyzed the cytotoxicity of different metal ions, and copper ions have been considered inductors of cell death. In particular, MC3T3-E1 preosteoblasts cultured in the presence of 0.049 μM CuCl or 0.2 μM $CuCl_2$ showed DNA fragmentation and cell death [30]. Although these levels are below the values encountered in our work, the MC3T3-E1 preosteoblasts were directly exposed to a solution containing the metal salts at the indicated concentrations, which is not exactly

comparable to a situation where cells are cultured onto a solid alloy that gradually releases copper ions to the medium. Moreover, the specific copper speciation that applies in each case might have an effect on the toxicity and immunogenic reactions. To confirm whether copper was released from the $Ti_{40}Cu_{38}Zr_{10}Pd_{12}$ alloy, we conducted a long term study during 21 days. As far as we know, there are not long-term studies on metal ions release from alloys and their effect on cell cultures. We observed a very fast release of copper ions into the culture medium during the first 24 h of culture, which then slowed down, reaching the highest concentration at 7 days. The dynamics of copper ions released was not modified by the presence or absence of cells in the cultures. The presence of released copper ions did not show any toxic effect, and even though the concentration of copper ions in the culture medium increased with time, the rates of cell death were not increased. Recently, it has been reported that the dissolution of copper when it is alloyed with Au is dose-dependent. For instance, the addition of 10 % Au to the copper plate reduces the dissolution of copper into the culture medium and the cell mortality [31]. It is possible that in the case of the $Ti_{40}Cu_{38}Zr_{10}Pd_{12}$ alloy, the other elements of the alloy could reduce copper ion dissolution, so that the amount of copper released is below the minimum necessary to induce cytotoxicity. On the other hand, it is important to point out that all experiments that we have conducted were performed in closed culture systems, where no medium replacement or addition takes place during the length of the experiment. However, in *in vivo* conditions, the concentration of copper ions near the implant would probably be lower than in a closed system, because human tissues are constantly irrigated and waste substances can be removed from the tissue and eliminated through urine. Therefore, in this situation, the chance of toxicity of a potential $Ti_{40}Cu_{38}Zr_{10}Pd_{12}$ implant would be very low. Nevertheless, *in vivo* studies with this alloy should be performed to completely rule out a toxic effect. If wear or corrosion of the implanted alloy did occur, then the release of copper ions could be much higher.

Up to now, we have demonstrated that $Ti_{40}Cu_{38}Zr_{10}Pd_{12}$ alloy is not cytotoxic for preosteoblasts exposed or grown onto this material for up to 21 days. However, even if a material is not cytotoxic, it can still trigger an immunogenic response. The biological response to corrosion products from alloys, such as metal ions and wear debris, can be responsible for the induction of an inflammatory reaction that could play an important

role in implant loosening [7]. For this reason, we decided to assess if the addition of a disk of $Ti_{40}Cu_{38}Zr_{10}Pd_{12}$ alloy in a culture of human macrophages would induce the secretion of inflammatory cytokines, as an indicator of an inflammatory response. The results obtained after an incubation of 5 and 24 h indicated that no significant amounts of inflammatory cytokines were secreted, in contrast with cytokine secretion in the presence of LPS (positive control). Basal levels of cytokine secretion in the negative control and in the alloy groups could be attributed to the addition of PMA to induce macrophage differentiation, as it has been described that THP-1 differentiation stimulates the secretion of proinflammatory cytokines [14]. Macrophages are activated when an inflammatory reaction takes place, resulting in the release of proinflammatory cytokines (IL-6, IL-1β and TNFα). The mechanisms by which particles or metal ions activate macrophages remain unclear. While some authors have proposed that particles have to be phagocyted by macrophages to activate cytokine secretion [32], others have suggested that phagocytosis is not necessary [13]. Studies on the inflammatory response caused by different metal ions and particles have been reported. For instance, it is known that Pd(II), Au(III) and Ni(II) do not induce secretion of inflammatory cytokines by macrophages without previous LPS activation [15]. However, NiCr alloy induces an increase of proinflammatory cytokine expression by oral keratinocyte cells, due to the release of Ni ions [16]. Therefore, inflammatory response activation seems to depend on the particle and ion concentration, and also on the cell type used. This is the first time, to the best of our knowledge, that the effect of copper ions release from bulk metallic alloys in inflammatory response has been analyzed. Taking together the values of copper ions released from the $Ti_{40}Cu_{38}Zr_{10}Pd_{12}$ alloy after 24 h in culture (59 ng) and the volume of medium used to assess cytokine secretion (200 μl), it can be assumed that a concentration of 295 μg/L copper ions does not activate an inflammation response.

Conclusions

In conclusion, the $Ti_{40}Cu_{38}Zr_{10}Pd_{12}$ alloy, with optimal mechanical properties, could be considered as a biomaterial because it is not cytotoxic for preosteoblasts cultured in its presence for up to 21 days, it allows preosteoblasts to adhere completely to its mirror-like surface and to differentiate into osteoblasts under the appropriate culture conditions, and it does not induce an inflammatory response. Therefore, this biomaterial is a potential material to be used for the construction of different sorts of implants. However, *in vitro* studies should be complemented with *in vivo* studies to discard any potential negative effects for the body before this material is used for biomedical purposes.

Acknowledgements

This work has been partially financed by the Spanish Ministerio de Ciencia e Innovación (TEC2011-29140-C03-03), the Generalitat de Catalunya (2009-SGR-282), the FP7-PEOPLE-2010-ITN-264635 (BioTiNet). A.B. was supported by a predoctoral grant from the Universitat Autònoma de Barcelona. M.D.B. was partially supported by an ICREA ACADEMIA award.

References

[1] M Geetha, AK Singh, R Asokamani, AK Gogia. Ti based biomaterials, the ultimate choice for orthopaedic implants – A review. Prog Mater Sci. 2009;54:397-425.

[2] MF Ashby, AL Greer. Metallic glasses as structural materials. Scr Mater. 2006;54:321-6.

[3] H Chang, Y Wang. Cell responses to surface and architecture of tissue engineering scaffolds. In: D Eberli, editor. Regenerative Medicine and Tissue Engineering—Cells and Biomaterials. Rijeka, Croatia: InTech; 2011. pp. 569-88.

[4] JC Wataha, CT Hanks, Z Sun. Effect of cell line on in vitro metal ion cytotoxicity. Dent Mater. 1994;10:156-61.

[5] A Yamamoto, R Honma, M Sumita. Cytotoxicity evaluation of 43 metal salts using murine fibroblasts and osteoblastic cells. J Biomed Mater Res. 1998;39:331-40.

[6] ME Percy, TPA Kruck, AI Pogue, WJ Lukiw. Towards the prevention of potential aluminum toxic effects and an effective treatment for Alzheimer's disease. J Inorg Biochem. 2011;105:1505-12.

[7] A Pizzoferrato, E Cenni, G Ciapetti, D Granchi, L Savarino, S Stea. Inflammatory response to metals and ceramics. In: R Barbucci, editor. Integrated Biomaterials Science. Italy; 2002. pp. 735-91.

[8] H Prigent, P Pellen-Mussi, G Cathelineau, M Bonnaure-Mallet. Evaluation of the biocompatibility of titanium-tantalum alloy versus titanium. J Biomed Mater Res. 1998;39:200-6.

[9] T Yamazaki, A Yamazaki, Y Hibino, SA Chowdhury, Y Yokote, Y Kanda, S Kunii, H Sakagami, H Nakajima, J Shimada. Biological impact of contact with metals on cells. In Vivo. 2006;20:605-11.

[10] JP Thyssen. Metal Allergy: A Review on Exposures, Penetration, Genetics, Prevalence, and Clinical Implications. Chem Res Toxicol. 2009;23:309.

[11] L Bacakova, E Filova, M Parizek, T Ruml, V Svorcik. Modulation of cell adhesion, proliferation and differentiation on materials designed for body implants. Biotechnol Adv. 2011;29:739-67.

[12] JR Popp, KE Laflin, BJ Love, AS Goldstein. In vitro evaluation of osteoblastic differentiation on amorphous calcium phosphate-decorated poly(lactic-co-glycolic acid) scaffolds. J Tissue Eng Regen Med. 2011;5:780-9.

[13] Y Nakashima, DH Sun, MC Trindade, WJ Maloney, SB Goodman, DJ Schurman, RL Smith. Signaling pathways for tumor necrosis factor-alpha and interleukin-6 expression in human macrophages exposed to titanium-alloy particulate debris in vitro. J Bone Joint Surg Am. 1999;81:603-15.

[14] G Vallés, P González-Melendi, JL González-Carrasco, L Saldaña, E Sánchez-Sabaté, L Munuera, N Vilaboa. Differential inflammatory macrophage response to rutile and titanium particles. Biomaterials. 2006;27:5199-211.

[15] JC Wataha, JB Lewis, KR Volkmann, PE Lockwood, RLW Messer, S Bouillaguet. Sublethal concentrations of Au (III), Pd (II), and Ni(II) differentially alter inflammatory cytokine secretion from activated monocytes. J Biomed Mater Res B. 2004;69B:11-7.

[16] EL McGinley, GJ Fleming, GP Moran. Development of a discriminatory biocompatibility testing model for non-precious dental casting alloys. Dent Mater. 2011;27:1295-306.

[17] L Li, JC Wataha, C Cate, H Zhang, D DiJulio, WO Chung. Ni(II) alters the NFkB signaling pathway in monocytic cells. J Biomed Mater Res B. 2012;100B:934-9.

[18] L Huang, Z Cao, HM Meyer, PK Liaw, E Garlea, JR Dunlap, T Zhang, W He. Responses of bone-forming cells on pre-immersed Zr-based bulk metallic glasses: Effects of composition and roughness. Acta Biomater. 2011;7:395-405.

[19] YB Wang, YF Zheng, SC Wei, M Li. In vitro study on Zr-based bulk metallic glasses as potential biomaterials. J Biomed Mater Res B. 2011;96B:34-46.

[20] X Gu, Y Zheng, S Zhong, T Xi, J Wang, W Wang. Corrosion of, and cellular responses to Mg–Zn–Ca bulk metallic glasses. Biomaterials. 2010;31:1093-103.

[21] S González, E Pellicer, J Fornell, A Blanquer, L Barrios, E Ibáñez, P Solsona, S Suriñach, MD Baró, C Nogués, J Sort. Improved mechanical performance and delayed corrosion phenomena in biodegradable Mg–Zn–Ca alloys through Pd-alloying. J Mech Behav Biomed Mater. 2012;6:53-62.

[22] E Pellicer, S Gonzalez, A Blanquer, S Surinach, MD Baro, L Barrios, E Ibanez, C Nogues, J Sort. On the biodegradability, mechanical behavior, and cytocompatibility of amorphous Mg72 Zn23 Ca5 and crystalline Mg70 Zn23 Ca5 Pd2 alloys as temporary implant materials. J Biomed Mater Res A. 2013;101:502-17.

[23] N Shimojo, C Kondo, K Yamashita, T Hoshino, T Hayakawa. Cytotoxicity analysis of a novel titanium alloy in vitro: adhesion, spreading, and proliferation of human gingival fibroblasts. Biomed Mater Eng. 2007;17:127-35.

[24] JJ Oak. Characterization of surface properties, osteoblast cell culture in vitro and processing with flow-viscosity of Ni-free Ti-based bulk metallic glass for biomaterials. J Biomech Sci Eng. 2009;4:384.

[25] J Fornell, N Van Steenberge, A Varea, E Rossinyol, E Pellicer, S Suriñach, MD Baró, J Sort. Enhanced mechanical properties and in vitro corrosion behavior of amorphous and devitrified Ti40Zr10Cu38Pd12 metallic glass. J Mech Behav Biomed Mater. 2011;4:1709-17.

[26] B Finke, F Luethen, K Schroeder, PD Mueller, C Bergemann, M Frant, A Ohl, BJ Nebe. The effect of positively charged plasma polymerization on initial osteoblastic focal adhesion on titanium surfaces. Biomaterials. 2007;28:4521-34.

[27] J Wei, T Igarashi, N Okumori, T Igarashi, T Maetani, B Liu, M Yoshinari. Influence of surface wettability on competitive protein adsorption and initial attachment of osteoblasts. Biomed Mater. 2009;4:045002.

[28] NR Washburn, KM Yamada, CG Simon Jr., SB Kennedy, EJ Amis. High-throughput investigation of osteoblast response to polymer crystallinity: influence of nanometer-scale roughness on proliferation. Biomaterials. 2004;25:1215-24.

[29] L Bacakova, V Svorcik, D Kimura. Cell colonization control by physical and chemical modification of materials. Cell Growth Processes: New Research. 2008:5-56.

[30] RG Contreras, JR Vilchis, H Sakagami, Y Nakamura, Y Nakamura, Y Hibino, H Nakajima, J Shimada. Type of cell death induced by seven metals in cultured mouse osteoblastic cells. In Vivo. 2010;24:507-12.

[31] T Yamazaki, M Kobayashi, K Hirano, H Onuki, J Shimada, A Yamazaki, Y Hibino, H Nakajima, Y Yokote, S Takemoto, Y Oda, H Sakagami. Protection against copper-induced cytotoxicity by inclusion of gold. In Vivo. 2012;26:651-6.

[32] TA Blaine, PF Pollice, RN Rosier, PR Reynolds, JE Puzas, RJ O'Keefe. Modulation of the production of cytokines in titanium-stimulated human peripheral blood monocytes by pharmacological agents. The role of cAMP-mediated signaling mechanisms. J Bone Joint Surg Am. 1997;79:1519-28.

3.2. Effect of surface modifications of $Ti_{40}Zr_{10}Cu_{38}Pd_{12}$ bulk metallic glass and Ti-6Al-4V alloy on human osteoblasts biocompatibility

Effect of Surface Modifications of $Ti_{40}Zr_{10}Cu_{38}Pd_{12}$ Bulk Metallic Glass and Ti-6Al-4V Alloy on Human Osteoblasts Biocompatibility

Andreu Blanquer[1], Anna Hynowska[2], Carme Nogués[1], Elena Ibáñez[1], Jordi Sort[2,3], Maria Dolors Baró[2], Berna Özkale[4], Salvador Pané[4], Eva Pellicer[2], Leonardo Barrios[1]

[1] Departament de Biologia Cel·lular, Fisiologia i Immunologia, Universitat Autònoma de Barcelona, Edifici Cc, Bellaterra, Spain

[2] Departament de Física, Universitat Autònoma de Barcelona, Edifici Cc, Bellaterra, Spain

[3] Institució Catalana de Recerca i Estudis Avançats, Spain

[4] Multi-Scale Robotics Lab, Institute of Robotics and Intelligent Systems, ETH Zurich, Zurich, Switzerland

Abstract

The use of biocompatible materials, including bulk metallic glasses (BMGs), for tissue regeneration and transplantation is increasing. The good mechanical and corrosion properties of $Ti_{40}Zr_{10}Cu_{38}Pd_{12}$ BMG and its previously described biocompatibility makes it a potential candidate for medical applications. However, it is known that surface properties like topography might play an important role in regulating cell adhesion, proliferation and differentiation. Thus, in the present study, $Ti_{40}Zr_{10}Cu_{38}Pd_{12}$ BMG and Ti6-Al-4V alloy were surface-modified electrochemically (nanomesh) or physically (microscratched) to investigate the effect of material topography on human osteoblasts cells (Saos-2) adhesion, proliferation and differentiation. For comparative purposes, the effect of mirror-like polished surfaces was also studied. Electrochemical treatments led to a highly interconnected hierarchical porous structure rich in oxides, which have been described to improve corrosion resistance, whereas microscratched surfaces showed a groove pattern with parallel trenches. Cell viability was higher than 96% for the three topographies tested and for both alloy compositions. In all cases, cells were able to adhere, proliferate and differentiate on the alloys, hence indicating that surface topography plays a minor role on these processes, although a clear cell orientation was observed on microscratched surfaces. Overall, our results provide further evidence that $Ti_{40}Zr_{10}Cu_{38}Pd_{12}$ BMG is an excellent candidate, in the present two topographies, for bone repair purposes.

Introduction

The use of biocompatible materials for tissue regeneration, tissue engineering and transplantation has increased in recent years. Among different types of biomaterials, metallic alloys are preferred for orthopaedic applications because of their excellent mechanical and physical properties, such as a relatively high elasticity (low Young's modulus) and hardness. Metallic biomaterials used as permanent surgical implants can be classified into three categories according to their composition: stainless steel, cobalt-chromium and titanium-based alloys [1,2]. The closer the elasticity of the metallic alloy is to that of the bone, the lower is the probability of implant loosening by the stress shielding effect [1]. Ti-based alloys are the most used in medicine for long-term bone implants because their Young's moduli (55 to 110 GPa) are closer to that of the cortical bone (4 to 30 GPa) in comparison with chromium-cobalt alloys (240 GPa) and stainless steel (210 GPa). Ti-based alloys are used to manufacture hip and knee joints or screws and pins suitable for orthopaedic implants. Among them, Ti-6Al-4V is widely used because of its good mechanical properties, although it has a high Young's modulus (110 GPa). During the last years, new alloys have been synthesized to improve the elastic properties. Bulk metallic glasses (BMG) are very promising due to their superior strength, relatively low Young's modulus, high elastic strain limit, excellent corrosion resistance and good wear resistance [3]. Nevertheless, before these new alloys can be applied, their possible toxicity and/or allergenic effects have to be studied. $Ti_{40}Zr_{10}$ $Cu_{38}Pd_{12}$ BMG has showed good mechanical and corrosion properties, it is not cytotoxic for mouse preosteoblasts cultured for 21 days in the presence of the alloy and it does not induce an inflammatory response by macrophages, making it a potential candidate for orthopaedic implants [4]. In addition, several authors have reported that Cu is an efficient alloying element to develop antibacterial Ti-based alloys, presenting good results against *Salmonella enteritidis* and *Salmonella typhimurium* [5,6].

Besides composition, surface topography of alloys can play an important role on bone integration, including cell adhesion, spreading, migration, proliferation and differentiation [7]. Surface topography can be classified by the scale of the irregularities (roughness) and by their distribution (morphology). According to the scale,

macroroughness (>100 μm), microroughness (1 μm -100 μm), submicron roughness (100 nm-1 μm) and nanoroughness (<100 nm) have been defined [8]. It has been described that microrough surfaces allow a better cell proliferation and differentiation than smooth surfaces [9,10]. Moreover, nanorough surfaces allow a better osseointegration and it is believed that irregularities smaller than 100 nm can mimic the nanoarchitecture of natural tissues [11,12]. According to the morphology, although there is not any classification, it has been reported that cells show different responses to different surface morphologies such as grooves [13], tubes [14], meshes [15] or columns [16].

In the present study, we have analyzed the biocompatibility of Ti-based alloys as a function of their surface topography. To alter the surface architecture of the alloys, two different approaches were employed: (a) electrochemical surface modification, in which a nanomesh surface is obtained; (b) physical surface modification, in which the surface becomes microscratched. Two alloys were investigated: $Ti_{40}Zr_{10}$ $Cu_{38}Pd_{12}$, previously reported by our group as a biocompatible material [4], and the commercially available Ti-6Al-4V. The biocompatibility of human osteosarcoma cells cultured on these alloys was assessed by evaluating the cytotoxicity, proliferation, morphology, adhesion, cytoskeleton distribution and differentiation.

Materials and Methods

Material synthesis

The master alloy $Ti_{40}Zr_{10}$ $Cu_{38}Pd_{12}$ (from now on TiZrCuPd) (at.%) was prepared by arc melting a mixture of the highly pure elements (>99,9%) under a Ti-gettered Ar atmosphere. Rods of 3 mm in diameter were obtained from the melt by Cu mold suction casting. Disks of approximately 500 □ m in thickness were cut from the as-prepared TiZrCuPd and from commercial Ti-6Al-4V (Alfa Aesar) rods, and carefully grinded with SiC paper (up to 4,000 grit), degreased with acetone and finally cleaned with distilled water in an ultrasonic bath.

Surface modification

For both compositions (TiZrCuPd and Ti-6Al-4V), two different surface treatments were applied: physical and electrochemical. The physical surface modification consisted of manually scratching mirror-like polished disks along one direction with 1,200 grit SiC paper. A linearly microscratched surface was obtained. The electrochemical surface modification consisted of polarizing the alloys in a 5 M NaOH solution at 25 °C. This was carried out in a one-compartment thermostatized three-electrode cell connected to a PGSTAT302N Autolab potentiostat/galvanostat (Ecochemie). An Ag| AgCl (3M KCl) and a Pt wire served as reference and counter electrodes, respectively. Single potentiodynamic polarization scans were run from –0.5 V to +2.0 V at 0.5 mV s^{-1}. A fraction of the disks was not subject to any special treatment (mirror-like finish).

Compositional, morphological and physicochemical characterization

The chemical composition of the electrochemically modified disks was studied by energy dispersive X-ray (EDX) spectroscopy on a Zeiss Merlin field-emission scanning electron microscope (FE-SEM) operated at 15 kV.

Surface roughness was determined by atomic force microscopy (AFM) using a Dual Scope TMC-26 system (Danish Micro Engineering) working in AC mode. A commercial silicon tip (50-100 KHz resonance frequency) was used to scan surface areas of 50 x 50

μm^2 in order to extract the peak-to-valley (PTV) distance and the root-mean-square (RMS) roughness values.

Cross-sections of electrochemically modified disks were obtained in a SEM equipped with a focused ion beam (FIB). A gallium ion source with currents in the range 300 pA – 1.5 nA was employed. Samples were sputtered with a thin layer of gold prior to FIB-cutting the area of interest in order to enhance sample conductivity and to prevent any drift or charging. A thin carbon coating was deposited during imaging prior to FIB cross-sectioning to provide smooth cross-sections.

The wettability of the surfaces resulting from the performed treatments was studied by sessile drop technique. A drop of 1.5 µl of Dulbecco's modified Eagle medium (DMEM; Invitrogen) was deposited onto the surface of the specimens using a microdispenser and the contact angle was determined with a Contact Angle Measuring System DSA 100 (Krüss) at room temperature (RT). Measurements were done in triplicate.

Cell culture

Osteoblast-like Saos-2 (ATCC, HTB-85) cells, derived from a primary human osteosarcoma, were cultured in DMEM with 10% foetal bovine serum (Gibco) under standard conditions (37°C and 5% CO_2).

Cell viability assay

Alloy disks were cleaned with absolute ethanol and glued onto glass coverslips with silicone (Bayer), introduced into a 4-multiwell culture plate and sterilized by UV light for at least 2 h. Once sterilized, 50,000 cells were seeded into each well and cultured for 24 h. Cell viability on disk surfaces was evaluated using the Live/Dead Viability/Cytotoxicity kit for mammalian cells (Invitrogen), according to the manufacturer's protocol. Images from different regions of the alloy disk and from the control culture (without disk) were captured using an Olympus IX71 inverted microscope equipped with epifluorescence. A minimum of 300 cells were analyzed per group.

Cell morphology analysis

After the cell viability assay, the same samples were prepared for observation in SEM. Cultured cells were rinsed twice in phosphate buffered saline (PBS), fixed in 4% paraformaldehyde (PFA, Sigma) in PBS for 45 min at RT and rinsed twice in PBS. Cell dehydration was performed in a series of ethanol (50%, 70%, 90% and twice 100%), 7 min each. Finally, samples were dried using hexamethyl disilazane (Electron Microscopy Sciences) for 15 min, mounted on special stubs and analysed using SEM.

Cell adhesion and actin cytoskeleton distribution analysis

Cell adhesion onto the alloy surface was analysed using an antibody against vinculin to determine the presence of focal contacts. At the same time, phalloidin was used to visualize actin filaments and their distribution, as reported previously [4]. The same cell culture protocol described for viability studies was employed, but after 24 h of culture the cells were fixed in 4 % PFA in PBS for 30 min at RT, permeabilized with 0.1 % Triton X-100 (Sigma) in PBS for 15 min and blocked for 25 min with 1 % bovine serum albumin (BSA; Sigma) in PBS at RT. Samples were then incubated with 2 μg/ml mouse anti-vinculin primary monoclonal-antibody (Chemicon, MAB3574) for 60 min at RT and washed with 1 % BSA-PBS. Then, samples were incubated with a mixture of 1.4 U/ml Alexa fluor 594-conjugated phalloidin (Invitrogen), 6 μg/ml Alexa fluor 488 goat anti-mouse IgG1 and Hoechst 33258 (both from Sigma) for 60 min at RT. Finally, samples were washed in 1 % BSA-PBS, air dried and mounted on specific bottom glass dishes (MatTek) using ProLong mounting solution (Life Technologies). Control analyses were performed in absence of the alloy. Sample evaluation was done with a confocal laser scanning microscope (CLSM, Olympus).

Cell proliferation assay

Saos-2 proliferation was determined at 72 h and 7 days using Alamar Blue (Invitrogen). A total amount of 250,000 cells were seeded into each well of a 4-multiwell plate containing the alloy disk. After 24 h, disks with adhered cells on the surface were transferred to a 96-multiwell plate and medium with 10 % of Alamar Blue was added into each well and incubated for 4 h at 37°C and 5% CO_2, protected from direct light. Then,

the supernatant was collected and the fluorescence was read using a Cary Eclipse fluorescence spectrophotometer (Agilent Technologies). Cells on the disk were incubated again with fresh medium, and the Alamar Blue analysis was repeated at 72 h and 7 days. All experiments were performed in triplicate. Negative controls without cells were run as well.

Cell differentiation assay

Differentiation of cells growing on the alloy was evaluated through the alkaline phosphatase (ALP) activity and the detection of calcium deposits, a sign of extracellular matrix (ECM) mineralization. A total amount of 500,000 cells were seeded into 35 mm culture dishes containing an alloy disk and cultured during 14 days, replacing the medium every 3-4 days. All experiments were done in triplicate.

After 14 days in culture, the alloy disk was transferred to an eppendorf tube and the cells were lysed, using CyQuant cell lysis buffer (Invitrogen), for 10 min and vortexed for 15 s. Cell lysates were centrifuged at 12,000 rpm for 4 min at 4°C and the supernatants were used to evaluate ALP activity by quantifying p-nitrophenol, produced by the hydrolysis of p-nitrophenyl phosphate (pNPP). Briefly, 25 µl of 1-step pNPP (ThermoScientific) was added to 25 µl of supernatant. After 30 min incubation at RT, 2M NaOH was added to stop the reaction. The absorbance was measured at 405 nm using a Nanodrop Spectophotometer (ThermoScientific). ALP activity was normalized to total protein content using the Micro BCA Protein Assay kit (ThermoScientific), according to the manufacturer's protocol.

Secreted calcium deposits were detected using Alizarin Red S staining. After 14 days in culture, cells were fixed in 4 % PFA in PBS for 30 min at RT. Then, cells were incubated with 2% Alizarin Red S (Sigma) for 30 min at RT. Finally, samples were washed with milliQ water and visualized using an Olympus IX71 inverted microscope.

Statistical analysis

Cell viability was analysed using the Fisher's exact test. Cell proliferation and cell differentiation were analysed using the Kruskal-Wallis test. Statistical significance was considered when $p < 0.05$.

Results

Samples characterization

The physicochemical properties of the surface resulting from the aforementioned treatments applied to TiZrCuPd and Ti-6Al-4V materials were studied by SEM, AFM and contact angle measurements. As expected, the mirror-like polished surfaces were smooth and did not show any relevant feature apart from some residual ultra-fine scratches caused by the polishing (Fig 1(a, b)). The grooves created during manual scratching of the surface with 1,200 grit SiC paper (microscratched) can be observed in Fig 1(c, d). Trenches run in parallel over the surface since polishing was conducted in only one direction. Finally, a highly interconnected hierarchical porous structure was observed on the TiZrCuPd surface following electrochemical treatment (nanomesh). The pore walls were very thin, of only a few nanometers in thickness (Fig 1(e, f)). The same porous structure was observed on Ti-6Al-4V surface (S1 Fig). During potentiodynamic polarization up to 2V, the sample undergoes severe oxidation revealing a nanomesh structure on the surface. A typical potentiodynamic polarization curve is shown in the supplementary data (S2 Fig). The thickness of this nanomesh layer was around 200 nm, as illustrated in the FIB-SEM cross-section displayed in Fig 2(a). Actually, a magnified detail reveals a two-layer structure; an upper highly porous layer and a more compact layer underneath. Below this 200 nm-thick layer, the alloy remains unaffected. The EDX spectrum of the electrochemically-treated surface is depicted in Fig 2(b). Chemical composition analysis revealed that the nanomesh is made of 27 at% Ti, 7 at% Zr, 21 at% Cu, 9 at% Pd and 36 at% O. This indicates that the network is rich in Ti and Cu oxides. Nevertheless, since the penetration of X-rays in EDX is of the order of a few microns, the elemental composition is likely influenced by the underlying metallic alloy. These results indicate that the applied treatments render surfaces with very distinct features, ranging from micro- to nanoscales. Similar results were observed for Ti-6Al-4V. For this alloy, the nanomesh layer obtained after anodic treatment contains 57 at% Ti, 6 at% Al, 2 at% V and 35 at% O; hence it is mostly made of titanium oxides. Again, taking into account the small thickness of the porous layer and the penetration of X-rays, the percentages are likely influenced by the underlying alloy.

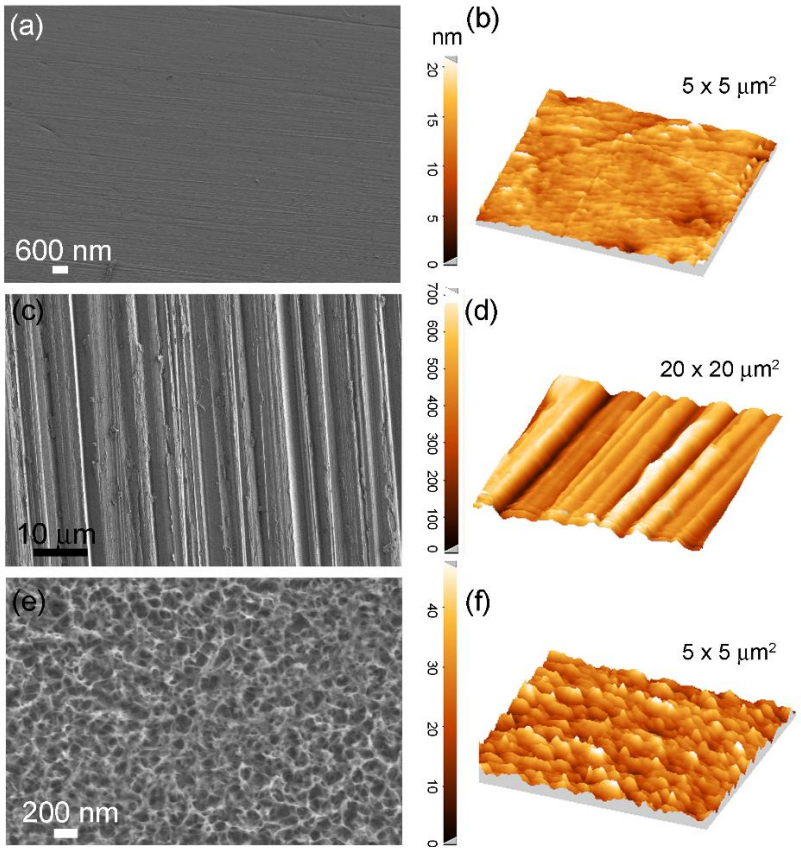

Fig 1. SEM (a, c, e) and AFM (b, d, f) images of mirror-like (a, b), micro-scracthed (c, d) and nanomesh (e, f) surfaces of TiZrCuPd alloy.

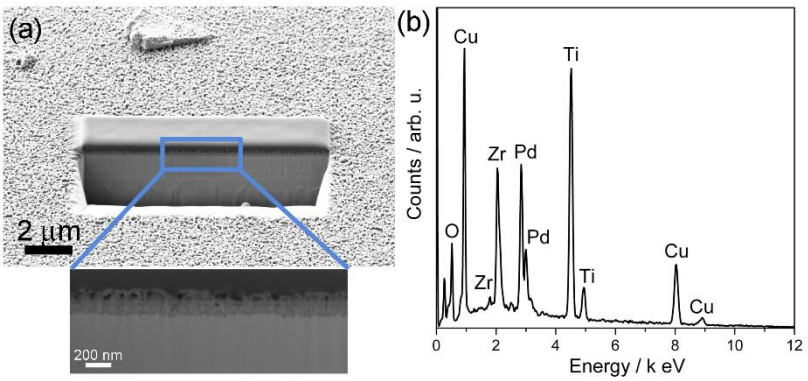

Fig 2. SEM-FIB cross-section (a) and EDX pattern (b) of a nanomesh layer formed by electrochemical treatment of TiZrCuPd alloy.

Table 1 lists the RMS roughness (R_q) and the PTV distance determined by AFM for the different surfaces. These values were obtained on scanned areas of 5 x 5 μm^2 in the case of the mirror-like finish and the nanomesh surfaces, and larger areas of 50 x 50 μm^2 in the case of the microscratched specimens (due to the higher lateral size of the trenches). As expected, the microscratched surfaces exhibit the highest R_q and PTV values, which are within the submicron scale domain (i.e., R_q values are well above 100 nm and PTV values approach 1 μm). On the contrary, both the mirror-like and the electrochemically-treated surfaces show R_q and PTV values falling within the nanoscale. The R_q and PTV values of the electrochemically-treated surfaces are slightly higher than those of the mirror-like surfaces, which is consistent with the existence of an oxide porous network. Therefore, the trends in R_q and PTV values go in the following direction for both alloys: microscratched > nanomesh > mirror-like.

Table 1. Root-mean-square (RMS) roughness (R_q) and peak-to-valley (PTV) distance determined by AFM, and contact angle values for the different surfaces.

	$Ti_{40}Zr_{10}Cu_{38}Pd_{12}$			Ti-6Al-4V		
	Mirror-like	Nanomesh	Microscratched	Mirror-like	Nanomesh	Microscratched
R_q (nm)	3	8	141	2	11	159
PTV (nm)	28	60	776	12	80	803
Contact angle (degree)	78	84	81	89	72	71

Concerning wettability properties, contact angles between 71° and 89° were measured regardless the surface condition. Table 1 lists the static contact angle measurements, showing that both the nanomeshed and microscratched Ti-6Al-4V surfaces exhibit the lowest contact angles.

Cell viability and cell proliferation

Cell viability was determined by analysing Saos-2 cells grown on the surface of TiZrCuPd and Ti-6Al-4V alloys. The number of live cells detected by Live/Dead kit was higher than 96% for the three topographies studied for both alloys (Fig 3).

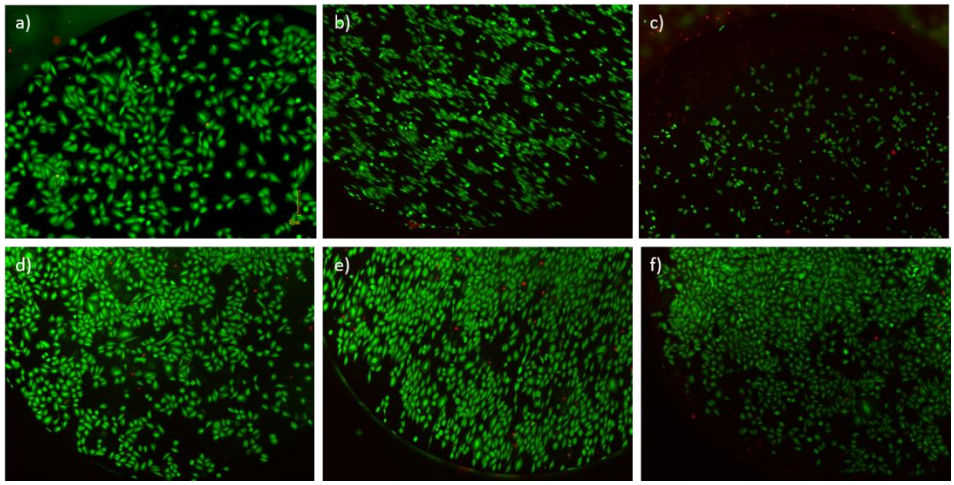

Fig 3. Viability of Saos-2 cells cultured onto TiZrCuPd (a-c) and Ti-6Al-4V (d-f) alloys: mirror-like (a, d), microscratched (b, e) and nanomesh (c, f). Live cells are stained in green whereas dead cells are stained in red.

Saos-2 cells proliferation was analysed at 24 h, 72 h and at 7 days of growth on the alloy disks for the three different surface topographies of the two compositions tested (Fig 4). For both alloys, the microscratched topography showed the highest cell numbers (Alamar blue intensities) at 7 days but the differences were not significant in relation to the other two topographies. Moreover, no significant differences between both alloys were observed for any topography.

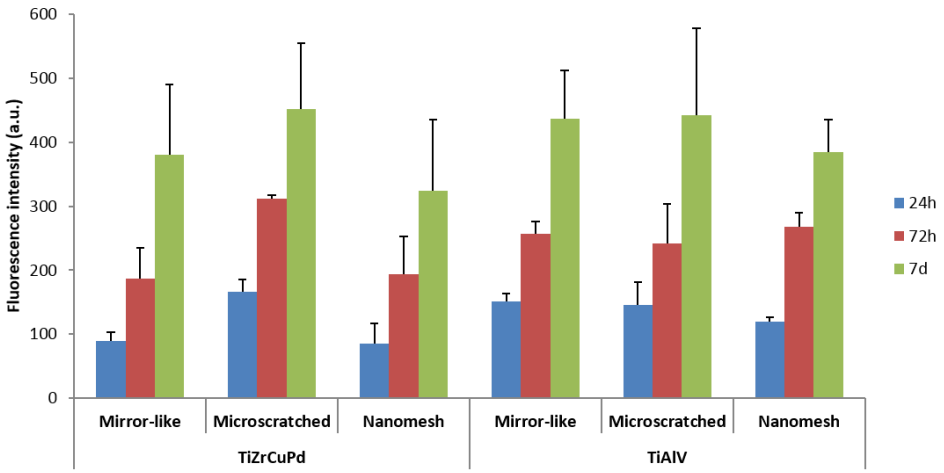

Fig 4. Saos-2 cells proliferation on TiZrCuPd and Ti-6Al-4V mirror-like, microscratched and nanomesh surfaces measured by Alamar Blue fluorescence at 24 h, 72 h and 7 days.

Cell adhesion and cell morphology

Cell adhesion and cell morphology were studied after 24 h of culture using CLSM and SEM. The presence and distribution of vinculin and actin microfilaments was analysed in cells growing on the surface of the alloys with different surface topographies (Fig 5). Clear focal adhesion plaques were observed on mirror-like and nanomesh surfaces, but no recognizable focal adhesion plaques were detected on microscratched surfaces. On the other hand, actin stress fibres were normally formed in cells growing on all surfaces, although for both alloys, the orientation of cells and the arrangement of actin bundles varied as a function of the alloy surface topography. Specifically, cells growing on the microscratched surfaces showed well-defined stress fibres and a more elongated morphology compared to cells growing on mirror-like and nanomesh surfaces. In addition, cells grown on nanomesh surfaces exhibited thin and long filopodia, not usually seen in cells grown on the other surfaces. In some cells, these cytoplasm projections crossed the grooves without touching the groove floor, whereas in some other cases, the filopodia crossed the grooves touching the floor (Fig 6).

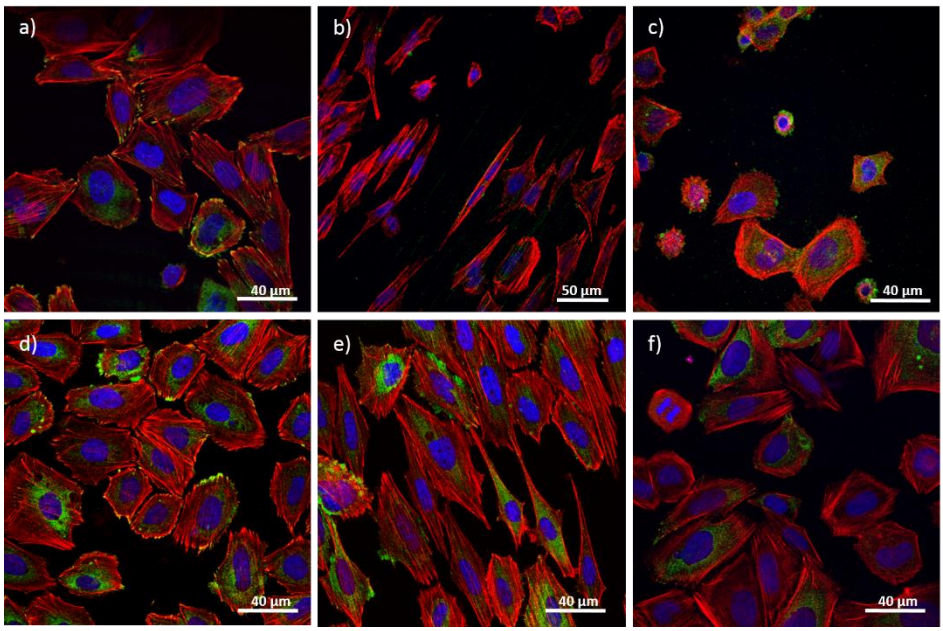

Fig 5. Saos-2 adhered onto the surface of TiZrCuPd (a-c) and Ti-6Al-4V (d-f) alloys: mirror-like (a, d), microscratched (b, e) and nanomesh (c, f). Stress fibers (red), focal contacts (green) and nuclei (blue) can be observed.

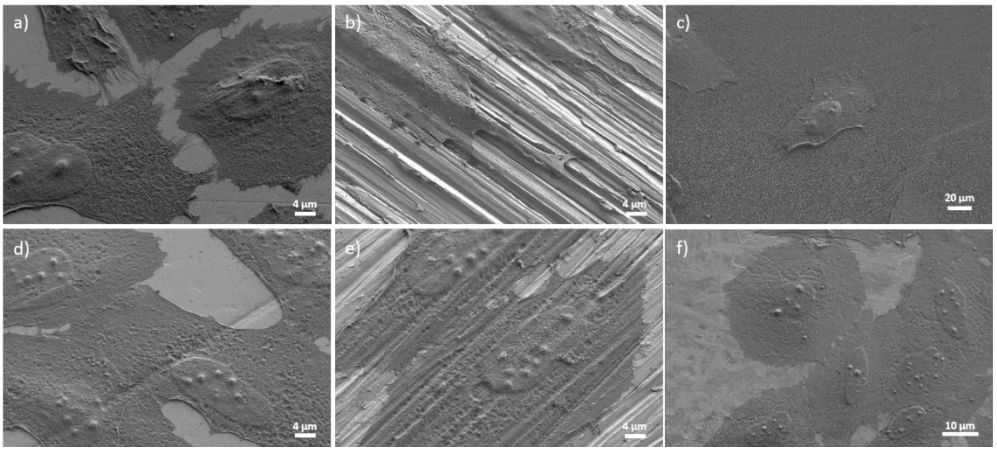

Fig 6. SEM images of Saos-2 cells grown on three different surface topographies of TiZrCuPd (a-c) and Ti-6Al-4V alloys (d-f): mirror-like (a, d), microscratched (b, e) and nanomesh (c, f).

Cell orientation

CLSM images of cells grown on the surface of the alloys were analyzed to determine the cytoskeleton distribution and the cell orientation. Cell orientation was measured by the angle formed between the major cell axis and the groove axis, with 0° indicating a perfect alignment and 45° a random orientation. Stress fibres were oriented along the longitudinal axis of the microscratched surface, but no defined orientation was observed in cells grown on mirror-like and nanomesh surfaces (Fig 5). Angular measurements revealed a strong orientation of cells grown on microscratched surfaces along the grooves with a mean angle of 15.9°. In contrast, cells grown on mirror-like or nanomesh surfaces showed a random orientation, with angles of 47° and 38°, respectively.

Cell differentiation and ECM mineralization

As a marker of osteoblasts differentiation, the increase of ALP activity after 7 and 14 days in culture was measured (Fig 7). No significant differences for ALP activity were observed, except for cells grown on Ti-6Al-4V microscratched surfaces when compared with cells grown on TiZrCuPd mirror-like surfaces after 7 days in culture. However, this difference disappeared after 14 days in culture, when no significant differences were observed for any alloy or surface topography.

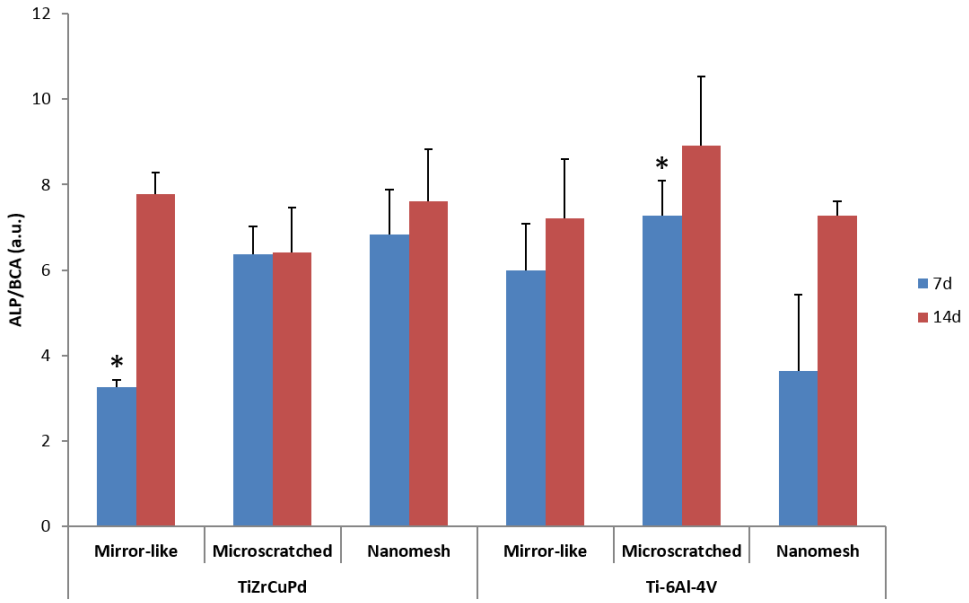

Fig 7. ALP activity of Saos-2 cells differentiated on three different surface topographies of TiZrCuPd and Ti-6Al-4V alloys, detected by p-nitrophenol absorbance normalized to total protein. Asterisks denote significant differences between the marked groups.

ECM mineralization after 14 days in culture, detected as calcium phosphate nodules using Alizarin Red S stain, showed calcium nodules and similar patterns of ECM mineralization for both alloys and all topographies (data not shown).

Discussion

Amorphous TiZrCuPd alloy shows high hardness, relatively low Young's modulus, moderate plasticity and good corrosion resistance [17], which constitute excellent characteristics for its use in orthopaedic implants. Regarding its biocompatibility, in a previous study we reported no cytotoxic effects on mouse MC3T3-E1 preosteoblasts cultured on top of TiZrCuPd disks up to 21 days, in spite of the release of Cu ions from the alloy into the culture medium [4]. Moreover, no inflammatory cytokines secretion was observed in macrophages grown in the presence of the alloy. In order to further demonstrate its safeness for medical applications, in vitro biocompatibility analyses have now been performed with human Saos-2 osteoblast-like cells, which show similarities with primary osteoblast cells and are the best choice for osteocompatibility studies [18]. Results of cell viability, adhesion and differentiation of human Saos-2 cells cultured on top of the mirror-like TiZrCuPd alloy were similar to those previously obtained with mouse MC3T3-E1 cells [4]. In addition, no differences in biocompatibility were detected in the present study between the TiZrCuPd alloy and the commercially available Ti-6Al-4V alloy, which was used as a control biomaterial due to its known biocompatibility and its current use in medical applications [1]. Altogether, these results show that mirror-like TiZrCuPd is not cytotoxic and allows cell adhesion and differentiation on flat surfaces. The results are in agreement with other studies of Ti-based and Zr-based alloys with mirror-like surfaces [19–21].

To survive and proliferate, osteoblasts need to adhere to a surface through focal contacts. In this sense, it is known that the surface topography of an alloy can influence cell adhesion, and thus cell proliferation and differentiation [7,22,23]. It has been reported that nanorough surfaces provide better cell proliferation and differentiation than smooth ones [11], even though other authors reported that better results are obtained with microrough surfaces [23]. A drawback for standardizing the knowledge on the importance of topography on cell behavior is the lack of consensus for surface topography characterization [24]. Because there are not many studies comparing the biological effect of different topographies of an alloy in the same cell line, we focused the present study on comparing the biological effect, in Saos-2 cells, of three different

topographies of the TiZrCuPd alloy: mirror-like, microscratched and nanomesh. As a control we used the commercial Ti-6Al-4V alloy, treated in the same fashion to obtain the same three topographies.

Electrochemical polarization and directional manual scratching was used to change the surface topography and the physicochemical properties of the alloys. In the present study, anodic oxidation generated an interconnected hierarchical porous structure by potentiodynamic polarization in 5M NaOH solution at 25 °C. Coral-like topographies have been reported to form upon soaking Ti in hot NaOH (70 °C) for 24h [25]. Under these conditions, chemical etching of Ti takes place. Here, a spongy morphology was developed by polarizing the material in NaOH at RT. A similar procedure has been previously applied to steels, by scanning the potential from +1.6 to +2.6 V in 50% NaOH at temperatures ranging from 30 °C to 70 °C [26]. EDX studies showed that the nanomesh layer of the TiZrCuPd alloy was rich in Ti and Cu oxides, and that of the Ti-6Al-4V alloy was rich in Ti oxides. Other authors have described that electrochemical anodization of Ti-based alloys produces TiO_2 structures on their surfaces, such as TiO_2 nanotubes [14] or a TiO_2 nanomesh [15]. This TiO_2 surface layer plays an important role acting as an inhibitor of metallic ions release and increasing the corrosion resistance of the alloy [15,27]. Moreover, TiO_2 has been considered biocompatible and an enhancer of the biological response [15,27,28]. Manual disk scratching created parallel trenches without changing the surface composition. R_q values of scratched surfaces were in the submicron microscale domain whereas those of the electrochemical-treated and mirror-like surfaces were at the nanoscale, showing higher values on the electrochemical-treated surfaces. Contact angle measurements of all surfaces were below 90°, which is the threshold for hydrophobicity. Therefore, the surfaces can be regarded as slightly polar. The value for the Ti-6Al-4V alloy with mirror-like finish is comparable to the previously reported contact angle for metal oxides (considering that a natural TiO_2 passivation layer forms on the surface) [27].

It has been described that when grown on Ti-6Al-4V microrough surfaces, primary human osteoblasts show a more differentiated phenotype than mesenchymal stem cells [23]. Moreover, Li et al. indicated that Ti and Zr BMG microroughness enhance MG63 osteosarcoma cells attachment, proliferation and differentiation [9]. It has also been

described that differentiation of human primary osteoblasts is enhanced by nanostructured superimposed onto micro-rough Ti-6Al-4V surfaces [29]. Similarly, Deng et al. concluded that nanostructured Ti is beneficial for MG63 osteosarcoma cells adhesion, viability and differentiation [11]. In contrast with all these previous reports, our study with Saos-2 cell line shows no significant differences in terms of cell viability, proliferation and differentiation among the three types of evaluated surfaces neither for the Ti-6Al-4V alloy, nor for the TiZrCuPd. The surface-modified-samples (microscratched and nanomesh) were as good as mirror-like ones for cell adhesion, proliferation and differentiation indicating that the three types of surfaces, can potentially be used in orthopaedic implants.

A previously described orientation effect has also observed on microscratched surfaces. It has been reported that cells are able to recognize the topography from few nanometers to hundred microns [24], and that cell morphology and orientation can change depending on topography. When topography presents specific patterns, such as grooves or ridges, cell orientation can be measured by the angle formed between the major cell axis and the groove axis. Some authors have described that cells can be aligned along defined substrates and, in most of the cases, orientation is obvious due to the formation of filopodia at opposite ends of the cell [30]. In our work, microscratched surfaces present grooves with a RMS of approximately 150 nm and the maximum PTV value is 789 nm. Measurements of cell orientation on microscratched surfaces showed a mean angle of 15.9°, indicating a good alignment with topography grooves. Indeed, most of the cells analysed had cytoplasm projections and actin microfilaments aligned along the grooves. In any case, taking into account our biocompatibility results, differences in cell orientation do not seem to influence Saos-2 osteoblast viability, proliferation or differentiation.

Conclusion

Our results show that $Ti_{40}Zr_{10}$ $Cu_{38}Pd_{12}$ BMG can be considered an excellent candidate to be used for orthopaedic implants. Moreover, we have demonstrated that electrochemical treatment generates a porous structure (nanomesh) rich in oxides on both Ti-6Al-4V and $Ti_{40}Zr_{10}$ $Cu_{38}Pd_{12}$ alloys, which improve corrosion resistance. Regarding biological studies, surface modifications do not show any impact on proliferation, adhesion and differentiation of human Saos-2 cells. A directional attachment of cells is observed on surfaces featuring parallel trenches created by manual scratching. The results provide an interesting contribution to the biological effect of surface modifications and their potential use to improve osseointegration.

Acknowledgements

This work has been partially financed by the Spanish Ministerio de Ciencia e Innovación (TEC2011-29140-C03-03 and MAT2014-57960-C03-3-R), the Generalitat de Catalunya (2014-SGR-524 and 2014-SGR-1015), and the FP7-PEOPLE-2010-ITN-264635 (BioTiNet). A.B. was supported by a predoctoral grant from the Universitat Autònoma de Barcelona. E.P. acknowledges the MINECO for the Ramón y Cajal contract (RYC-2012-10839).

References

[1] M. Geetha, A.K. Singh, R. Asokamani, A.K. Gogia, Ti based biomaterials, the ultimate choice for orthopaedic implants – A review, Prog. Mater. Sci. 54 (2009) 397–425.

[2] H. Hermawan, D. Ramdan, J.R. P. Djuansjah, Metals for Biomedical Applications, in: Biomed. Eng. - From Theory to Appl., InTech, 2011.

[3] M.F. Ashby, A.L. Greer, Metallic glasses as structural materials, Scr. Mater. 54 (2006) 321–326.

[4] A. Blanquer, E. Pellicer, A. Hynowska, L. Barrios, E. Ibáñez, M.D. Baró, et al., In vitro biocompatibility assessment of Ti40Cu38Zr10Pd12 bulk metallic glass., J. Mater. Sci. Mater. Med. 25 (2014) 163–72.

[5] L. Zhu, J. Elguindi, C. Rensing, S. Ravishankar, Antimicrobial activity of different copper alloy surfaces against copper resistant and sensitive Salmonella enterica, Food Microbiol. 30 (2012) 303–310.

[6] E. Zhang, L. Zheng, J. Liu, B. Bai, C. Liu, Influence of Cu content on the cell biocompatibility of Ti–Cu sintered alloys, Mater. Sci. Eng. C. 46 (2015) 148–157.

[7] A. Zareidoost, M. Yousefpour, B. Ghaseme, A. Amanzadeh, The relationship of surface roughness and cell response of chemical surface modification of titanium, J. Mater. Sci. Mater. Med. 23 (2012) 1479–1488.

[8] L. Bacakova, E. Filova, M. Parizek, T. Ruml, V. Svorcik, Modulation of cell adhesion, proliferation and differentiation on materials designed for body implants, Biotechnol. Adv. 29 (2011) 739–767.

[9] H.F. Li, Y.B. Wang, Y.F. Zheng, J.P. Lin, Osteoblast response on Ti- and Zr-based bulk metallic glass surfaces after sand blasting modification, J. Biomed. Mater. Res. - Part B Appl. Biomater. 100 B (2012) 1721–1728.

[10] D.B.S. Mendonça, P. a. Miguez, G. Mendonça, M. Yamauchi, F.J.L. Aragão, L.F. Cooper, Titanium surface topography affects collagen biosynthesis of adherent cells, Bone. 49 (2011) 463–472.

[11] Z. Deng, B. Yin, W. Li, J. Liu, J. Yang, T. Zheng, et al., Surface characteristics of and in vitro behavior of osteoblast-like cells on titanium with nanotopography prepared by high-energy shot peening, Int. J. Nanomedicine. 9 (2014) 5565–5573.

[12] M. Vandrovcová, L. Bačáková, Adhesion, growth and differentiation of osteoblasts on surface-modified materials developed for bone implants, Physiol. Res. 60 (2011) 403–417.

[13] F. Zhou, L. Yuan, H. Huang, H. Chen, Phenomenon of "contact guidance" on the surface with nano-micro-groove-like pattern and cell physiological effects, Chinese Sci. Bull. 54 (2009) 3200–3205.

[14] S. Minagar, J. Wang, C.C. Berndt, E.P. Ivanova, C. Wen, Cell response of anodized nanotubes on titanium and titanium alloys, J. Biomed. Mater. Res. - Part A. 101 A (2013) 2726–2739.

[15] W.E. Yang, H.H. Huang, Improving the biocompatibility of titanium surface through formation of a TiO2 nano-mesh layer, Thin Solid Films. 518 (2010) 7545–7550.

[16] M.J. Dalby, M.O. Riehle, D.S. Sutherland, H. Agheli, A.S.G. Curtis, Changes in fibroblast morphology in response to nano-columns produced by colloidal lithography, Biomaterials. 25 (2004) 5415–5422.

[17] J. Fornell, S. González, E. Pellicer, N. Van Steenberge, P. Pérez, S. Suriñach, et al., Deformation and fracture behavior of corrosion-resistant, potentially biocompatible, Ti40Zr10Cu38Pd12 bulk metallic glass, J. Alloys Compd. 536 (2012) S74–S77.

[18] E.M. Czekanska, M.J. Stoddart, R.G. Richards, J.S. Hayes, In search of an osteoblast cell model for in vitro research, Eur. Cells Mater. 24 (2012) 1–17.

[19] A. Hynowska, A. Blanquer, E. Pellicer, J. Fornell, S. Suriñach, M.D. Baró, et al., Novel Ti-Zr-Hf-Fe nanostructured alloy for biomedical applications, Materials (Basel). 6 (2013) 4930–4945.

[20] L. Huang, Y. Yokoyama, W. Wu, P.K. Liaw, S. Pang, A. Inoue, et al., Ni-free Zr-Cu-Al-Nb-Pd bulk metallic glasses with different Zr/Cu ratios for biomedical applications, J. Biomed. Mater. Res. - Part B Appl. Biomater. 100 B (2012) 1472–1482.

[21] A. Hynowska, A. Blanquer, E. Pellicer, J. Fornell, S. Suriñach, B. MD, et al., Nanostructured Ti-Zr-Pd-Si- (Nb) bulk metallic composites : Novel biocompatible materials with superior mechanical strength and elastic recovery, J. Biomed. Mater. Res. Part B Appl. Biomater. online (2014) 1–11.

[22] G.M. de Peppo, H. Agheli, C. Karlsson, K. Ekström, H. Brisby, M. Lennerås, et al., Osteogenic response of human mesenchymal stem cells to well-defined nanoscale topography in vitro., Int. J. Nanomedicine. 9 (2014) 2499–515.

[23] R. Olivares-Navarrete, S.L. Hyzy, M.E. Berg, J.M. Schneider, K. Hotchkiss, Z. Schwartz, et al., Osteoblast lineage cells can discriminate microscale topographic features on titanium-aluminum-vanadium surfaces., Ann. Biomed. Eng. 42 (2014) 2551–61.

[24] K. Anselme, L. Ploux, a Ponche, Cell/Material Interfaces: Influence of Surface Chemistry and Surface Topography on Cell Adhesion, J. Adhes. Sci. Technol. 24 (2010) 831–852.

[25] M. Pisarek, A. Roguska, L. Marcon, M. Andrzejczuk, Biomimetic and Electrodeposited Calcium-Phosphates Coatings on Ti - Formation, Surface Characterization, Biological Response, in: Biomed. Eng. - Tech. Appl. Med., InTech, 2012: pp. 20–22.

[26] T.D. Burleigh, P. Schmuki, S. Virtanen, Properties of the Nanoporous Anodic Oxide Electrochemically Grown on Steel in Hot 50% NaOH, J. Electrochem. Soc. 156 (2009) C45–C53.

[27] S.B. Patel, A. Hamlekhan, D. Royhman, A. Butt, J. Yuan, T. Shokuhfar, et al., Enhancing surface characteristics of Ti–6Al–4V for bio-implants using integrated anodization and thermal oxidation, J. Mater. Chem. B. 2 (2014) 3597.

[28] M. Vandrovcova, J. Hanus, M. Drabik, O. Kylian, H. Biederman, V. Lisa, et al., Effect of different surface nanoroughness of titanium dioxide films on the growth of human osteoblast-like MG63 cells., J. Biomed. Mater. Res. A. 100 (2012) 1016–32.

[29] R.A. Gittens, R. Olivares-Navarrete, T. McLachlan, Y. Cai, S.L. Hyzy, J.M. Schneider, et al., Differential responses of osteoblast lineage cells to nanotopographically-modified, microroughened titanium–aluminum–vanadium alloy surfaces, Biomaterials. 33 (2012) 8986–8994.

[30] A. Curtis, C. Wilkinson, Topographical control of cells, Biomaterials. 18 (1997) 1573–1583.

Supporting information

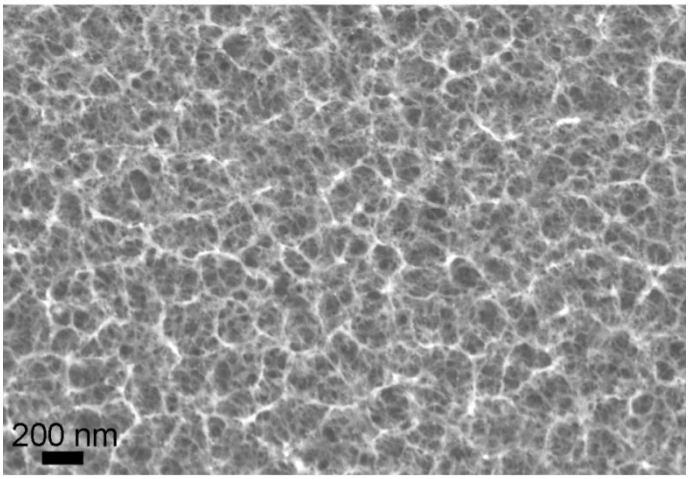

S1 Fig. SEM image of the nanomesh layer formed by electrochemical treatment on Ti-6Al-4V alloy.

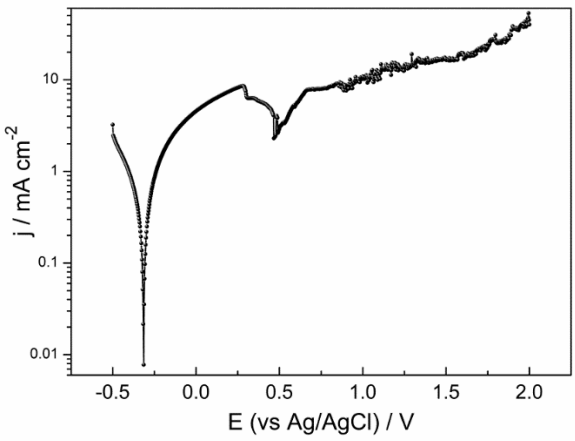

S2 Fig. Potentiodynamic polarization curve in logarithmic scale of $Ti_{40}Zr_{10}Cu_{38}Pd_{12}$ alloy in 5 M NaOH at 25 ºC (scan rate 0.5 mV s^{-1}).

3.3. Biocompatibility assessment of Ti-Zr-Pd-Si-(Nb) alloys with low Young's modulus, increased hardness and enhanced osteoblast differentiation for biomedical applications

Biocompatibility assessment of Ti-Zr-Pd-Si-(Nb) alloys with low Young's modulus, increased hardness and enhanced osteoblast differentiation for biomedical applications

Andreu Blanquer[1], Jana Musilkova[2], Leonardo Barrios[1], Elena Ibáñez[1], Marta Vandrovcova[2], Eva Pellicer[3], Jordi Sort[4], Lucie Bacakova[2], Carme Nogués[1]

[1]Departament de Biologia Cellular, Fisiologia i Immunologia, Universitat Autònoma de Barcelona, E-08193 Bellaterra, Spain

[2]Institute of Physiology, Academy of Sciences of the Czech Republic, 14220 Prague 4 Czech Republic

[3]Departament de Física, Universitat Autònoma de Barcelona, E-08193 Bellaterra, Spain

[4]Institució Catalana de Recerca i Estudis Avançats (ICREA) and Departament de Física, Universitat Autònoma de Barcelona, E-08193 Bellaterra, Spain

Abstract

Ti-based alloys have increased importance for biomedical applications due to their excellent properties. In particular, TiZrPdSi(Nb) alloys, with a predominant β-Ti phase microstructure, have good mechanical properties, such as a relatively low Young's modulus and high hardness. Biocompatibility of TiZrPdSi(Nb) alloys was assessed using human osteoblast-like cells. Cells grown on the alloys showed larger spreading areas and higher vinculin contents when compared with cells grown on glass control surfaces, indicating a better cell adhesion. Fibronectin and bovine serum albumin adsorption was higher on the alloy containing Nb than on the one lacking it. The number of cells growing on both alloys was also higher than on controls. Osteogenic differentiation was evaluated by quantifying the expression of four osteogenic genes (osteonectin, osteocalcin, osteopontin and bone sialoprotein), the presence of three osteogenic proteins (alkaline phosphatase, collagen I and osteocalcin) and the activity of alkaline phosphatase at different time-points. The different methodologies showed concordant results and demonstrated that TiZrPdSi and TiZrPdSiNb alloys enhance osteoblast differentiation, and that cells grown on TiZrPdSiNb alloy presented higher levels of some late osteogenic markers during the first week in culture. These results suggest that the TiZrPdSi(Nb) alloys can be considered as excellent candidates for orthopaedical uses.

Introduction

Titanium-based alloys have attracted much attention in the orthopedic field for bone repair purposes because of their better physico-chemical and mechanical properties compared with other metallic alloys and biocompatible materials. Different Ti-based alloys, with different combinations of non-toxic elements, are being investigated in order to improve their properties, including elasticity and hardness. Suitable elastic properties, meaning a not exceedingly high Young's modulus, are among the key factors to be taken into account when evaluating the potential use of an alloy in bone implants. Alloys with a Young's modulus close to that of the cortical bone (20-30 GPa) tend to be more suitable for orthopedic applications, as this reduces the "stress shielding effect", a biomechanical incompatibility that can result in implant loosening [1]. Hardness is also an important property, and current efforts are focused on trying to synthesize new alloys with reduced Young´s moduli, while maintaining or increasing their hardness. Nowadays, one of the most used Ti-based alloys is the commercially available Ti-6Al-4V, with a hardness of 5 GPa and a Young's modulus of 110 GPa, which is much higher than that of the cortical bone. Thus, new Ti-based alloys with higher elasticity (lower Young's modulus) and hardness, but maintaining other good properties such as low corrosion and wear resistance, are under development.

The physical, chemical and mechanical properties of an alloy can be readily modified by changing its composition (elements and percentage). But, because some elements have been described as cytotoxic, they should not be used for the synthesis of alloys for biomedical applications. The cytotoxicity of the most commonly used elements in implant alloys has been studied by many researchers, and, in 2012, Biesiekierski et al. published an extensive review on the biocompatibility, carcinogenicity, genotoxicity, mutagenicity, cytotoxicity, allergenicity and the proneness to corrosion of 27 transition metals [2]. On the one hand, Vanadium, Beryllium, Cadmium and Cobalt are considered cytotoxic elements, whereas Aluminum is known to have adverse effects and it seems to be involved in severe neurological diseases and to play a role in neurodegeneration [3,4]. All authors agree on the allergenic effect of Nickel [5,6], and some of them also consider Nickel ions to be cytotoxic and to have a potential carcinogenic effect. On the other

hand, Titanium, Zirconium, Tantalum, Niobium and Palladium are considered low cytotoxicity elements and, thus, they can be safely used to synthesize biocompatible medical alloys [7].

Regarding alloy biocompatibility, osseointegration is an important issue, and thus the interactions between cells and the alloy surface should carefully be analyzed. Topography, wettability and surface charge are parameters that can modulate cell response. In general, cell adhesion increases with surface hydrophilicity, and it is mediated through the recognition and adhesion to extracellular matrix molecules (collagen, fibronectin, laminin, etc.). Proteins from the serum are adsorbed onto alloy surfaces, facilitating the contact with the cell membrane receptors. Fibronectin, collagen and laminin are considered promoters of cell adhesion whereas proteins like albumin are considered inhibitors of cell adhesion. Thus, cell adhesion can be modulated depending on the affinity of different types of proteins for the alloy surface. Adhesion is mandatory for all anchorage-dependent cells, like osteoblasts, to resume the cell cycle and hence to allow cell proliferation[8]. Osteoblast adhesion to the implant material and consequent spreading is mediated by integrins, a family of adhesion proteins that act as receptors for the extracellular matrix proteins collagen, laminin or fibronectin. When integrins contact fibronectins, they cluster and trigger the formation of focal contacts together with other cytosolic proteins such as talin, vinculin and paxillin.

Adhesion, however, is not the only biological property that a biomaterial must permit. It should also allow osteoblast differentiation, that is, cells should be allowed to synthesize the proteins needed to produce and mineralize the extracellular matrix. Osteoblast differentiation in the bone is a continuous process that can be divided in three different stages: i) proliferation, ii) osteogenic proteins expression and secretion, and iii) mineralization of extracellular matrix [9]. During the osteogenic protein expression stage, several proteins can be detected *in vitro* at different time-points. For example, collagen I (COLI) and alkaline phosphatase (ALP) activity are considered early osteogenic markers, whereas osteocalcin (OC), bone sialoprotein (BSP), osteopontin (OPN) and osteonectin (ON) are considered late osteogenic markers. The study of the expression of specific osteogenic genes, and the detection of specific proteins at different time-points is therefore important to determine whether the alloy affects the differentiation patterns.

The microstructure, mechanical properties and short-term biological response of the TiZrPdSi(Nb) alloy were studied in a previous work by our group [10]. Microstructure consisted of a predominant β-Ti phase and additional phases in smaller volume fractions. In terms of mechanical properties, the $Ti_{45}Zr_{15}Pd_{30}Si_5Nb_5$ alloy exhibited lower Young's modulus and hardness (85 GPa and 10.4 GPa, respectively) than the $Ti_{45}Zr_{15}Pd_{35}Si_5$alloy (117 GPa and 14.2 GPa, respectively). Moreover, preliminary short-term biological tests at 24 h indicated high cell viability and complete osteoblast adhesion on both alloy surfaces. These previous results suggested that these alloys possess a great potential to be used as permanent implants for bone repair purposes.

In the present study, we aimed at deepening on the biocompatibility analysis by performing short- and medium-term studies with the two metallic $Ti_{45}Zr_{15}Pd_{35}Si_5$ and $Ti_{45}Zr_{15}Pd_{30}Si_5Nb_5$ alloys. First, we evaluated the capacity of both alloys to adsorb two proteins present in the serum: albumin and fibronectin. Second, we analyzed the initial adhesion response (cell spreading and vinculin quantification), proliferation over 7 days in culture and osteogenic differentiation of human osteoblast-like Saos-2 cells. Third, we quantified the expression of four osteogenic genes (ON, OC, BSP and OPN), the presence of three osteogenic proteins (ALP, COL I and OC) and the activity of ALP at different time-points to determine whether cell differentiation on both alloys followed the expected pattern.

Material and Methods

Alloy samples

Master alloys with composition $Ti_{45}Zr_{15}Pd_{35-x}Si_5Nb_x$ (where x=0 and 5 at. %) were prepared by arc melting a mixture of the highly pure elements (>99.99% wt %) under a Ti-gettered Ar atmosphere on a water-cooled Cu heart. Rods of 3 mm in diameter were obtained from the melt by suction casting into a Cu mould.

From now on, we will refer to$Ti_{45}Zr_{15}Pd_{35}Si_5$ as TiZrPdSi and to $Ti_{45}Zr_{15}Pd_{30}Si_5Nb_5$ as TiZrPdSiNb.

Contact angle measurements

To assess the wettability of the alloys surfaces, the contact angle of an aqueous drop (1.5 µl) of McCoy's culture medium (Sigma) supplemented with 10% foetal bovine serum (FBS; Gibco) and deposited onto the surface of the alloy was measured using a Contact Angle Measuring System DSA 100 (Krüss) at room temperature (RT). Wettability of the glass coverslip surface was used as a control.

Quantification of protein adsorption

To quantify the amount of protein adsorbed on the surface of the alloy, samples were submerged overnight at 4°C in a phosphate buffered solution (PBS; Sigma) containing 5 µg/ml of bovine serum albumin (Sigma) or fibronectin (Roche Diagnostics). After incubation, samples were washed thrice with PBS and non-specific binding sites were blocked by 1% Tween (Sigma) in PBS for 20 min at room temperature (RT). Then, samples were incubated with anti-albumin (Sigma) or anti-fibronectin (Sigma) antibodies (1:200) at RT for 1 h, washed thrice with PBS and incubated with HRP peroxidase-conjugated secondary antibody (1:1000) (Sigma) at RT for 1 h. Afterwards, samples were washed four times with PBS and transferred to a new plate where 2,2'-azino-bis(3-ethylbenzothiazoline-6-sulfonic acid) (ABTS) solution (0.1M NaOAc; 0.05 NaH_2PO_4; 21.9 mg/ml ABTS (Sigma) in ddH_2O at pH 5) and 30% H_2O_2 were added and incubated for 20 min at RT in agitation. Finally, supernatants were transferred to an ELISA plate

and read with a spectrophotometer at 405 nm (Synergy HT). Experiments were performed in triplicate and with negative controls without primary antibody.

Cell culture

Alloy disks were individually inserted into 24-well cell culture plates and 50,000 Saos-2 cells (European Collection of Cell Cultures, Salisbury) were seeded and cultured in McCoy's 5A medium supplemented with 10% FBS (Sebak GmbH) and gentamicin (40 µg/ml, LEK) under standard conditions (37°C and 5% CO_2). Cells grown directly on polystyrene wells and on glass coverslips were used as controls.

Spreading area measurement

The spreading area of the cells adhered onto the alloy (with or without Nb) and control (polystyrene and glass) surfaces was evaluated after 24 h of seeding. Cells were rinsed with PBS, fixed with 70% frozen ethanol at RT for 20 min, and stained with a combination of the cell membrane dye Texas Red C_2-maleimide (Thermo Fisher Scientific) and the nuclear dye Hoechst 33258 (Sigma) at RT for 1 h. Microphotographs of adhered cells were captured under an IX-50 microscope, equipped with a DP 70 digital camera (both from Olympus). The spreading area of each individual cell (a minimum of 215 cells/sample) was measured using the Atlas software (Tescan). Cells with intercellular contacts were excluded from the evaluation. Four independent samples were analysed for each alloy tested and for controls.

Vinculin immunodetection and actin staining

The presence of focal adhesion plaques by vinculin immunodetection was analysed after 3 days of cells growing on top of the alloys and glass coverslips. Cells were rinsed twice in PBS, fixed with 70% frozen ethanol for 20 min, incubated with 1% bovine serum albumin (BSA) in PBS containing 0.05% Triton X-100 (Sigma) for 20 min at RT, and treated with 1% Tween for 20 min. Then, cells were incubated with a mouse monoclonal anti-human vinculin primary antibody (Sigma) at 4°C, overnight. After rinsing twice in PBS, goat anti-mouse IgG secondary antibody conjugated with Alexa Fluor 488 (Thermo Fisher Scientific) was applied for 1 h at RT simultaneously with the nuclear dye Hoechst 33258 and phalloidin conjugated with TRITC (1:1000, Sigma). Images of different

regions of the samples were taken under both an IX-50 inverted fluorescence microscope (Olympus) and a laser scanning confocal microscope (Leica TCS SP2).To measure the fluorescence intensity, micrographs from each sample were taken with the same exposure time and analysed using Fluorescence Image Analyser software (ver. 1.1, 2013, available from http://alice.fbmi.cvut.cz/software/fia). A single colour plane threshold was set on each image to remove the non-protein area from the image data. The same threshold and colour plane settings were used for all images. Then the cumulative sum of all pixel intensities was evaluated and the background intensity of the negative staining control was subtracted. The total immunofluorescence intensity of the protein was normalized to the pixels evaluated.

Quantification of cell proliferation

Cell proliferation on metallic alloys and control surfaces was evaluated by counting the number of cells at different time-points. After 1, 3 and 7 days of cell seeding, cells were stained with the nuclear dye Hoechst #33258and randomly selected fields were photographed in order to quantify the number of nuclei (cells) on each sample. Three independent experiments were performed.

Quantitative real-time PCR (qPCR)

The qPCR was performed to determine the expression profile of four osteoblast genes expression. Saos-2 cells were grown for 7 and 14 days on the alloy and glass (control) surfaces. Total RNA was extracted from the cell cultures using Total RNA purification micro kit (Norgen Biotek) according to the manufacturer's protocol. The mRNA concentration was measured using the NanoPhotometer (Implen). Reverse transcription was performed on 100 ng of total RNA using the ProtoScript M-MuLV First Strand cDNA synthesis kit (New England BioLabs) according to manufacturer's protocol using a T Personal Thermocycler (Biometra). The mRNA levels were quantified using quantitative real time 5xHOT FIREPol Probe qPCR Mix Plus (ROX) (Solis BioDyne, Tartu, Estonia) and with TaqMan Gene Expression Assays (Thermo Fischer Scientific, Waltham, MA, USA) labelled with FAM reporter dye specific for human osteocalcin (OC; Hs01587814_g1), osteonectin (ON; Hs00234160_m1), osteopontin (OPN; Hs00959010_m1), bone sialoprotein (BSP; Hs00173720_m1) as target genes,and

glyceraldehyde 3-phosphate dehydrogenase (GAPDH; Hs02758991_g1) as a reference gene, in final reaction volume of 20 μl per well on a 96-well optical reaction plate using the ViiaTM 7 Real-time PCR System. Data are the mean of 4–5 experimental points from 2 independent experiments. Expression values were obtained from Ct numbers. The target gene levels are expressed as a relative value, the ratio of the target gene expression towards the reference ACTB gene. The relative gene expression was calculated as $2^{-\Delta Ct}$.

Osteogenic markers immunodetection

Quantification of osteogenic markers was performed by immunodetection of three different proteins involved in osteoblast differentiation: COL I, OC and ALP. Saos-2 cells were cultured during 7 days onto alloys and control glass coverslips. Cells were then fixed in 4% paraformaldehyde in PBS for 30 min at RT, permeabilised with 1% BSA in PBS containing 0.05% Triton X-100 for 20 min and treated with 1% Tween for 20 min at RT. Samples were then incubated overnight at 4ºC with primary antibodies: rabbit anti-osteocalcin (1:200; Peninsula Laboratories), mouse monoclonal anti-collagen I (1:200; Sigma) or mouse anti-ALP (Sigma). After being rinsed twice with PBS, cells were incubated for 1 h at RT with the secondary antibody Alexa Fluor 488-conjugated goat anti-rabbit (Thermo Fisher Scientific) or Alexa Fluor 488-conjugated goat anti-mouse (Thermo Fisher Scientific) diluted 1:400 in PBS together with the nuclear dye Hoechst 33258. Images from randomly selected regions were captured and fluorescence intensity was measured as previously described for vinculin immunodetection.

Quantification of ALP activity

Saos-2 cells differentiation on alloys and control surfaces was also studied measuring the ALP activity. Cells were cultured onto the samples during 7 and 14 days. Each sample was transferred to an Eppendorf tube and cells were lysed for 10 min in CyQuant cell lysis buffer (Invitrogen) and then vortexed for 10 sec. Cell lysates were centrifuged at 12,000 rpm for 4 min at 4°C, and supernatants were collected. ALP activity was determined by the hydrolysis of p-nitrophenyl phosphate (pNPP), which produces p-nitrophenol (pNP). Briefly, 25 μl of 1-step pNPP (Thermo Fisher Scientific) was added to 25 μl of supernatant. After 30 min incubation at RT, 2M NaOH was added to stop the reaction. The absorbance was measured at 405 nm using a spectrophotometer. ALP

activity was normalized to total protein content using Micro BCA Protein Assay kit (Thermo Fisher Scientific), according to the manufacturer's protocol.

Statistical analysis

The quantitative data is presented as mean ± SD (Standard Deviation). Statistical comparisons were performed using one-way analysis of variance (ANOVA) with Tukey-Kramer multiple comparison test for protein immunodetection and cell proliferation assays. The Kruskal-Wallis test with Dunn's multiple comparisons was used for protein adsorption, spreading area and ALP activity assays. Multiple comparison procedures were performed with ANOVA using the Student-Newman-Keuls mehthod for gene expression values. In all cases, the analysis was performed using GraphPad Prism (GraphPad software) and a value of $p<0.05$ was considered statistically significant.

Results

Wettability

The contact angle values were 57.6 ° for the TiZrPdSi alloy and 64.8 ° for the TiZrPdSiNb alloy, both slightly lower than the value for the glass coverslip used as control (78.6 °).

Albumin and fibronectin adsorption

Albumin was significantly more adsorbed on the TiZrPdSiNb alloy surface than in TiZrPdSi and control surfaces (Fig. 1a). The amount of protein adsorbed was similar on TiZrPdSi and glass surfaces, and significantly lower in polystyrene surface. A similar tendency was observed for fibronectin, with a significantly increased adsorption on TiZrPdSiNb surface.

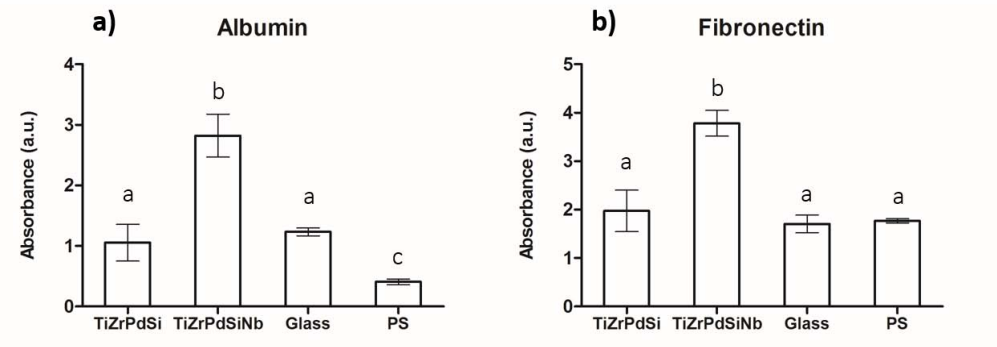

Figure 1. Albumin and fibronectin adsorption on the different sample surfaces measured by ELISA. PS: polystyrene. Different letters above the columns indicate significant differences ($p < 0.05$).

Cell spreading

Individual cell spreading areas of Saos-2 cells grown on tested alloys and controls were measured after 24 h. Osteoblasts adhered on all surfaces tested and no significant differences were found between cells growing on the two alloy compositions tested (TiZrPdSi 784 ± 27 and TiZrPdSiNb 734 ± 27 μm^2), and the polystyrene control (739 ± 31 μm^2). However, a significantly reduced spreading area was observed on cells grown on the glass coverslip (352 ± 15 μm^2) (Fig. 2).

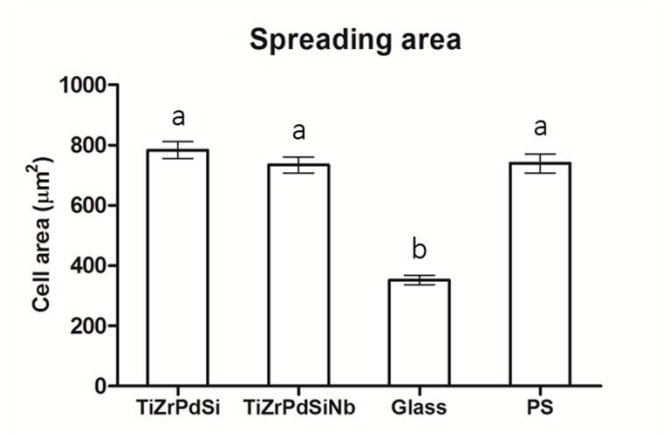

Figure 2. Mean spreading area of Saos-2 cells after 24h in culture on alloys and controls surfaces (glass and polystyrene, PS). Different letters above the columns indicate significant differences ($p < 0.05$).

Cell adhesion and vinculin immunodetection

Immunofluorescence detection of vinculin, a protein involved in focal contacts, and staining of actin filaments, the constituents of stress fibres, was next performed in order to further investigate osteoblasts adhesion on the sample surfaces. After 3 days in culture, Saos-2 cells presented diffuse free vinculin in the cytoplasm and defined spots of vinculin integrated in focal adhesion plaques that co-localized at the cell periphery with the ends of the stress fibres on all surfaces tested (Fig. 3). Well-defined stress fibres, some of them crossing the cell from end to end, were observed in all cases. Moreover, images of vinculin immunodetection were used to quantify the fluorescence intensity. Results indicated no significant differences in fluorescence intensity between the two alloys tested, but both showed significantly higher intensities than the glass coverslip control (Fig. 3d).

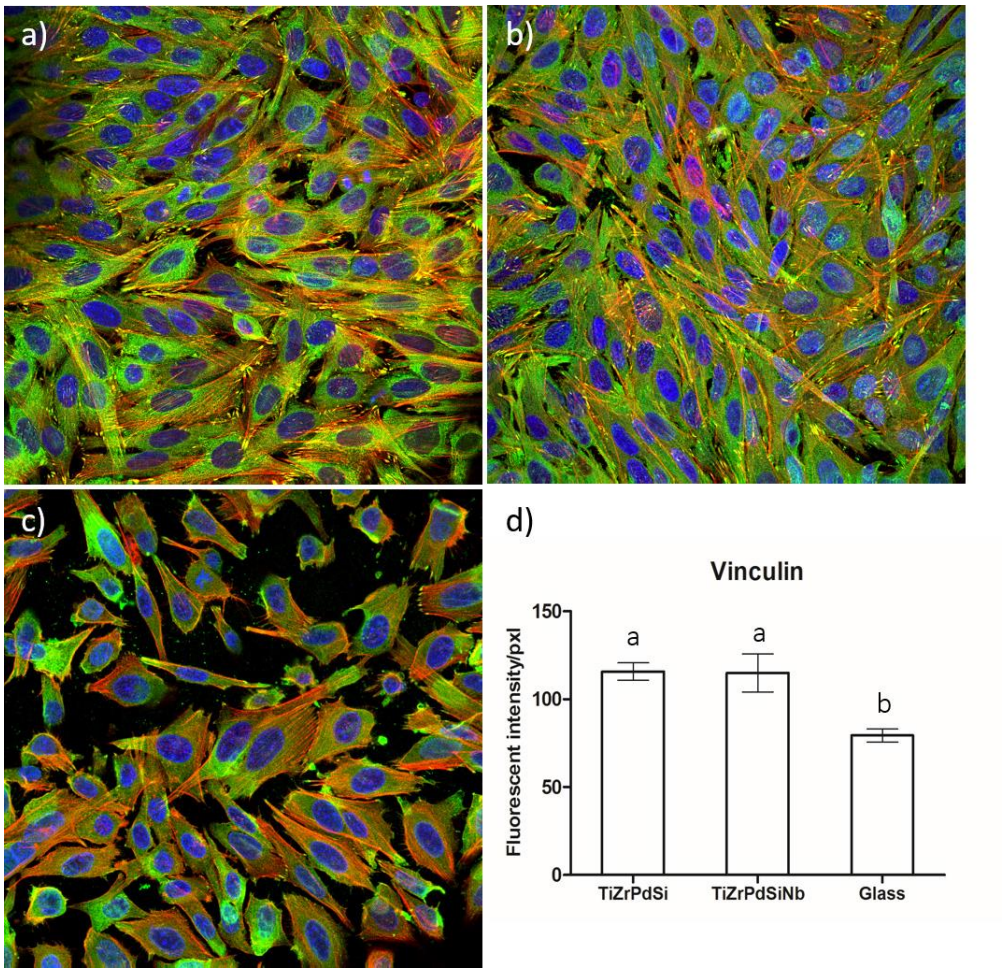

Figure 3. Vinculin and actin distribution in human Saos-2 cells grown on TiZrPdSi (a) and TiZrPdSiNb (b) alloys, and on a glass coverslip (c). Stress fibres (red), focal contacts (green) and nuclei (blue) can be observed. Fluorescence intensity of vinculin signal normalized to the total amount of pixels evaluated (d).Different letters above the columns indicate significant differences ($p < 0.05$).

Cell proliferation

The proliferation of Saos-2 cells grown on the two alloys was quantified at days 1, 3 and 7 and compared with the proliferation on control samples (glass and PS). As it can be seen in figure 4, the number of cells growing on both alloys was significantly higher than the cells growing on both controls after 1 day in culture. The same tendency was observed after 3 and 7 days. On the other hand, no significant differences in cell proliferation were observed between the two alloyed compositions, or between both controls.

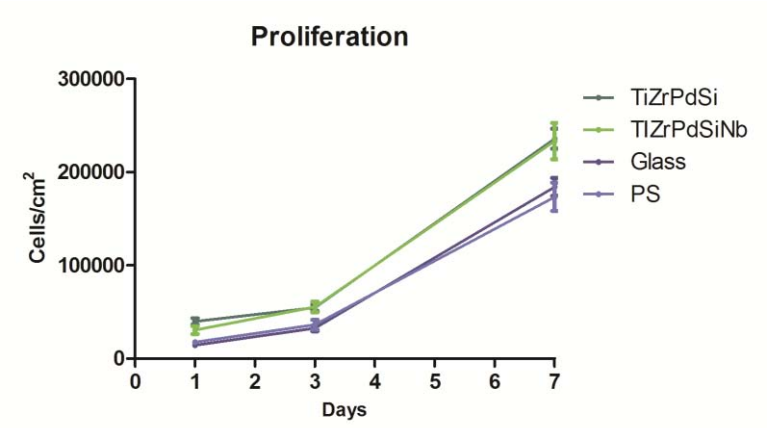

Figure 4. Proliferation of Saos-2 cells grown on TiZrPdSi and TiZrPdSiNb alloys, and on glass coverslip and polystyrene (PS) surfaces at 1, 3 and 7 days in culture.

Expression of osteogenic markers

The expression of four specific osteoblast differentiation markers (OC, OPN, ON, BSP) was evaluated after 7 and 14 days in culture on both alloys and on glass surfaces. The level of OC mRNA after 7 days was nearly twice in TiZrPdSiNb compared with the level in TiZrPdSi and glass. However, after 14 days, the level of OC mRNA was similar in cells growing on both alloys, and significantly higher than in cells growing on the glass coverslip. Expression of OPN was similar to that of OC at 7 days, but at 14 days of culture it was significantly lower in cells grown on TiZrPdSiNb than on the TiZrPdSi alloy. Differences in ON mRNA levels were detected only between TiZrPdSi and glass at 7 days in culture. Finally, the expression of BSP was similar for both alloys, and significant lower for the glass control at 7 days of culture. However, the situation was reversed at 14 days of culture, being BSP expression significantly higher in cells growing on glass than on both alloys.

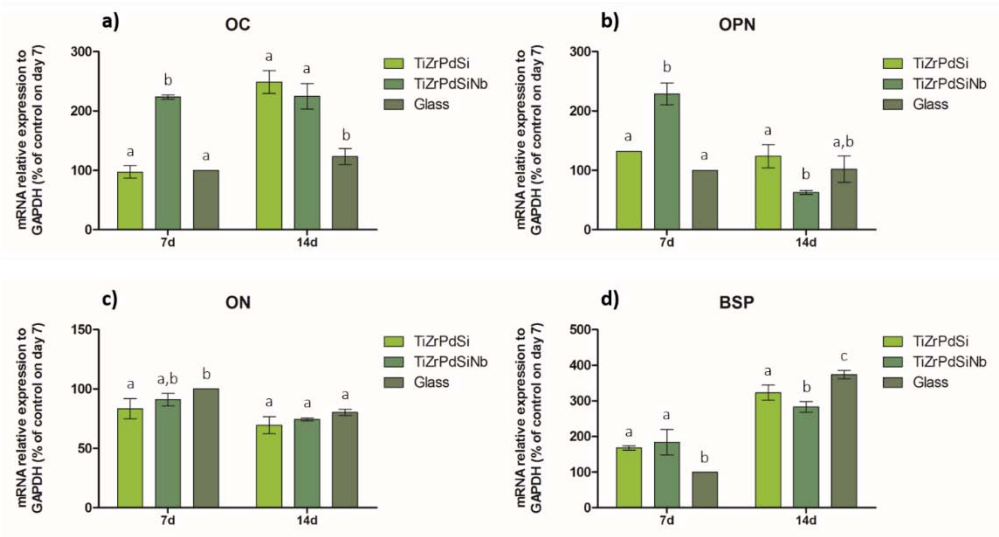

Figure 5. Quantification of mRNA levels. Relative expression of Osteocalcin (OC), Osteopontin (OPN), Osteonectin (ON) and Bone sialoprotein II (BSP) in Saos-2 cells on day 7 and 14 after seeding on TiZrPdSi and TiZrPdSiNb alloys, and on a glass coverslip. The target gene levels are expressed as a relative value, i.e. the ratio of the target gene expression toward the reference *GAPDH* gene. Different letters above the columns indicate significant differences ($p < 0.05$) among the materials at the same time-point.

Osteogenic proteins

Osteoblast differentiation was also evaluated by quantifying the immunodetection of COLI, OC and ALP after 7 days in culture. No significant differences in COLI levels were found between the two alloys tested, but a significantly smaller amount of this protein was detected in cells grown on the glass coverslip (Fig. 6a). Cells grown on TiZrPdSiNb presented a larger amount of OC (117 a.u.) than on TiZrPdSi (77 a.u.) and glass coverslip (60 a.u) (Fig. 6b). Finally, TiZrPdSi alloy showed the largest amount of ALP protein (Fig. 6c).

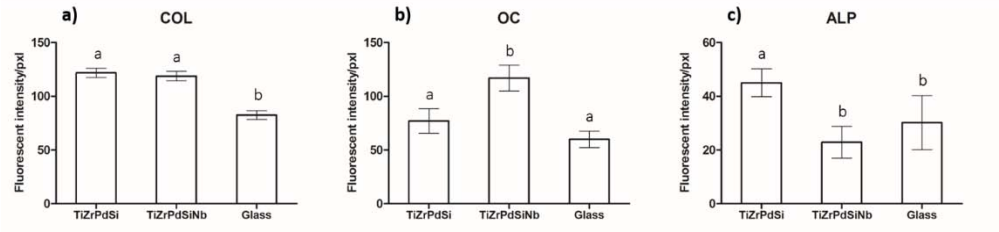

Figure 6. Fluorescence intensity of COLI (a), OC (b) and ALP (c) osteoblast differentiation proteins in Saos-2 cells grown on TiZrPdSi, TiZrPdSiNb and glass surfaces for 7 days. Different letters above the columns indicate significant differences ($p < 0.05$).

ALP activity

ALP activity is also a marker for osteoblast differentiation. After 7 days, no significant differences were observed among the two alloys tested and the control glass surfaces (Fig. 7). However, after 14 days, ALP activity had strongly increased in both alloys, but decreased on cells grown on glass coverslips.

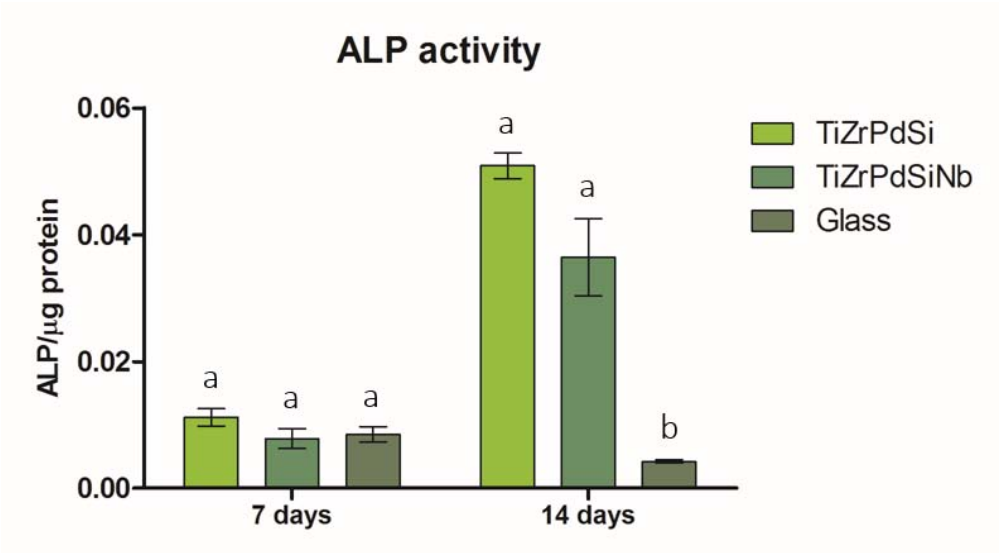

Figure 7. ALP activity of Saos-2 cells grown on TiZrPdSi alloy, TiZrPdSiNb alloy and glass coverslip after 7 and 14 days in culture. Values are normalized with total protein content. Different letters above the columns indicate significant differences ($p < 0.05$).

Discussion

Nanostructured TiZrPdSi(Nb) alloys were characterized by our group in a previous work and we demonstrated that they present a good combination of relatively high elasticity and hardness, better than the commercially available Ti-6Al-4V and Ti-40Nb alloys [10]. The addition of Nb to the alloy (TiZrPdSiNb) resulted in a lower Young's modulus, close to that of the bone, but also lower hardness than its counterpart (TiZrPdSi). Importantly, the addition of Nb to the alloy did not produce cytotoxicity at 24 h of culture. Altogether, the results of this previous work suggested that TiZrPdSi(Nb) is a promising candidate to be used in bone implants. However, further analyses of biocompatibility were necessary to demonstrate its safeness in medium- and long-term biological conditions.

Hydrophobicity of the alloy surface is an important parameter for cell adhesion and growth. In general, osteoblast adhesion and spreading improves with an increase in surface hydrophilicity, measured by the contact angle [11]. Protein adsorption is the first biological event that occurs when a biomaterial is immersed in a medium supplemented with serum, and it depends on hydrophobic interactions. *In vitro* studies have shown that hydrophilic surfaces are able to adsorb proteins in a more flexible conformation than hydrophobic ones, and this flexibility allows their reorganization and improves cell adhesion and spreading [11]. Other factors like pH, surface charge and roughness are also important for protein adsorption. Cell response can differ depending on the type and concentration of the proteins adsorbed on the alloy. Some authors have suggested that fibronectin promotes cell adhesion, whereas albumin prevents it [12]. In the present work, we show that TiZrPdSiNb adsorbed more albumin and fibronectin than the TiZrPdSi alloy, glass and PS, although results on wettability of the TiZrPdSi alloy indicated slightly more hydrophilicity than for the TiZrPdSiNb alloy.

Anchorage-dependent cells, like Saos-2, need to adhere to survive and avoid the induction of anoikis, a type of regulated cell death. Cell adhesion is mediated by integrins, a family of membrane receptors that bind to the extracellular ligands like fibronectin, collagen and laminin and that cluster to form focal adhesion plaques together with intracellular proteins such as vinculin. We found that, even though the alloy containing Nb (TiZrPdSiNb) adsorbed more fibronectin than the one lacking Nb, vinculin signal

intensity was similar in cells grown on top of both alloys, suggesting an equivalent degree of cell adhesion to the alloy surface. A possible explanation is that although fibronectin and albumin are components of the serum, they compete to be adsorbed on the same surface and the increase in fibronectin adsorption is balanced by the increase in albumin adsorption. Moreover, the protein conformation once adsorbed to the surface of both alloys is unknown, and it is a key point in the subsequent cell response [13].

On the other hand, cell adhesion and spreading was lower on the glass coverslip, where more rounded cells were observed, which is in agreement with the lower detection of vinculin in this sample compared with the alloys. The higher contact angle of the glass coverslip (close to 80 °) compared with that of the two alloys (57.6 ° and 64.8 °) can explain the differences in cell adhesion and spreading between the two different surfaces. These results are in agreement with those of other authors showing that contact angles of 60 ° or 64 ° allowed optimal cell adhesion and spreading compared to 90 ° [14]. Direct osteoblast adhesion and spreading on metal surfaces is important to prevent aseptic loosening of metal implants caused by fibroblast layer attachment and, for this reason, successful implant integration is highly dependent on the correct osteoblast adhesion on implant surface [15]. As cell adhesion was higher on both alloys, it is not surprising that cell proliferation was also better on the alloys than on the controls, because Saos-2 cells cannot divide without previous adhesion [11].

Finally, the last item we analysed to assess the biocompatibility of the alloys was the ability of Saos-2 cells to differentiate onto the alloys. Osteoblast differentiation and extracellular matrix mineralization play an important role in osseointegration. OC, OPN, ON and BSP are osteogenic genes expressed by Saos-2 cells during the extracellular matrix maturation and mineralization [13,16]. COLI is the major component of organic bone extracellular matrix, representing 90% of extracellular matrix proteins, and it is considered an early marker of osteoblast differentiation [17]. Another important marker in osteoblast differentiation is the ALP enzyme, which activity is necessary for extracellular matrix mineralization and reaches its maximum during early stages of differentiation [9]. We studied osteoblast differentiation at three different levels, first by quantifying the expression of four genes (OC, OPN, ON and BSP) at 7 and 14 days of culture; second, by detecting and quantifying three proteins (COLI, OC and ALP) at 7

days of culture; and third, by quantifying the activity of a protein (ALP) at 7 and 14 days of culture. In global, we can summarise that expression, presence and activity of the proteins analysed were similar or higher in cells cultured during 7 days on the alloys than on glass coverslip, except for ON. Between both alloys, differentiation seemed to be higher in the alloy containing Nb, according to the results of OC and OPN expression and of OC protein detection. At 14 days, the differences between alloys and glass were minimum in terms of gene expression, except for a still higher OC expression in both alloys, but ALP activity was still much higher in cells grown on the alloys than on glass coverslips. These results are in agreement with the good biological response that has been described for β-Ti alloys [18], the same microstructure present in TiZrPdSi and TiZrPdSiNb alloys. Guo et al. (2013) developed another β-Ti alloy, Ti-35Nb-2Ta-3Zr, and demonstrated, in *in vitro* studies, that the alloy enhanced cell proliferation and osteoblast differentiation [19]. Thus, it seems that this microstructure, the β-Ti phase, is an excellent structure to obtain biocompatible materials.

Conclusion

In conclusion, the TiZrPdSi(Nb) alloy system presents excellent mechanical properties and good biological response. Both alloys enhanced Saos-2 cells adhesion, spreading and proliferation. Using three different methodologies to analyse osteoblast differentiation we obtained concordant results that demonstrated that TiZrPdSi and TiZrPdSiNb alloys allow better osteoblast differentiation than the control glass coverslip. Furthermore, our results showed that cells grown onto the TiZrPdSiNb alloy presented higher levels of some late osteogenic markers during the first week in culture. Thus, TiZrPdSi and TiZrPdSiNb alloys can be considered as excellent candidates to be used in orthopaedical implants.

Acknowledgements

The study was supported by the Grant Agency of the Czech Republic (GACR, grant No. 15-01558S), the Spanish Ministerio de Ciencia e Innovación (MAT2014-57960-C03-1-R – co-financed by the Fondo Europeo de Desarrollo Regional, FEDER, and MAT2014-57960-C03-3-R projects), and the Generalitat de Catalunya (2014-SGR-524 and 2014-SGR-1015). AB was supported by a predoctoral grant from the Universitat Autònoma de Barcelona.

References

[1] M. Geetha, A.K. Singh, R. Asokamani, A.K. Gogia, Ti based biomaterials, the ultimate choice for orthopaedic implants – A review, Prog. Mater. Sci. 54 (2009) 397–425. doi:10.1016/j.pmatsci.2008.06.004.

[2] A. Biesiekierski, J. Wang, M. Abdel-Hady Gepreel, C. Wen, A new look at biomedical Ti-based shape memory alloys, Acta Biomater. 8 (2012) 1661–1669. doi:10.1016/j.actbio.2012.01.018.

[3] S.S.A. El-Rahman, Neuropathology of aluminum toxicity in rats (glutamate and GABA impairment), Pharmacol. Res. 47 (2003) 189–194. doi:10.1016/S1043-6618(02)00336-5.

[4] M.E. Percy, T.P. a Kruck, A.I. Pogue, W.J. Lukiw, Towards the prevention of potential aluminum toxic effects and an effective treatment for Alzheimer's disease, J. Inorg. Biochem. 105 (2011) 1505–1512. doi:10.1016/j.jinorgbio.2011.08.001.

[5] V. Bordignon, F. Palamara, P. Cordiali-Fei, A. Vento, A. Aiello, M. Picardo, et al., Nickel, palladium and rhodium induced IFN-gamma and IL-10 production as assessed by in vitro ELISpot-analysis in contact dermatitis patients., BMC Immunol. 9 (2008) 19. doi:10.1186/1471-2172-9-19.

[6] A. Faurschou, T. Menné, J.D. Johansen, J.P. Thyssen, Metal allergen of the 21st century - A review on exposure, epidemiology and clinical manifestations of palladium allergy, Contact Dermatitis. 64 (2011) 185–195. doi:10.1111/j.1600-0536.2011.01878.x.

[7] H. Matsuno, A. Yokoyama, F. Watari, M. Uo, T. Kawasaki, Biocompatibility and osteogenesis of refractory metal implants, titanium, hafnium, niobium, tantalum and rhenium, Biomaterials. 22 (2001) 1253–1262. doi:10.1016/S0142-9612(00)00275-1.

[8] J.-W. Lee, K.-B. Lee, H.-S. Jeon, H.-K. Park, Effects of surface nano-topography on human osteoblast filopodia., Anal. Sci. 27 (2011) 369. doi:10.2116/analsci.27.369.

[9] J. Popp, K. Laflin, B. Love, A. Goldstein, In vitro evaluation of osteoblastic differentiation on amorphous calcium phosphate-decorated poly(lactic-co-gylolic acid) scaffolds, J. Tissue Eng. Regen. Med. 5 (2011) 780–789. doi:10.1002/term.376.

[10] A. Hynowska, A. Blanquer, E. Pellicer, J. Fornell, S. Suriñach, B. MD, et al., Nanostructured Ti-Zr-Pd-Si- (Nb) bulk metallic composites : Novel biocompatible materials with superior mechanical strength and elastic recovery, J. Biomed. Mater. Res. Part B Appl. Biomater. online (2014) 1–11. doi:10.1002/jbm.b.33346.

[11] L. Bacakova, E. Filova, M. Parizek, T. Ruml, V. Svorcik, Modulation of cell adhesion, proliferation and differentiation on materials designed for body implants, Biotechnol. Adv. 29 (2011) 739–767. doi:10.1016/j.biotechadv.2011.06.004.

[12] J. Wei, T. Igarashi, N. Okumori, T. Igarashi, T. Maetani, B. Liu, et al., Influence of surface wettability on competitive protein adsorption and initial attachment of osteoblasts., Biomed. Mater. 4 (2009) 045002. doi:10.1088/1748-6041/4/4/045002.

[13] M. Vandrovcova, I. Jirka, K. Novotna, V. Lisa, O. Frank, Z. Kolska, et al., Interaction of Human Osteoblast-Like Saos-2 and MG-63 Cells with Thermally Oxidized Surfaces of a Titanium-Niobium Alloy, PLoS One. 9 (2014) e100475. doi:10.1371/journal.pone.0100475.

[14] D.P. Dowling, I.S. Miller, M. Ardhaoui, W.M. Gallagher, Effect of Surface Wettability and Topography on the Adhesion of Osteosarcoma Cells on Plasma-modified Polystyrene., J. Biomater. Appl. 26 (2011) 327–347. doi:10.1177/0885328210372148.

[15] W. Wang, C.K. Poh, Titanium Alloys in Orthopaedics, Titan. Alloy. - Adv. Prop. Control. (2013) 1–20. doi:10.5772/55353.

[16] V. Goriainov, R. Cook, J. M. Latham, D. G. Dunlop, R.O.C. Oreffo, Bone and metal: An orthopaedic perspective on osseointegration of metals, Acta Biomater. 10 (2014) 4043–4057. doi:10.1016/j.actbio.2014.06.004.

[17] J. Liskova, O. Babchenko, M. Varga, A. Kromka, D. Hadraba, Z. Svindrych ZdenekBurdikova, et al., Osteogenic cell differntation on H-terminated and O-terminated nanocrystalline diamond films, Int. J. Nanomedicine. 10 (2015) 1–

16.

[18] I. Jirka, M. Vandrovcova, O. Frank, Z. Tolde, J. Plsek, T. Luxbacher, et al., On the role of Nb-related sites of an oxidized beta-TiNb alloy surface in its interaction with osteoblast-like MG-63 cells, Mater. Sci. Eng. C. 33 (2013) 1636–1645. doi:10.1016/j.msec.2012.12.073.

[19] Y. Guo, D. Chen, W. Lu, Y. Jia, L. Wang, X. Zhang, Corrosion resistance and in vitro response of a novel Ti35Nb2Ta3Zr alloy with a low Young's modulus, Biomed. Mater. 8 (2013) 055004. doi:10.1088/1748-6041/8/5/055004.

3.4. Piezoelectric nanogenerators for electrical stimulation of living cells

Piezoelectric nanogenerators for electrical stimulation of living cells

G Murillo[1*], A Blanquer[2*], L Barrios[2], E Ibañez[2], C Nogues[2] and J Esteve[1]

[1]Department of Nano and Microsystems, Instituto de Microelectrónica de Barcelona.

[2]Departament de Biologia Cel·lular, Fisiologia i Immunologia, Universitat Autònoma de Barcelona, Edifici C, 08193, Bellaterra, Spain.

*This authors contributed equally to this work

Abstract

Piezoelectric materials are smart materials that can generate an electrical activity in response to minute deformations. Here, we demonstrate that the interaction of human cells with piezoelectric nanogenerators (NGs) based on a network of two-dimensional ZnO nanosheets induces a local electric field that can alter cell behavior in a cell type-dependent manner. When cells were cultured on top of the NGs, the electromechanical NGs-cells interactions stimulated the motility of macrophages and triggered the opening of ion channels present in the plasma membrane of osteoblast-like cells inducing intracellular calcium transients. In addition, excellent cell viability, proliferation and differentiation was validated. These results pave the way for the future use of NGs for "in situ" stimulation of other electrically responsive cells like neurons or muscle cells.

Nanostructured ZnO has become very popular over the last few years for its application as piezoelectric nanogenerator (NG) (*1*–*3*). For biological applications, ZnO devices are being used as sensors or generators for animal muscles, but at millimeter-scale sizes (*4*, *5*). No applications at the nanoscale have been demonstrated so far.

Here, we propose the use of a network of ZnO nanosheets (NSs) as piezoelectric NGs for the electrical stimulation of living cells. This concept is based on the creation of a local electric potential difference near the plasma membrane of cells cultured on top of the NSs network (Fig. 1A). The reduced thickness of less than 20 nm with an aspect ratio higher than 100, makes possible the deflection of these nanostructures by inherent cell forces. This deflection is translated into the generation of an electric field due to the piezoelectric effect of the ZnO NSs. Ultimately, this electric field, locally produced near the cell plasma membrane, could trigger the activation of cell signalling patwhways and a change in cell behavior. The main features that make these nanoscale voltage generators suitable for this biological application are that: (1) the NGs have a size smaller than a cell, (2) the typical cell membrane potential is comparable to the voltage generated by a single NG and (3) the generated electric power is used instantaneously to stimulate the cell, without the need for any energy storage mechanism.

The fabrication of the NGs used as cell culture substrate is based on the hydrothermal synthesis of ZnO NSs. This method was chosen due to its simplicity and compatibility with other technologies and materials. It is based on a chemical reaction under mild hydrothermal conditions, which is one of the most powerful low-cost, low-temperature and simple approaches. It ordinarily consists of an aqueous solution of Zinc nitrate ($Zn(NO_3)_2$) and hexamethylenetetramine (HMTA, a highly water soluble, non-ionic tetradentate cyclic tertiary amine) undergoing hydrothermal process at temperatures <100 ºC (*6*). Thermal degradation of HMTA releases hydroxyl ions which react with Zn^{2+} ions to form ZnO (*7*–*12*). Different ZnO morphologies have been reported in literature, mainly governed by epitaxial growth over a seed layer and/or by the effect of pH (*13*, *14*).

To obtain the NSs morphology, we used a (100) silicon substrate covered by an AlN thin-film acting as seed layer (Fig. S1A). This seed layer generates a local pH gradient due

to AlN hydrolysis that eases the growth of ZnO NSs in contrast to the typical nanowire shape commonly obtained with other seed layers such as gold, ZnO or zinc acetate. The AlN thin layer was deposited by reactive RF magnetron sputtering on top of a thin layer of Ti/Pt that improves the AlN crystallinity (*15–18*). They show high crystallinity quality, good uniformity and growth reproducibility (Fig. S1). In order to study the dependence of the NS aspect ratio on the electric field strengths generated by the NG-cell interaction, two different NS geometries were synthesized in this work. We will use the term 'thick nanogenerator' (thick-NG) to refer to structures with a mean thickness of 40 ± 4.5 nm and 'thin nanogenerator' (thin-NG) for those with a mean thickness of 20 ± 1.34 nm (Fig. 1B and C). Mean diameters were 3.08 ± 0.82 μm and 1.34 ± 0.09 μm, respectively. It has been calculated that the thin-NGs generate a higher piezopotential than the thick-NGs for the same force (Fig. 1D and E).

To demonstrate the NG direct piezoelectric effect, we fabricated a flexible test device composed of polymer-embedded ZnO NSs sandwiched between a gold top electrode and a conducting polyimide substrate (Fig. 1F). The voltage peaks generated after periodically bending the test device validated the theoretical piezoelectricity of the ZnO NS (Fig. 1G).

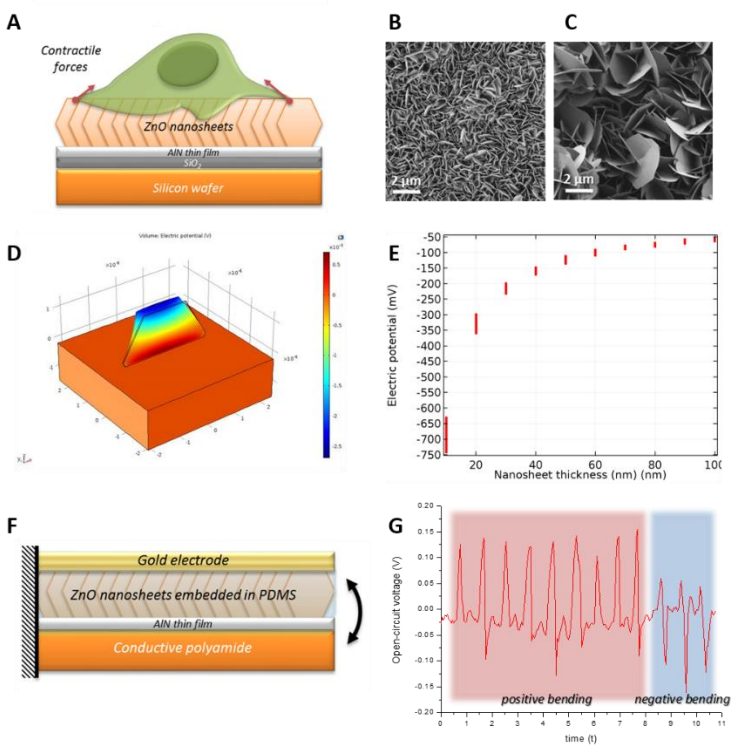

Figure 1. Piezoelectric nanogenerators (NGs) based on a network of ZnO nanosheets (NSs). Inherent cell forces of cells grown on NGs are able to bend the NSs (A). Scanning electron microscopy images of both geometries: thin-NGs (B) and thick-NGs (C). Field emission scanning electron microscopy simulation of a thin-NG generated 6 mV when strained by 1 nN (D), whereas 2.5 mV were generated for thick-NG. Relationship between NS thickness and electric potential generated (E). Cross-section diagram of the NS-based prototype demonstrator (F) and the open-circuit voltage generated by the demonstrator while applying a periodic positive and negative bending (G).

We next evaluated the NG-cell interaction using two different human cell lines: THP1 monocytes differentiated into macrophages and Saos-2 osteoblast-like cells. The former are motile cells whereas the latter present voltage-gated calcium channels (VGCCs) and stretch-activated cation channels (SACCs) in their membrane. Both motility and channel opening can be stimulated by electric fields (*19*, *20*). In addition, it is known that electrical stimulation of osteoblasts increases cell proliferation and differentiation (*21*). To evaluate the feasibility of using the NGs as electrical stimulators of living cells, we first assessed the biocompatibility of the thin- and thick-NGs, using AlN thin-films as control

substrate. Cell viability, proliferation and differentiation were similar between both NGs and between them and the control at all time-points analyzed (Fig. 2A and Fig. 3A-C). Thus, ZnO NSs do not seem to interfere with these cell activities, in contrast to ZnO nanoflowers (*22*) or nanorods (*23*), where a decrease in cell proliferation was observed when compared with control substrates.

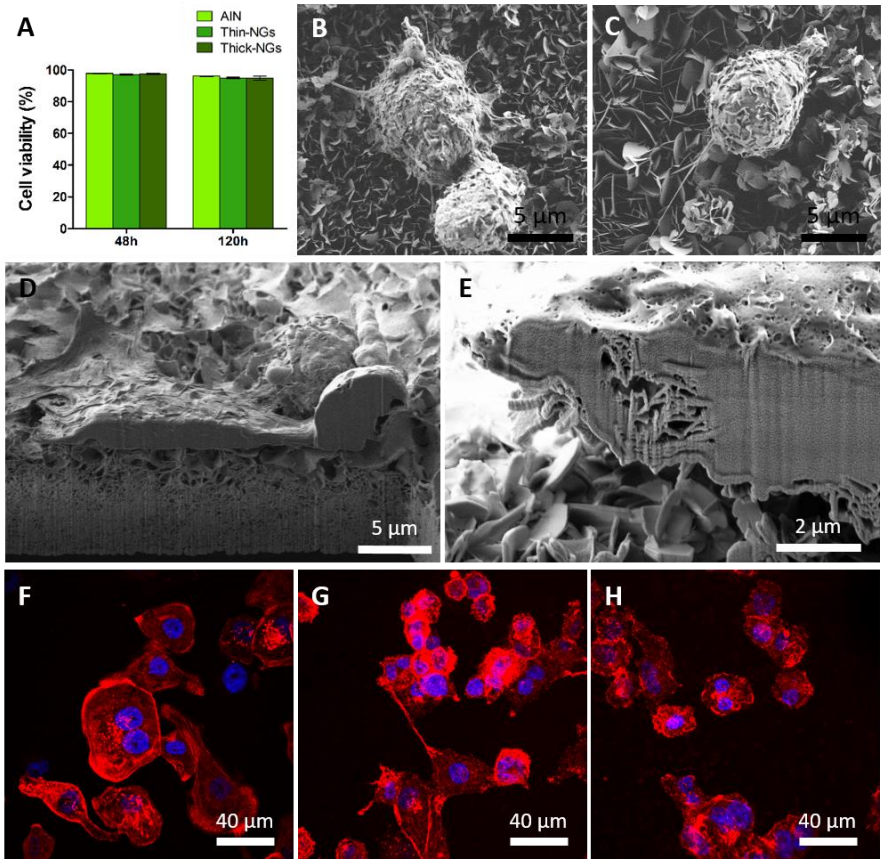

Figure 2. Biocompatibility of thin ZnO nanogenerators (thin-NG), thick-NG and control AlN for macrophages. Cytotoxicity was analyzed by the live/dead kit at 2 and 5 days of culture (A). No differences were found among samples and time-points analyzed (χ^2 test). Cell morphology and NG-cell interaction, assessed by scanning electron microscopy and focus ion beam after 2 days in culture, showed that macrophages were adhered to both thin- (B) and thick-NGs (C). The plasma membrane was in direct contact with the thick-NGs (D) and some macrophages even appeared to have engulfed the NGs (E). Confocal laser scanning microscopy images of actin filaments (red) detection showed that the distribution of stress fibers was similar on cells grown on AlN (F), thin-NGs (G) and thick-NGs (H).

Next, cell adhesion to the NGs was assessed, as this is a key parameter for the induction of the piezoelectric effect. It is well-known that the intracellular tension can be transmitted, via focal contacts, to the underlying substrate (*24*). Consequently, if the cells are firmly adhered on the NGs surface they would apply a force on the NGs that could result in the generation of an electric field near the cell plasma membrane. We observed that the plasma membrane of cells cultured on top of the NGs was in close contact with the NSs network, and that cells emitted short and long projections that firmly attached to individual NSs (Fig. 2B-E and Fig. 3D-G). Adhesion to the NSs was confirmed by the presence of focal contacts (Fig. 3H-J). Slight differences in Saos-2 cells morphology, length of actin stress fibers and distribution and number of focal contacts were observed among the three substrates analyzed.

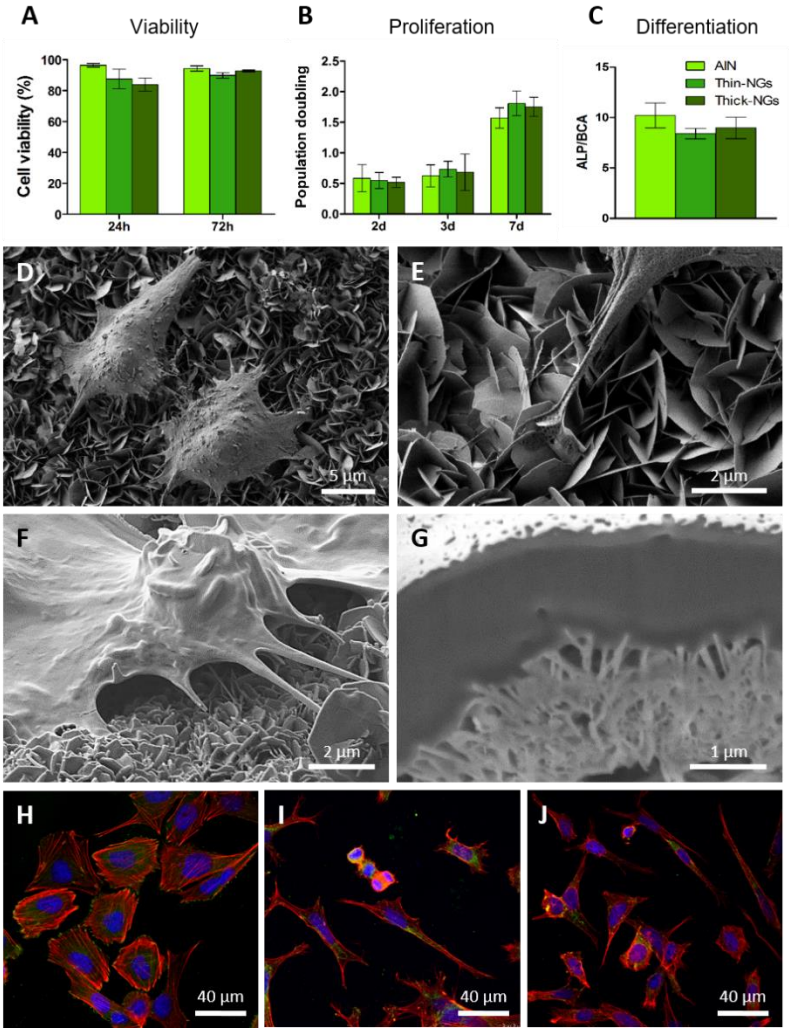

Figure 3. Biocompatibility of thin ZnO nanogenerators (thin-NGs), thick-NGs and control AlN for Saos-2 cells. Viability was analysed by the live/dead kit at 24 and 72 h of culture (A), proliferation by the Alamar Blue assay at 1, 2, 3 and 7 days (B) and differentiation by a quantitative analysis of ALP activity, a differentiation osteoblast marker, at 14 days of culture (C). No significant differences among materials were observed for any of the parameters (χ^2 test and Kruskal-Wallis test). Morphology and NG-cell interaction, assessed by scanning electron microscopy and focus ion beam, showed that cells were firmly adhered to the NGs (D) and emitted long projections that anchored on the nanosheets (E). Cells were completely adapted to the topography of the nanosheets (F), which were in direct contact with the plasma membrane (G). Confocal laser scanning microscopy analysis after immunodetection of vinculin (focal contacts, green) and detection of actin (stress fibers, red) showed a high number of focal contacts at the end of long parallel bundles of actin filaments on cells grown on AlN, displaying a polygonal shape (H). Shorter actin bundles and less focal contacts were present in cells grown on thin-NGs (I) and thick-NGs (J), which also displayed a more elongated, spindle-shape morphology.

Finally, we analyzed changes in cell behavior, i.e. motility and intracellular calcium concentration ([Ca^{2+}]), induced by the NGs. It is well known that electric fields can stimulate macrophage migration (*19*) and that osteoblasts exposed to an electrical field can undergo changes in their cytosolic [Ca^{2+}] (*20*, *25*). We observed that macrophage motility was increased by their culture on top of the two NGs (trajectory length median of 58.1 μm for thin-NGs and 64.0 μm for thick-NGs) when compared with the control glass coverslip (median of 53.4), being the cells more active on the thick-NG (Fig. 4A). On the other hand, 64±19% of Saos-2 cells grown over thin-NGs experimented increases in [Ca2+] (Fig. 4B), with amplitudes of Ca^{2+} transients (Fig. 4C and Fig. S2) compatible with an influx of extracellular calcium (*25*). By contrast, only 19±9% of Saos-2 cells grown over thick-NGs presented increases in [Ca^{2+}] (Fig. 4A), with low amplitudes of Ca^{2+} transients (Fig. S3), and the percentage dropped to 6±3% (Fig. 4A and Fig. S4) in Saos-2 cells grown on glass coverslips. These results suggest that cell adhesion forces are able to bend the NSs, inducing the generation of a local electric field large enough to stimulate the cells and alter their behavior. The differential effect of thin- and thick-NGs on both cell types deserves further investigation, but could be related to the different geometry of the NSs and the magnitude of the piezoelectric potential generated, as well as to the type of cell response analyzed.

In Saos-2 cells grown on the NGs, especially on thin-NGs, calcium peaks varied in duration and amplitude from cell to cell, and even in the same cell along time (Fig. 4C-D and Fig. S2, S3 and S4). We hypothesize that the mechanical stress produced on each NS in contact with the cell membrane varies, affecting the extent of the NS bending and thus the intensity of the local voltage generated. This in turn would determine the type of ion channel that it is activated, as it has been reported that the type of channels that open in response to an electric field depends on the voltage (*25*). Voltages able to locally change the membrane potential would trigger the opening of VGCCs or SACCs (Fig. 3E), allowing an influx of extracellular Ca^{2+} that would produce high amplitudes of Ca^{2+} transients. High-amplitude and duration (in order of minutes) of Ca^{2+}transients have been reported in neural-like cells (*26*) using piezoelectric nanoparticles activated through ultrasounds to electrically stimulate those cells, and were attributed to voltage-gated ion channels. On the other hand, electrical stimulation can reorganize plasma membrane

proteins that via phospholipase C, can induce the release of intracellular Ca^{2+} stores, resulting in low-amplitude Ca^{2+} transients (*20*). Accordingly, the different types of Ca^{2+} peaks registered in Saos-2 cells grown on thin-NGs could be caused by a different combination of the three types of ion channels.

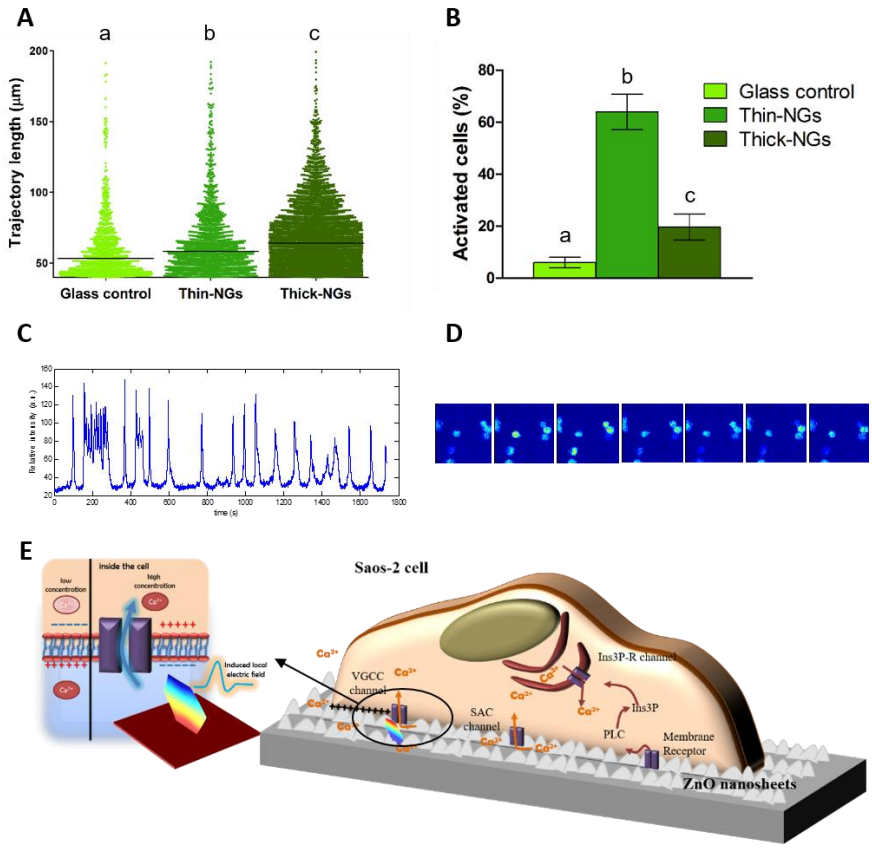

Figure 4. Effect of thin- and thick-nanogenerators (NGs) on macrophages and Saos-2 cells behavior. (A) Macrophages motility quantified as trajectory lengths. Distances shorter than 40 µm were considered in-situ motions. (B) Quantification of Saos-2 cells undergoing changes in Ca^{2+} concentration (activated cells). Different letters above the columns indicate significant differences (Kruskal-Wallis test and $\chi 2$ test). (C) Ca^{2+} influxes pattern of a selected cell grown on thin-NGs. (D) Sequential images of some Saos-2 showing changes in Ca^{2+} concentration over time. (E) Sketch of a cell grown on top of a nanogenerator microarray indicating the possible pathways involved in changes in the Ca^{2+}concentration. Extracellular Ca^{2+} influx is due to the opening of plasma membrane channels, either voltage gated Ca^{2+} (VGCC) or stretch-activated cation channels (SACC), whereas intracellular Ca^{2+} comes from endoplasmic reticulum stores through the activation of membrane receptors and the opening of Ins3P-receptor channels. The bending of a NG would induce a local electrical field that alter the membrane potential and/or the configuration of membrane receptors and results in the opening of the Ca^{2+} channels.

The work herein provides evidence that cell interaction with the developed NGs results in the generation of local electrical fields that can alter cell behavior, stimulating motility or triggering the opening of ion channels and increasing cytosolic [Ca^{2+}], depending on the cell type. Importantly, cells are able to proliferate and differentiate when cultured for up to 14 days on the NGs, i.e. under repetitive electrical stimulation. Therefore, NGs could be used to electrically self-stimulate bone fractures and increase bone regeneration. This in-situ cell-scale stimulation could be extrapolated to other excitable cells, such as neurons or muscle cells, leading to future bioelectronic medicines based on cell-targeted local electrical impulses.

Materials and methods

Substrate and seed layer preparation

The substrate used for the wafer-level hydrothermal growth was a 4-inch n-type silicon (1 0 0) wafer which had been covered by a silicon oxide layer of 2 μm by chemical vapour deposition. Afterwards, a Ti/Pt bilayer of 30 nm/20 nm was sputtered followed by a layer of AlN with two different thicknesses, 100 nm and 300 nm. Finally, the wafer was diced to obtain 6 mm × 6 mm samples. These two different substrates were used as seed layer of the subsequent hydrothermal method. In addition, the substrate with the 300nm-thick AlN layer was also used as control substrate.

ZnO nanosheets synthesis

Prior to the growth step, every sample was cleaned with acetone, isopropanol, ethanol and deionized water. Zinc nitrate hexahydrate (98%, Sigma) and hexamethylenetetramine (99%, Sigma) were mixed to create an equimolar aqueous solution at 5 mM. Afterwards, every sample was placed floating facing down in a wide-mouth jar containing 50 mL of aqueous solution. The jar was then hermetically closed and placed in a convection oven at 80 °C for 14 h and 16 h to grow the thin and thick nanosheets, respectively. Finally, the samples were rinsed with deionized water, dipped in ethanol to avoid stiction of the grown nanostructures, and dried at room temperature (RT).

Fabrication of test device

In order to demonstrate the NG direct piezoelectric effect, a test film structure, comprised of conducting polyimide, AlN thin, ZnO NS, a polydimethylsiloxane (PDMS) layer and a gold top electrode, was fabricated (Fig.1F).

Physical Characterization

High resolution transmission electron microscopy (HRTEM), and selected area electron diffraction (SAED) experiments were performed with a TEM Jeol JEM 2011 instrument operating at 200 kV. In order to prepare the samples, the substrates were immersed in ethanol and introduced in an ultrasound bath for 10 min to release the nanosheets from the substrate. Then, a drop of the resulting solution containing the released nanosheets

was deposited on a holey carbon grid and dried at RT. SAED patterns analyses were performed by comparing measured distances and related measured angles among them with the help of CaRIne 3.1 crystallography software. Subsequently, d-spacings were assigned to their corresponding reflections under the criteria of the best fit with respect to reported d-spacings and related angles according to ZnO structure (Crystallography Open Database,COD, ID: 1011259, hexagonal).

Field emission scanning electron microscopy (FESEM) and energy-dispersive X-ray spectroscopy (EDX) analyses were performed with a SEM/EDX Zeiss AURIGA over similar samples placed on a carbon conductive tab. For imaging, a voltage of 2 kV and a secondary electrons detector were used. EDX measurements were obtained applying a voltage of 10 kV.

X-Ray powder diffraction (XRD) patterns of the samples were collected on a Bruker D8 Advance diffractometer (CuKα, λ=1.5418Å) equipped with a bidimensional General Area Detector Diffraction System (GADDS) detector. A 2θ angle ranging from 17 º to 80 º, a voltage of 40 KV and a current of 40 mA were used.

Cell lines

Human THP-1 monocyte cells were grown under standard conditions (37ºC and 5% CO^2) in RPMI 1640 medium (Life Technologies) supplemented with 25% foetal bovine serum (FBS, Life Technologies) and 5% L-glutamine (Biowest). To differentiate monocytes into macrophages, cells were treated with 0.16 μM phorbol-12-myristate-13-acetate (Sigma) a minimum of 24 h.

Human osteosarcoma Saos-2 cells (ATCC) were cultured in Dulbecco's modified Eagle medium (DMEM) (Invitrogen) with 10% FBS under standard conditions.

Cell viability assay

The samples (AlN, thin-NGs and thick-NGs) were sterilized with absolute ethanol and individually introduced into a 4-well plate. For Saos-2 cells studies, 50,000 cells were seeded into each well and cultured under standard conditions for 24 and 72 h, whereas for macrophage analysis, 100,000 monocytes were seeded into each well and

differentiated into macrophages for 48 and 120 h. In parallel, control cells were seeded directly onto a glass coverslip in the absence of samples.

Cytotoxicity was analysed using the Live/Dead Viability/Cytotoxicity kit for mammalian cells (Invitrogen), according to the manufacturer's protocol. Live cells with intracellular esterase activity show green fluorescence, whereas dead cells show red fluorescence because of the permeability of their damaged plasma membrane to the ethidium homodimer. Cultures were observed under an Olympus IX71 inverted microscope equipped with epifluorescence. Images from different regions were captured, and a minimum of 300 cells were analysed. All experiments were performed in triplicate.

Cell morphology and adhesion analysis

The same samples used for the viability assay were processed to be analysed by scanning electron microscopy (SEM) and focused ion beam (FIB). Cells were washed in phosphate buffered saline (PBS), fixed in 4 % paraformaldehyde in PBS for 15 min at RT and washed again in PBS. Cell dehydration was performed in a series of increasing ethanol concentrations (50, 70, 90 and twice 100 %) for 8 min each. Finally, samples were dried using hexamethyldisilazane (Electron Microscope Science) for 15 min. Samples were mounted on special stubs and analysed using a SEM (Zeiss Merlin) in order to observe cell morphology. In addition, samples were cut using a FIB in order to observe the interaction between cells and piezoelectric material.

Cytoskeleton organization and focal contacts were assessed by actin filaments and vinculin detection, respectively. Following the same protocol described for the viability assay, cells were seeded onto samples and, after 24 h in the case of Saos-2 cells and 48 h for macrophages, cells were fixed in 4 % paraformaldehyde in PBS for 15 min at RT. Then, cells were permeabilized with 0.1% Triton X-100 (Sigma) in PBS for 15 min and blocked for 25 min with 1% bovine serum albumin (BSA; Sigma) in PBS at RT. Samples were then incubated with a mouse anti-vinculin primary antibody (Chemicon) for 60 min at RT and washed with 1% BSA-PBS. Then, samples were incubated with a mixture of Texas Red-conjugated phalloidin (Invitrogen), Alexa fluor 488 goat anti-mouse IgG1 and Hoechst 33258 (both from Invitrogen) for 60 min at RT. Finally, cells were washed in PBS, air dried and mounted on a specific bottom glass dishes (MatTek) using

ProLongAntifade mounting solution (Life Technologies). Samples were analyzed in a confocal laser scanning microscope (CLSM, Olympus XT7).

Saos-2 cells proliferation assay

Saos-2 cells proliferation was determined using Alamar Blue cell viability reagent (Invitrogen). A total of 250,000 cells were seeded into each well of a 4-multiwell plate containing each sample type. After 24 h, samples were moved to a new 4-multiwell plate containing fresh medium with 10% Alamar Blue. After 4 h in standard conditions, the supernatant was collected and its fluorescence quantified using a fluorimeter. Fresh medium was added to the cultures and the assay was repeated after 72 h and 7 days. Experiments were performed in triplicate.

Saos-2 cells differentiation assay

Saos-2 differentiation onto the sample surfaces was analysed by quantifying alkaline phosphatase (ALP) activity, considered an early stage marker of osteoblast differentiation. Thus, 500,000 cells were seeded into 35 mm culture dishes containing a pre-sterilized sample. After 14 days in culture, replacing the medium every 3-4 days, ALP activity was measured. Briefly, each sample was transferred to an Eppendorf tube and cells were lysed using 2x CyQuant cell lysis buffer (Invitrogen) for 10 min and vortexed for 15 s. Cell lysates were centrifuged at 12,000 rpm for 4 min at 4°C and supernatants were collected. ALP activity was evaluated quantifying the p-nitrophenol (pNP) produced by the hydrolysis of pNP phosphate (ThermoScientific), according to the manufacturer's protocol. The absorbance was measured at 405 nm using NanodropSpectrphotometer (ThermoScientific). ALP activity was normalized to total protein content using the Micro BCA Protein Assay kit (ThermoScientific).

Intracellular calcium quantification

CLSM (Leica SP5) was used to detect the intracellular calcium increase over time. Saos-2 cells were cultured on samples surface for 24 h in standard conditions, then cells were loaded with 2 μM Fluo-4 AM and 0.02% pluronic acid (both from Life Technologies) in serum free DMEM for 30 min in the dark at RT. Samples were washed with serum free DMEM and then transferred to MatTek dishes with fresh medium. Images of

osteoblasts were captured every 1 sec during 30 min. Changes in fluorescence intensity during the time of monitoring were processed using Image J software. A MATLAB code was developed to automatically detect Ca^{2+} increase in cells, taking the time-lapse movies recorded in the CLSM as data source. Several image enhancement routines and a perimeter detection algorithm were used to detect all the cultured cells. Then, mean relative intensity along time was calculated for each particular cell, using the automatic suitable threshold for every different measurement. Finally, every cell relative intensity was used as input of a ad-hoc peak detector to estimate whether the cell was activated by the nanogenerators

Macrophage motility assay

Macrophages motility on the sample surface was studied using time-lapse CLSM (Leica SP5). Monocytes were differentiated to macrophages onto the sample surface as explained before. Then, macrophage cultures were incubated with the CellTracker green CMFDA (Life Technologies), according to manufacturer's protocol. Samples with attached cells were transferred to MatTek dishes containing fresh medium and images from different regions were captured in 20 different z-stacks every 5 min for 4 h using a 10x objective. Captured images were analyzed using Imaris software (Bitplane) to determine cells trajectories length. Trajectories shorter than 40 μm were considered in-situ motions and were not taken into account.

Acknowledgments

This work was supported by FP7-NMP-2013-SMALL-7, SiNERGY (Silicon Friendly Materials and Device Solutions for Microenergy Applications), Contract n. 604169, MINAHE V project (TEC2013-41767-R/MINECO) and ENV-BIO-PORAL project (MAT2014-57960-C3-3-R). Dr. GM acknowledges his JAE-Doc contract from the Spanish National Research Council (CSIC) under the "Junta para la Ampliación de Estudios" Programme, co-funded by the European Social Fund (ESF)".

References

1. Z. L. Wang, J. Song, Piezoelectric Nanogenerators Based on Zinc Oxide Nanowire Arrays. *Science.* **312**, 242–246 (2006).

2. Z. L. Wang *et al.*, Lateral nanowire/nanobelt based nanogenerators, piezotronics and piezo-phototronics. *Mater. Sci. Eng. R Reports.* **70**, 320–329 (2010).

3. X. Wang, J. Song, J. Liu, Z. L. Wang, Direct-Current Driven Nanogenerator by Ultrasonic Waves. *Science.* **316**, 102–105 (2007).

4. R. Yang, Y. Qin, C. Li, G. Zhu, Z. L. Wang, Converting biomechanical energy into electricity by a muscle-movement- driven nanogenerator. *Nano Lett.* **9**, 1201–1205 (2009).

5. G. Zhu, A. C. Wang, Y. Liu, Y. Zhou, Z. L. Wang, Functional electrical stimulation by nanogenerator with 58 v output voltage. *Nano Lett.* **12**, 3086–3090 (2012).

6. S. Xu, Z. L. Wang, One-dimensional ZnO nanostructures: Solution growth and functional properties. *Nano Res.* **4**, 1013–1098 (2011).

7. M. T. Doan, X. V. Ho, T. Nguyen, V. N. Nguyen, Influence of doping Co to characterization of ZnO nanostructures. *Adv. Nat. Sci. Nanosci. Nanotechnol.* **5**, 25011 (2014).

8. N. H. Al-Hardan *et al.*, A wide-band UV photodiode based on n-ZnO/p-Si heterojunctions. *Sensors Actuators, A Phys.* **207**, 61–66 (2014).

9. M. Y. a. Rahman, a. a. Umar, R. Taslim, M. M. Salleh, Effect of surfactant on the physical properties of ZnO nanorods and the performance of ZnO photoelectrochemical cell. *J. Exp. Nanosci.* **10**, 599–609 (2015).

10. F. Bamiduro, M. B. Ward, R. Brydson, S. J. Milne, Hierarchical growth of ZnO particles by a hydrothermal route. *J. Am. Ceram. Soc.* **97**, 1619–1624 (2014).

11. A. Phuruangrat, T. Thongtem, S. Thongtem, Controlling morphologies and growth mechanism of hexagonal prisms with planar and pyramid tips of ZnO microflowers by microwave radiation. *Ceram. Int.* **40**, 9069–9076 (2014).

12. F. S. Tsai, S. J. Wang, Enhanced sensing performance of relative humidity sensors using laterally grown ZnO nanosheets. *Sensors Actuators, B Chem.* **193**, 280–287 (2014).

13. C. H. Lu, C. H. Yeh, Influence of hydrothermal conditions on the morphology and particle size of zinc oxide powder. *Ceram. Int.* **26**, 351–357 (2000).

14. S. Baruah, J. Dutta, Hydrothermal growth of ZnO nanostructures. *Sci. Technol. Adv. Mater.* **10**, 13001 (2009).

15. J. X. Zhang *et al.*, Growth of AlN films on Si (100) and Si (111) substrates by reactive magnetron sputtering. *Surf. Coatings Technol.* **198**, 68–73 (2005).

16. L. R. Yao, F. H. Lu, Low vacuum deposition of aluminum nitride thin films by sputtering. *Int. J. Appl. Ceram. Technol.* **10**, 51–59 (2013).

17. H. Jin *et al.*, Deposition of c-axis orientation aluminum nitride films on flexible polymer substrates by reactive direct-current magnetron sputtering. *Thin Solid Films.* **520**, 4863–4870 (2012).

18. H. Campanella *et al.*, Sensitivity considerations in localized mass detection based on thin-film bulk acoustic wave resonators. *Proc. - IEEE Ultrason. Symp.* **1**, 1828–1831 (2006).

19. M. R. Cho, H. S. Thatte, R. C. Lee, D. E. Golan, Integrin-dependent human macrophage migration induced by oscillatory electrical stimulation. *Ann. Biomed. Eng.* **28**, 234–43 (2000).

20. L. Khatib, D. E. Golan, M. Cho, Physiologic electrical stimulation provokes intracellular calcium increase mediated by phospholipase C activation in human osteoblasts. *FASEB J.* **18**, 1903–1905 (2004).

21. S. Meng, Z. Zhang, M. Rouabhia, Accelerated osteoblast mineralization on a conductive substrate by multiple electrical stimulation. *J. Bone Miner. Metab.* **29**, 535–544 (2011).

22. J. K. Park *et al.*, The topographic effect of zinc oxide nanoflowers on osteoblast growth and osseointegration. *Adv. Mater.* **22**, 4857–4861 (2010).

23. J. Lee *et al.*, The control of cell adhesion and viability by zinc oxide nanorods. *Biomaterials*. **29**, 3743–9 (2008).

24. B. Li, J. H. C. Wang, Application of sensing techniques to cellular force measurement. *Sensors*. **10**, 9948–9962 (2010).

25. N. Özkucur, T. K. Monsees, S. Perike, H. Q. Do, R. H. W. Funk, Local calcium elevation and cell elongation initiate guided motility in electrically stimulated osteoblast-like cells. *PLoS One*. **4**, e6131 (2009).

26. A. Marino *et al.*, Piezoelectric Nanoparticle-Assisted Wireless Neuronal Stimulation. *ACS Nano*. **9**, 7678–7689 (2015).

Supplementary materials

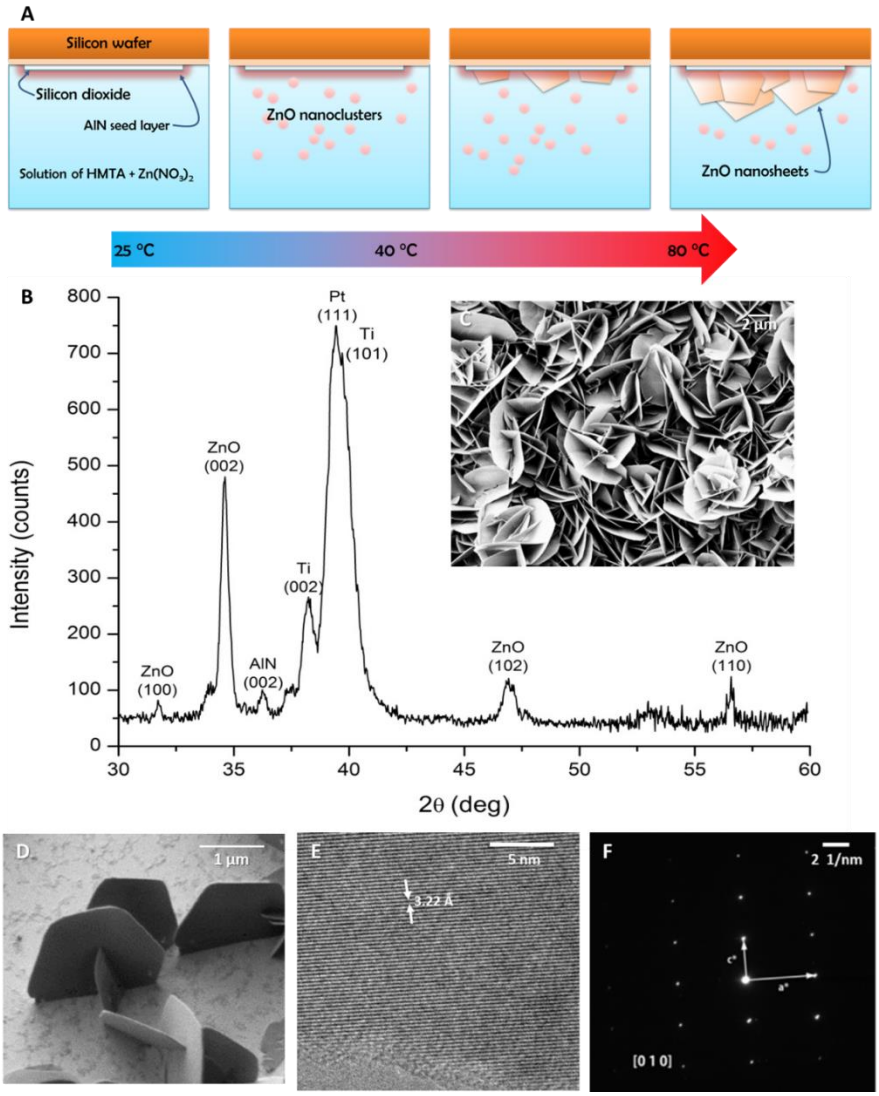

Figure S1. Physical characterization of the ZnO nanosheets (NSs). A mild hydrothermal method was used to synthesize the ZnO NS by using a special seed layer of AlN (A). XRD pattern shows good crystallinity (B) corresponding to the ZnO NSs grown over AlN shown in SEM image (C). In addition, to determine the lattice constant of a single NS (D), HRTEM was performed (E) and the associated calculated SAED image (F) shows the crystal orientation.

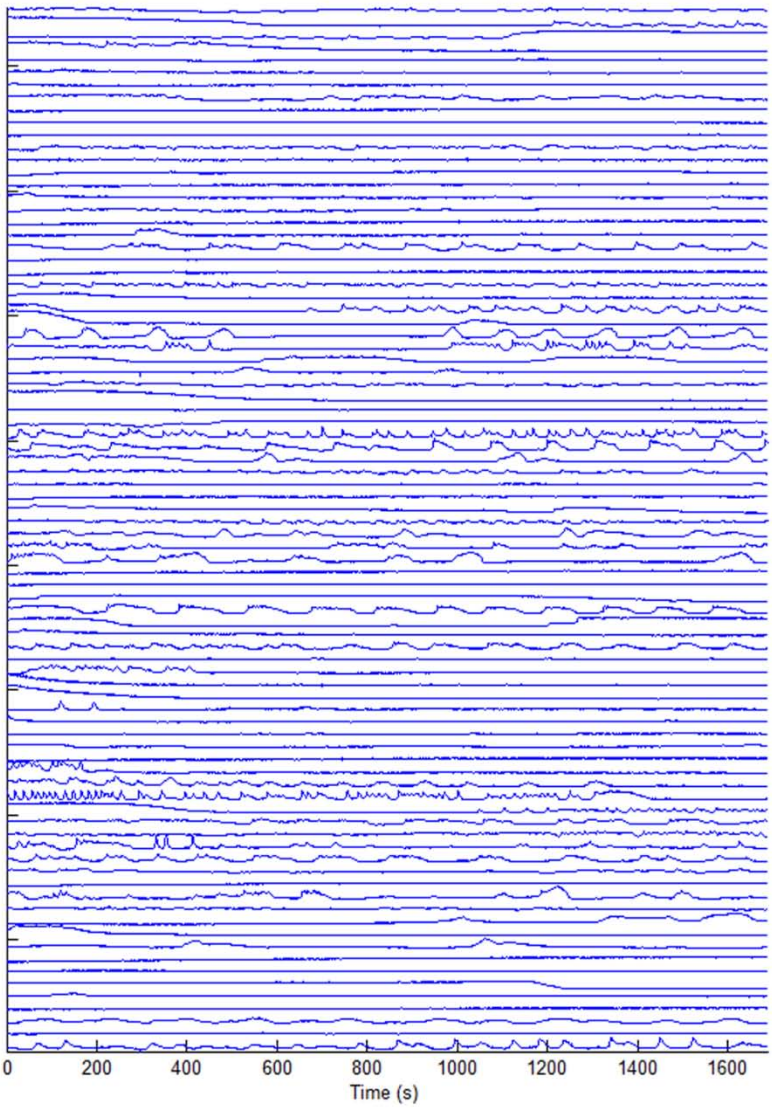

Fig. S2. Relative fluorescence intensity of Saos-2 cells cultured over thin-NGs versus time. A high number of cells present changes in their calcium concentration. The amplitude and duration of the Ca^{2+} peaks varies from cell to cell and in the same cell along time.

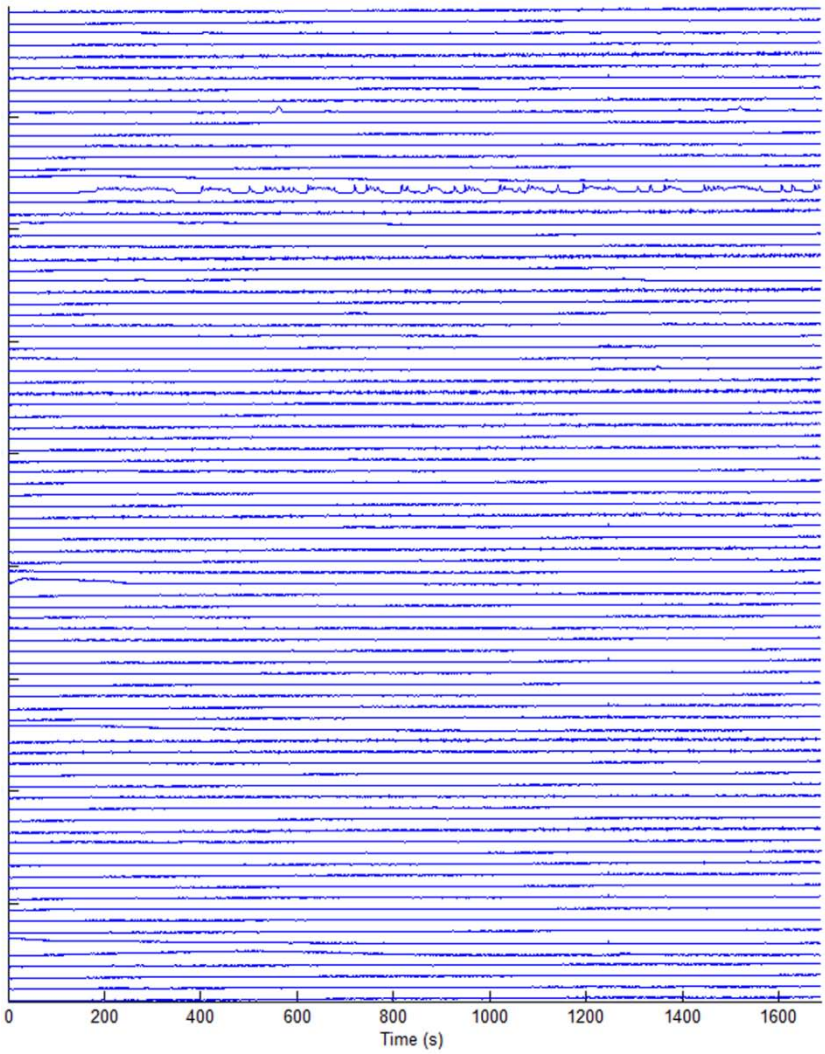

Fig. S3. Relative fluorescence intensity of Saos-2 cells cultured over thick-NG versus time. Several osteoblasts present changes in their Ca^{2+} concentration, but the amplitude of the Ca^{2+} peaks is generally low.

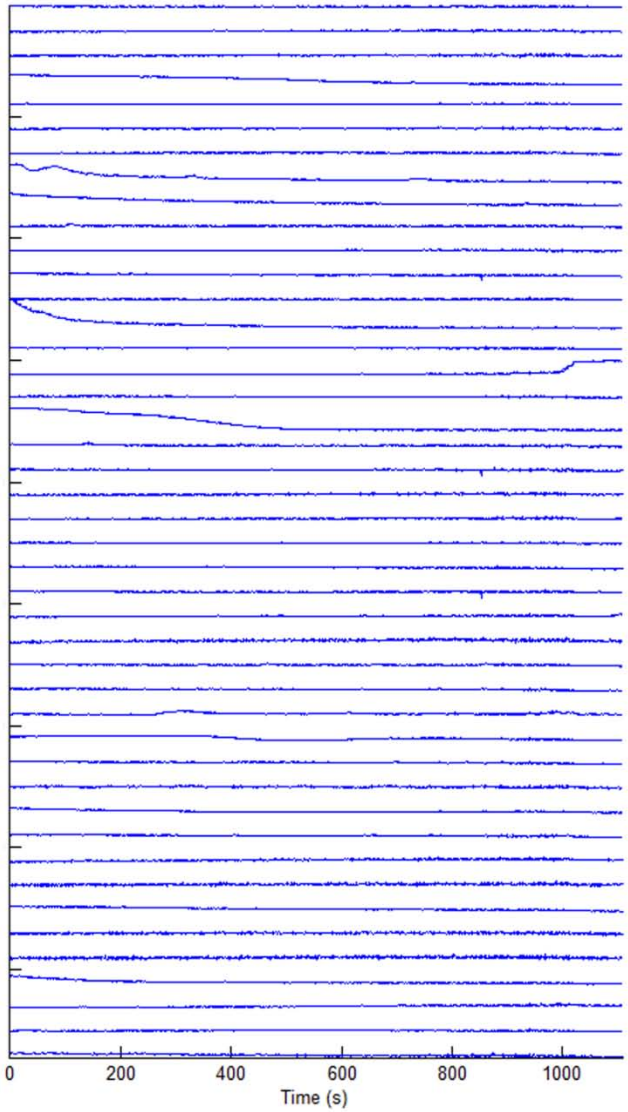

Fig. S4. Relative fluorescence intensity of Saos-2 cells cultured over glass coverslip versus time. The number of cells presenting high amplitud Ca^{2+} peaks is very low.

4. Discussion

The use of orthopaedic implants is continuously growing due to the increased demand derived from an aging population as well as from the increase in the average weight of this population (Viteri & Fuentes 2013). In this regard, development of new biomaterials with improved physical, mechanical and biocompatibility properties is of paramount importance to ensure the long-term success of the implants.

In the present thesis, we have performed in vitro biocompatibility studies of three newly synthesised Ti-based alloys and of two ZnO piezoelectric nanogenerators (NGs), with interesting properties for their use in the fabrication of new orthopaedic implants. These biocompatibility studies, performed with mouse and human cell lines, included the analysis of several key biological parameters such as cytotoxicity, cell adhesion, cell differentiation and inflammatory cytokines secretion.

4.1. Ti-based metallic alloys

The three new Ti-based alloys include a BMG (TiZrCuPd) and two crystalline alloys (TiZrPdSi and TiZrPdSiNb). The three alloys present better physical and mechanical properties than the commercial available Ti-6Al-4V alloy (Table 2). The TiZrCuPd BMG exhibits high hardness, a relatively low Young's modulus, good wear resistance and excellent corrosion behaviour (Fornell et al. 2012). On the other hand, the TiZrPdSi and TiZrPdSiNb alloys show a microstructure consisting of several phases, with a predominant beta-titanium, and additional phases in smaller volume fraction (Hynowska et al. 2014). The TiZrPdSiNb alloy has lower Young's modulus and hardness than the TiZrPdSi alloy.

Table 2. Summary of physical and mechanical properties corresponding to the three new Ti-based alloys and commercial Ti-6Al-4V.

Ti-based alloys	*Structure*	*Hardness (GPa)*	*Young´s modulus (GPa)*
$Ti_{40}Cu_{38}Zr_{10}Pd_{12}$	BMG	7.5	100
$Ti_{45}Zr_{15}Pd_{35}Si_{5}$	β-Ti	14.2	117
$Ti_{45}Zr_{15}Pd_{30}Si_{5}Nb_{5}$	β-Ti	10.4	85
Ti-6Al-4V	(α+β)-Ti	5	121

First, we studied the in vitro cytotoxicity of TiZrCuPd BMG using mouse preosteoblasts (MC3T3-E1). Among the elements used to synthesize this alloy, two of them are considered biocompatible (Ti and Zr), whereas Cu and Pd have showed controversial results (Biesiekierski et al. 2012), being reported as non-toxic by some authors and as slightly cytotoxic by others (Prigent et al. 1998; Yamamoto et al. 1998; Geurtsen 2002; Yamazaki et al. 2006). Our results showed a high viability of preosteoblasts when cultured both in the presence of medium that had been in contact with the alloy as well as directly on the surface of the alloy, suggesting that the presence of Cu and Pd in the TiZrCuPd alloy was not cytotoxic.

Next, as it has been reported that the corrosion of metallic alloys can produce cytotoxicity due to the release of metal ions and debris (Geetha et al. 2010), we analysed the release of Cu ions for 21 days in culture. The TiZrCuPd alloy showed a very fast release of Cu ions during the first 24 h, but then it slowed down, reaching the highest concentration after 7 days. In spite of this, as our viability results show, the amount of Cu released from the alloy was not enough to induce toxicity on preosteoblasts at any time-point. These results are in agreement with those of recent studies reporting that alloys containing Cu are not cytotoxic and can be considered biocompatible (Subramanian 2015; Zhang et al. 2015), probably because alloying Cu with other elements reduces the release of Cu ions into the medium (Yamazaki et al. 2012).

Since the material tested is a potential candidate to be used in orthopaedic implants in clinical applications, we decided to corroborate the cytotoxicity results obtained with mouse preosteoblasts using a human cell line. We chose the Saos-2 osteoblast-like cell line because it shows similarities with primary osteoblast cells and it is considered by other authors as the best choice for osteocompatibility studies (Czekanska et al. 2012). Results of cell viability and proliferation were similar to those obtained with mouse MC3T3-E1 preosteoblasts. Together, the results with mouse and human cells clearly demonstrated that the TiZrCuPd alloy is not cytotoxic, despite the Cu ions released and its Pd content.

On the other hand, ions released from the alloy may induce an inflammatory response, which can promote implant loosening. For this reason, we quantified inflammatory

cytokine secretion by human macrophages in response to the alloy, and we observed that the TiZrCuPd alloy and/or the Cu ions released from it did not result in an increased cytokine secretion. To our knowledge, there are no previous studies on the effect of Cu ions release on the inflammatory response, although several authors have studied the inflammatory response caused by other metal ions and particles (Wataha et al. 2004; McGinley et al. 2011).

Although some authors have suggested that alloys containing Cu are not cytotoxic, and our results agree with this idea, the use of Cu has been proposed to be avoided for new orthopaedic alloys (Abdel-Hady Gepreel & Niinomi 2013). Thus, despite the good cell viability results with the TiZrCuPd alloy, a new alloy was synthesized, TiZrPdSi, in which Cu was replaced by Si. This change in composition resulted in a higher hardness but a lower elasticity. In order to improve the elasticity, Nb was next added to the TiZrPdSi alloy, through a partial replacement of Pd. The resulting alloy, TiZrPdSiNb, presented a higher elasticity while maintaining a high hardness. None of the alloys showed cytotoxicity, and Saos-2 cells were able to proliferate on the alloys surface, indicating that the substitution of Cu by Si, and the addition of Nb does not have any effect in terms of toxicity. Si is an element considered biocompatible and widely used to fabricate wafers, nanostructures substrates and microparticles, without a cytotoxic effect (Petrochenko et al. 2014; Liskova et al. 2015; Fernández-Rosas et al. 2010). Nb is also biocompatible, cheap and often used as alloying element in orthopaedic Ti-based alloys. In fact, alloys containing Nb are being used in medicine since 1986, when the Ti-6Al-7Nb alloy was developed to replace V in the Ti-6Al-4V alloy by Nb, as V is considered a cytotoxic element. Since then, several authors have studied Ti-based alloys with Nb and have described good mechanical properties and biocompatibility, indicating the potential of these alloys to be used in implantable materials (Guo et al. 2013; Vandrovcova et al. 2014; Wang et al. 2010).

Osseointegration is necessary to ensure the stable fixation between the implant and the bone, thus avoiding implant loosening. In this sense, cell adhesion and spreading on the alloys are important parameters to analyse, because osteoblasts need to adhere in order to proliferate and differentiate. For this reason, we next studied the adhesion and morphology of cells growing on the three Ti-based alloys. Clear focal contacts and well-

developed stress fibres were observed in mouse preosteoblasts and human osteoblasts grown on the TiZrCuPd alloy, indicating that the alloy allows initial cell adhesion and spreading. Similarly, Saos-2 cells were found to adhere on TiZrPdSi and TiZrPdSiNb alloys surfaces, and spreading area and vinculin quantification showed higher values on both alloys compared with glass coverslip controls. These cell adhesion and spreading results agree with the wettability measurements, which revealed that the three Ti-based alloys were hydrophilic. Previous studies have indeed reported that cell adhesion is higher on hydrophilic surfaces than on hydrophobic ones, as the former allow the adsorption of proteins in an appropriate configuration showing their specific binding sites to be recognized by the cell adhesion receptors (Bacakova et al. 2011a). Because protein adsorption on the alloy surface is important for cell adhesion, we studied the adsorption of albumin (non-adhesion protein) and fibronectin (adhesion promoter protein) on TiZrPdSi and TiZrPdSiNb alloys, and results showed an increase in the adsorption of both proteins on the TiZrPdSiNb alloy. However, adhesion and spreading of Saos-2 cells were similar in cells grown on top of both alloys, probably because the higher amount of albumin adsorbed on top of the TiZrPdSiNb alloy is compensated by the higher amount of fibronectin also adsorbed.

The studies described so far were performed with mirror-like surfaces of the Ti-based alloys. But because several authors have described that osseointegration can be enhanced by microrough and nanorough surfaces (Deng et al. 2014; Li et al. 2012), we next analysed the effect of two surface modifications of the TiZrCuPd alloy and of the commercially available Ti-6Al-4V alloy on Saos-2 cells viability, adhesion and morphology. A physical modification was performed to obtain a microscratched surface, whereas an electrochemical polarization was performed to obtain a nanomesh surface. Whereas the physical modification did not result in changes in surface composition of the alloys, electrochemical polarization resulted in the formation of a layer rich in Ti and Cu oxides on the TiZrCuPd alloy and rich in Ti oxides on the Ti-6Al-4V alloy. The presence of an oxide layer is important for corrosion resistance of alloys, because it protects the alloy against chemical attacks and reduces the corrosion rate (Geetha et al. 2009). In addition, it has been described that the Ti oxide layer is biocompatible and enhances the cellular response (Yang & Huang 2010; Vandrovcova et al. 2012; Patel et al. 2014). In spite of

this, viability of cells was similarly high on all types of surfaces, suggesting that, in our case, the presence of the oxide layer had no apparent effect on cell viability. Although the high cell viability indicated that cells were able to adhere to all surfaces, we decided to measure the wettability of the surfaces and the initial cell attachment. Wettability measurements were, in all cases, in the range considered hydrophilic, with only minor differences among surfaces, and cell adhesion occurred in all cases. The only substantial effect of surface modifications was seen on cell orientation. In particular, the long axis of the cells was clearly oriented along the parallel grooves of the microscratched surfaces, in agreement with observations by other authors (reviewed by Curtis & Wilkinson 1997).

In addition to cell adhesion and spreading, osteoblast differentiation plays a major role in osseointegration. For this reason, we analysed the capacity of osteoblasts to differentiate on the three Ti-based alloys and on the different topographies of the TiZrCuPd and control Ti-6Al-4V alloys. Regarding the effect of the alloy composition, the mirror-like TiZrCuPd BMG allowed the differentiation of mouse and human osteoblasts, measured as extracellular matrix mineralization. These results, together with the cell viability and adhesion results, are in agreement with other studies that have demonstrated the biocompatibility and osteoblast differentiation on Ti-based and Zr-based BMGs (Oak et al. 2009; Huang et al. 2012; Li et al. 2012). On the other hand, the differentiation of Saos-2 cells grown on the TiZrPdSi and TiZrPdSiNb alloys, with a predominant β-Ti phase, was assessed by analysing the transcription of osteogenic marker genes, protein synthesis and ALP activity, quantified at different culture time-points. Noteworthily, the results obtained using these different methodologies were consistent. In global, the expression and activity of protein markers in cells cultured during 7 days were similar or higher for cells growing on the alloys than on the glass controls surface, and minimal differences among alloys and control were observed at 14 days. These results are in agreement with those of others using β-Ti alloys (Jirka et al. 2013; Guo et al. 2013), indicating that this microstructure is excellent in terms of biocompatibility and osteoblasts differentiation.

Osteoblasts differentiation on the different topographies of the TiZrCuPd and Ti-6Al-4V alloys was next analysed by ECM mineralization and ALP activity, in order to determine whether surface modifications of the alloy alter the cell differentiation process.

Similar to the differences in terms of cell viability, proliferation and adhesion, cell differentiation was also equivalent among the three topographies and alloy compositions. Several authors have described the effect of micro- and nanoroughness on cell response. In general, authors agree that cells are able to recognize topography (Anselme et al. 2010), but there is no consensus about which scale and morphology is better for osseointegration. On the one hand, it has been described that microrough surfaces enhance cell adhesion, proliferation and differentiation. For example, human mesenchymal stem cells showed a more differentiated phenotype to osteoblasts on microrough and submicrorough surfaces than on smooth ones (Gittens et al. 2012; Mendonça et al. 2011). Moreover, osteoblasts seem to attach, proliferate and differentiate better on microrough surfaces compared to smoother ones (Li et al. 2012; Huang et al. 2011; Olivares-Navarrete et al. 2014). On the other hand, nanorough surfaces have been described to improve cell adhesion, viability and differentiation of osteoblasts (Deng et al. 2014; Gittens et al. 2012; Zareidoost et al. 2012). The unclear relation between topography and cell behaviour could be attributed to the different types of topographies used in these studies and the lack of consensus for their characterization, as indicated by Anselm et al. (Anselme et al. 2010). In addition, surface modification can result in changes in wettability and surface charge, which can affect cell adhesion and differentiation, and obscure the effects of the topography. Another parameter to take into account is that the cell response to topography varies depending on the relationship between cell size and the size of the features present on the material surface (Anselme et al. 2010). All these variables hinder the comparison between results obtained in the different studies reported in the literature, in which different materials, surface modifications and cell lines are used. To clarify the effect of topography on cell behaviour, these variables should be taken into account, and the studies should be performed using the same cell line and trying to minimize the changes in wettability and surface chemistry when modifying the topography. In line with this, in our study we used the same alloy composition for all topographies and the same cell line. Still, as previously mentioned, electrochemical polarization used to obtain the nanomesh surface inevitably resulted in changes in surface chemistry when compared with microscratched and mirror-like surfaces.

4.2. Piezoelectric materials

Piezoelectric materials are smart materials that can generate an electrical activity in response to minute deformations, constituting promising materials to be used in orthopaedic and tissue engineering applications (Rajabi et al. 2015). In this thesis, we used two new piezoelectric NGs consisting of arrays of ZnO hexagonal nanosheets grown on an AlN thin-film acting as seed layer.

To assess the biocompatibility of the newly developed NGs, we used two cell lines with an important role on osseointegration, macrophages derived from human THP-1 monocytes and human Saos-2 osteoblast-like cells. Macrophages are phagocytic cells involved in the immunological response, whereas Saos-2 cells are bone cells that can respond to electrical stimulation (Özkucur et al. 2009; Griffin et al. 2013). The same experiments performed to assess the biocompatibility of Ti-based alloys were carried out with the two NGs. The results with macrophages indicated that the two types of NGs were not cytotoxic and allowed cell adhesion. Likewise, Saos-2 cells cultured on ZnO nanosheets showed a high viability, good cell adhesion with detectable focal contacts, and a similar proliferation rate as cells grown on AlN control. In addition, the two NGs allowed osteoblast differentiation up to 14 days in culture. Several authors have studied the biocompatibility of other nanostructures made of ZnO with controversial results. For example, ZnO films have shown an antibacterial effect, which can be a key point to avoid infections in biomedical implants (Colon et al. 2006; Petrochenko et al. 2013). On the other hand, hydroxyapatite-ZnO composites allowed cell attachment, spreading and proliferation of eukaryotic cells, like osteoblasts and fibroblasts (Saha et al. 2012). Results for ZnO nanorods showed that adhesion and viability of anchorage-dependent cells was reduced, indicating that these substrates cannot be used for biomedical implants when cell adhesion is needed (Lee et al. 2008; Zaveri et al. 2010). In contrast, ZnO nanoflowers improved mouse MC3T3-E1 osteoblast adhesion, proliferation and differentiation when compared with ZnO films, although cell adhesion and differentiation were higher on polystyrene control (Park et al. 2010). All of these results suggest that ZnO biocompatibility may depend on its structure. In our case, the results for ZnO nanosheets demonstrated their biological safety in in vitro studies and make them potential candidates for the use in bone repair and other clinical applications.

With regard to cells-material interaction, lateral images and FIB cross-sections observed by SEM showed a direct contact between macrophages or Saos-2 cells and the ZnO nanosheets. Cells adapted to the surface shape, covering the nanosheets, and emitted multiple long projections that attached to the nanosheet surface. Because of this, stress fibres could not cross the cell as lineal and parallel bundles, as usually observed in cells cultured on flat surfaces, but were instead observed as short fibres surrounding the nanosheets. However, this irregular distribution did not disturb cell adhesion, as previously mentioned.

On the other hand, it is well-known that topography can modulate macrophage motility (Wójciak-Stothard et al. 1995). Recording and analysis of macrophages trajectories on the two NGs over the course of four hours showed that macrophages cultured on thick-NGs, with a thickness of 40 nm, moved more than those cultured on thin-NGs, with a thickness of 20 nm. Moreover, cells moved more on both NGs than on AlN control. Cell migration can be regulated by the extent of initial cell adhesion, and cells are more active in migration and proliferation when the adhesion strength is weak (Bacakova et al. 2004). Although focal adhesions were observed in macrophages cultured in both NGs and AlN surfaces, it is possible that macrophages grown on thick-NGs presented a weaker adhesion strength than those grown on the thin-NGs and the AlN surfaces, due to the topography, and this would explain their increase motility. On the other hand, it has been reported that direct current fields can stimulate macrophage migration along the electric fields lines (Cho et al. 2000). In our case, the constant movement of macrophages on the NGs could bend the nanosheets, resulting in the generation of an electric field that would in turn intensify macrophage migration. This could explain the enhanced motility of macrophages on the NGs, compared with the AlN control. Thus, in our study, macrophages motility could be influenced by the topography and/or the generated electric field.

Adhesion and movement of Saos-2 cells on the NGs could also result in the generation of an electric field. As Saos-2 cells presented local voltage-gated Ca^{2+} channels (VGCCs) in their plasma membrane (Özkucur et al. 2009), this electric field could induce changes in their intracellular Ca^{2+} concentration. Quantification of intracellular Ca^{2+} levels over a period of 30 min showed that in Saos-2 cells grown on thin NGs, a higher percentage of

cells displayed increases in the intracellular Ca^{2+} levels than in cells grown on thick NGs. As expected, changes in intracellular Ca^{2+} concentration were rarely observed on cells grown on the glass control. Differences observed between the two NGs can be explained because the thin-NG generates a higher piezopotential for the same force, and the mean electrical excitation created by the thick-NG was probably insufficient to trigger the opening of Ca^{2+} channels in the majority of the cells cultured on this material.

Ca^{2+} is a second messenger involved in multiple signal transduction pathways leading to cytoskeleton reorganization, cell proliferation and cell differentiation. The Ca^{2+} concentration in the cytosol of resting cells is very low, but when signalling is activated, a large increase occurs due to the release of Ca^{2+} ions from intracellular stores (endoplasmic reticulum, mainly) and/or to the entry of Ca^{2+} ions into the cell through plasma membrane ion channels. In the case of excitable cells, like osteoblasts, at least three types of Ca^{2+} channels can be involved in the response of electrical stimulation: VGCCs, stretch-activated cation channels (SACCs), and the inositol triphosphate receptor (Khatib et al. 2004). The first two are located on the plasma membrane whereas the third is located on the endoplasmic reticulum membrane and opens through the binding of inositol triphosphate released from the plasma membrane in response to the activation of certain cell surface receptors. The type of channels that open in response to an electric field depends on the voltage. According to Özkucur et al. (2009), electric fields of 2 V/cm activate the release of Ca^{2+} from intracellular stores, whereas exposures to 14 V/cm open the VGCCs. In our work, the voltage of the electric field generated by the two NGs is different. Moreover, the mechanical stress produced by each osteoblast every time it moves may also differ, depending on the intensity of the strength necessary to adhere to the nanosheets. Thus, the local voltage produced by each osteoblast and by each osteoblast movement may vary, making it difficult to predict which type of Ca^{2+} channels are responsible for the observed Ca^{2+} transients. Further experiments could be performed in the future, using specific inhibitors for each type of channel, to elucidate their contribution in the cytosolic Ca^{2+} increase induced by the piezoelectric NGs.

Repetitive increases in intracellular Ca^{2+} concentration could disturb important intracellular pathways mediated by Ca^{2+}. However, in spite that Saos-2 cells grown on thin-NGs presented several Ca^{2+} spikes during the 30 min of the assay, they remained

viable, proliferated and were able to differentiate after 14 days on the piezoelectric material. Therefore, neither the repetitive electric stimulation to which the cells were supposedly exposed to, nor the repetitive Ca^{2+} influxes that they supposedly underwent during this 14 day period had a cytotoxic effect.

Due to their biological safety, piezoelectric NGs have a potential use in bone regeneration and neuro-muscular applications. Bone has natural piezoelectric properties, where mechanical stress produces electrical signals that promote bone growth and remodeling. At the cellular level, several studies have demonstrated that electrical stimulation can enhance osteogenic activities (Ribeiro et al. 2015). In this regard, the activation effect created by the NGs in Saos-2 cells could lead to new bone regeneration methods or be extrapolated to other electrostimulable cells such as neurons and muscle cells, paving the way for future bioelectronic medicines based on cell-targeted local electrical impulses instead of common drugs.

In summary, the biocompatibility study of new materials with potential applications in medicine is of outmost importance to ensure their biosafety. All the studies presented in this thesis assess the biological response of new materials using in vitro techniques. We used cell types with an important role in osseointegration to test candidate materials for orthopaedic applications, and to perform several cell biology methodologies that allow to analyse a large variety of biocompatibility parameters. We demonstrated that all the alloys tested, with better mechanical properties than the alloys currently used, are biocompatible. Changes in topography did not modify the cellular response, and all topographies assessed presented good biological parameters. On the other hand, a new smart material with interesting piezoelectric properties for its use in several biomedical devices, has also been studied and determined to be safe and to stimulate cellular response. The results obtained in our studies contribute to the progress in the development of better materials for bone repair and regeneration.

5. Conclusions

1. TiZrCuPd bulk metallic glass allows mouse preosteoblasts and human osteoblast-like cells adhesion, proliferation and differentiation. Moreover, it does not induce the secretion of inflammatory cytokines by human macrophages. Thus, it can be considered a biocompatible material.

2. Electrochemical anodization and microscratched physical modification of TiZrCuPd and commercial Ti-6Al-4V alloy surfaces have no effect on osteoblast-like cells behaviour, allowing cell adhesion, proliferation and differentiation.

3. TiZrPdSi and TiZrPdSiNb alloys are biocompatible and enhance osteoblast-like cells adhesion, spreading and proliferation.

4. The study of osteoblast differentiation on TiZrPdSi and TiZrPdSiNb alloys using three different methodologies, osteogenic genes expression, protein quantification and protein activity, provided concordant results, and demonstrated that cells can differentiate on both alloys.

5. Piezoelectric nanogenerators based on a network of two-dimensional ZnO nanosheets are biocompatible for human macrophages and osteoblast-like cells.

6. The electrochemical nanogenerators-cells interactions were able to stimulate macrophages motility and to trigger the opening of ion channels present in the membrane of osteoblast-like cells inducing intracellular calcium transients. Thus, the piezoelectric nanogenerators developed are capable of altering cell behaviour, opening the door to the local stimulation of electrically responding cells.

6. References

A

Abdel-Hady Gepreel, M. & Niinomi, M., 2013. Biocompatibility of Ti-alloys for long-term implantation. *Journal of the Mechanical Behavior of Biomedical Materials*, 20, pp.407–415.

Aerssens, J. et al., 1998. Interspecies differences in bone composition, density, and quality: Potential implications for in vivo bone research. *Endocrinology*, 139(2), pp.663–670.

Aksakal, B., Yildirim, Ö.S. & Gul, H., 2004. Metallurgical Failure Analysis of Various Implant Materials Used in Orthopedic Applications. *Journal of Failure Analysis & Prevention*, 4(3), pp.17–23.

Alberts, B. et al., 2014. *Molecular Biology of the Cell*, 6th edn. Garland Science, Taylor & Francis Group, New York, US.

Anselme, K. & Bigerelle, M., 2014. On the relation between surface roughness of metallic substrates and adhesion of human primary bone cells. *Scanning*, 36, pp.11–20.

Anselme, K., Ploux, L. & Ponche, a, 2010. Cell/Material Interfaces: Influence of Surface Chemistry and Surface Topography on Cell Adhesion. *Journal of Adhesion Science and Technology*, 24(5), pp.831–852.

B

Bacakova, L. et al., 2004. Cell adhesion on artificial materials for tissue engineering. *Physiol Res*, 53 Suppl 1, pp.S35–45.

Bacakova, L. et al., 2011. Modulation of cell adhesion, proliferation and differentiation on materials designed for body implants. *Biotechnology Advances*, 29(6), pp.739–767.

Badami, V. & Ahuja, B., 2014. Biosmart materials: Breaking new ground in dentistry. *The Scientific World Journal*, 2014.

Beyersmann, D. & Hartwig, A., 2008. Carcinogenic metal compounds: recent insight into molecular and cellular mechanisms. *Archives of Toxicology*, 82(8), pp.493–512.

Biesiekierski, A. et al., 2012. A new look at biomedical Ti-based shape memory alloys. *Acta Biomaterialia*, 8(5), pp.1661–1669.

Bitar, D., 2015. Biological response to prosthetic debris. *World Journal of Orthopedics*, 6(2), p.172.

Bordignon, V. et al., 2008. Nickel, palladium and rhodium induced IFN-gamma and IL-10 production as assessed by in vitro ELISpot-analysis in contact dermatitis patients. *BMC immunology*, 9, p.19.

Branemark, P. et al., 1964. Regeneration of bone marrow. *Acta anat*, 59, pp.1–46.

Branemark, P.I., 1983. Osseointegration and its experimental background. *The Journal of Prosthetic Dentistry*, 50(3), pp.399–410.

Burger, E.H., Klein-Nulend, J. & Smit, T.H., 2003. Strain-derived canalicular fluid flow regulates osteoclast activity in a remodelling osteon - A proposal. *Journal of Biomechanics*, 36, pp.1453–1459.

C

Caicedo, M.S. et al., 2009. Soluble and particulate Co-Cr-Mo alloy implant metals activate the inflammasome danger signaling pathway in human macrophages: A novel mechanism for implant debris reactivity. *Journal of Orthopaedic Research*, 27(July), pp.847–854.

Chang, H. & Wang, Y., 2011. Cell responses to surface and architecture of tissue engineering scaffolds. *Regenerative Medicine and Tissue Engineering - Cells and Biomaterials*, pp.569–588.

Cho, M.R. et al., 2000. Integrin-dependent human macrophage migration induced by oscillatory electrical stimulation. *Annals of biomedical engineering*, 28(3), pp.234–43.

Clarke, B., 2008. Normal Bone Anatomy and Physiology. *Clinical Journal of the American Society of Nephrology*, 3(Supplement 3), pp.S131–S139.

Colon, G., Ward, B.C. & Webster, T.J., 2006. Increased osteoblast and

decreasedStaphylococcus epidermidis functions on nanophase ZnO and TiO2. *Journal of Biomedical Materials Research Part A*, 78A(3), pp.595–604.

Curtis, A. & Wilkinson, C., 1997. Topographical control of cells. *Biomaterials*, 18(24), pp.1573–1583.

Czekanska, E.M. et al., 2012. In search of an osteoblast cell model for in vitro research. *European Cells and Materials*, 24, pp.1–17.

D

Dalby, M.J. et al., 2004. Changes in fibroblast morphology in response to nano-columns produced by colloidal lithography. *Biomaterials*, 25(23), pp.5415–5422.

Deng, Z. et al., 2014. Surface characteristics of and in vitro behavior of osteoblast-like cells on titanium with nanotopography prepared by high-energy shot peening. *International journal of nanomedicine*, 9, pp.5565–5573.

Disegi, J.A., 2000. Stainless steel in bone surgery. , 31.

Dobnig, H. & Turner, R.T., 1995. Evidence that intermittent treatment with parathyroid hormone increases bone formation in adult rats by activation of bone lining cells. *Endocrinology*, 136(8), pp.3632–3638.

E

Eisenstein, M., 2013. Neurodevice startups target peripheral nervous system. *Nature Biotechnology*, 31(10), pp.865–866. Available at:

El-Rahman, S.S.A., 2003. Neuropathology of aluminum toxicity in rats (glutamate and GABA impairment). *Pharmacological Research*, 47, pp.189–194.

F

Faurschou, A. et al., 2011. Metal allergen of the 21st century - A review on exposure, epidemiology and clinical manifestations of palladium allergy. *Contact Dermatitis*, 64(4), pp.185–195.

Fernández-Rosas, E. et al., 2010. Internalization and cytotoxicity analysis of silicon-based microparticles in macrophages and embryos. *Biomedical Microdevices*, 12(3), pp.371–379.

Finke, B. et al., 2007. The effect of positively charged plasma polymerization on initial osteoblastic focal adhesion on titanium surfaces. *Biomaterials*, 28(30), pp.4521–4534.

Fornell, J. et al., 2012. Deformation and fracture behavior of corrosion-resistant, potentially biocompatible, Ti40Zr10Cu38Pd12 bulk metallic glass. *Journal of Alloys and Compounds*, 536, pp.S74–S77.

Fukada, E. & Yasuda, I., 1957. On the piezoelectric effect of bone. *J. Phys. Soc. Japan*, 12(10), pp.1158–1162.

G

Geetha, M. et al., 2009. Ti based biomaterials, the ultimate choice for orthopaedic implants – A review. *Progress in Materials Science*, 54, pp.397–425.

Geetha, M., Durgalakshmi, D. & Asokamani, R., 2010. Biomedical Implants: Corrosion and its Prevention - A Review. *Recent Patents on Corrosion Science*, 2(1), pp.40–54.

Geurtsen, W., 2002. Biocompatibility of dental casting alloys. *Critical reviews in oral biology and medicine : an official publication of the American Association of Oral Biologists*, 13(1), pp.71–84.

Gittens, R.A. et al., 2012. Differential responses of osteoblast lineage cells to nanotopographically-modified, microroughened titanium–aluminum–vanadium alloy surfaces. *Biomaterials*, 33(35), pp.8986–8994.

Goriainov, V. et al., 2014. Bone and metal: An orthopaedic perspective on osseointegration of metals. *Acta Biomaterialia*, 10(10), pp.4043–4057.

Griffin, M. et al., 2013. Enhancement of Differentiation and Mineralisation of Osteoblast-like Cells by Degenerate Electrical Waveform in an In Vitro Electrical Stimulation Model Compared to Capacitive Coupling M. Soncini, ed. *PLoS ONE*,

8(9), p.e72978.

Grossmann, J. et al., 2001. Apoptotic signaling during initiation of detachment-induced apoptosis ("anoikis") of primary human intestinal epithelial cells. *Cell growth & differentiation : the molecular biology journal of the American Association for Cancer Research*, 12(March), pp.147–155.

Guo, Y. et al., 2013. Corrosion resistance and in vitro response of a novel Ti35Nb2Ta3Zr alloy with a low Young's modulus. *Biomedical Materials*, 8(5), p.055004.

H

Häfeli, U.O., Aue, J. & Damani, J., 2007. The biocompatibility and toxicity of magnetic particles. In *Laboratory Techniques in Biochemistry and Molecular Biology*. pp. 163–223.

Hallab, N.J. et al., 2005. Effects of soluble metals on human peri-implant cells. *Journal of Biomedical Materials Research Part A*, 74A(1), pp.124–140.

Hamlet, S. & Ivanovski, S., 2011. Inflammatory cytokine response to titanium chemical composition and nanoscale calcium phosphate surface modification. *Acta Biomaterialia*, 7(5), pp.2345–2353.

Harb, A., 2011. Energy harvesting: State-of-the-art. *Renewable Energy*, 36(10), pp.2641–2654.

Hermawan, H., Ramdan, D. & P. Djuansjah, J.R., 2011. Metals for Biomedical Applications. In *Biomedical Engineering - From Theory to Applications*. InTech.

Horowitz, S.M. & Gonzales, J.B., 1996. Inflammatory response to implant particulates in a macrophage/osteoblast coculture model. *Calcified Tissue International*, 59(5), pp.392–396.

Hua, N. et al., 2014. Biocompatible Ni-free Zr-based bulk metallic glasses with high-Zr-content: compositional optimization for potential biomedical applications. *Materials science & engineering. C, Materials for biological applications*, 44, pp.400–10.

Huang, L. et al., 2013. Macrophage responses to a Zr-based bulk metallic glass. *Journal of Biomedical Materials Research - Part A*, pp.1–10.

Huang, L. et al., 2012. Ni-free Zr-Cu-Al-Nb-Pd bulk metallic glasses with different Zr/Cu ratios for biomedical applications. *Journal of Biomedical Materials Research - Part B Applied Biomaterials*, 100 B(6), pp.1472–1482.

Huang, L. et al., 2011. Responses of bone-forming cells on pre-immersed Zr-based bulk metallic glasses: Effects of composition and roughness. *Acta Biomaterialia*, 7(1), pp.395–405.

Hynowska, A., 2014. Biocompatible Ti-based metallic glasses and nanocomposite materials. , (September).

Hynowska, A. et al., 2014. Nanostructured Ti-Zr-Pd-Si- (Nb) bulk metallic composites : Novel biocompatible materials with superior mechanical strength and elastic recovery. *Journal of Biomedical Material Research Part B: Applied Biomaterials*, online, pp.1–11.

I

Ikeda, M., Komatsu, S. & Nakamura, Y., 2004. Effects of Sn and Zr Additions on Phase Constitution and Aging Behavior of Ti-50 mass%Ta Alloys Quenched from β Single Phase Region. *Materials Transactions*, 45(4), pp.1106–1112.

Imai, Y. et al., 2013. Nuclear Receptors in Bone Physiology and Diseases. *Physiological Reviews*, 93(2), pp.481–523.

Inoue, A., 2000. Stabilization of metallic supercooled liquid and bulk amorphous alloys. *Acta Materialia*, 48(1), pp.279–306.

J

Jirka, I. et al., 2013. On the role of Nb-related sites of an oxidized beta-TiNb alloy surface in its interaction with osteoblast-like MG-63 cells. *Materials Science and Engineering: C*, 33(3), pp.1636–1645.

K

Keselowsky, B.G., Collard, D.M. & García, A.J., 2004. Surface chemistry modulates focal adhesion composition and signaling through changes in integrin binding. *Biomaterials*, 25, pp.5947–5954.

Khatib, L., Golan, D.E. & Cho, M., 2004. Physiologic electrical stimulation provokes intracellular calcium increase mediated by phospholipase C activation in human osteoblasts. *The FASEB journal : official publication of the Federation of American Societies for Experimental Biology*, 18(15), pp.1903–1905.

Kim, I.S. et al., 2006. Biphasic electric current stimulates proliferation and induces VEGF production in osteoblasts. *Biochimica et Biophysica Acta (BBA) - Molecular Cell Research*, 1763(9), pp.907–916.

L

Lee, D.H. et al., 2006. Effects of hydrogen peroxide (H2O2) on alkaline phosphatase activity and matrix mineralization of odontoblast and osteoblast cell lines. *Cell Biology and Toxicology*, 22(1), pp.39–46.

Lee, J. et al., 2008. The control of cell adhesion and viability by zinc oxide nanorods. *Biomaterials*, 29(27), pp.3743–9.

Li, H.F. et al., 2012. Osteoblast response on Ti- and Zr-based bulk metallic glass surfaces after sand blasting modification. *Journal of Biomedical Materials Research - Part B Applied Biomaterials*, 100 B(7), pp.1721–1728.

Lian, J.B. & Stein, G.S., 1995. Development of the osteoblast phenotype: molecular mechanisms mediating osteoblast growth and differentiation. *The Iowa orthopaedic journal*, 15, pp.118–140.

Liskova, J. et al., 2015. Osteogenic cell differntation on H-terminated and O-terminated nanocrystalline diamond films. *International journal of nanomedicine*, 10, pp.1–16.

M

Mantripragada, V.P. et al., 2013. An overview of recent advances in designing orthopedic and craniofacial implants. *Journal of Biomedical Materials Research - Part A*, 101, pp.3349–3364.

Marino, A. et al., 2015. Piezoelectric Nanoparticle-Assisted Wireless Neuronal Stimulation. *ACS Nano*, 9(7), pp.7678–7689.

Matsuno, H. et al., 2001. Biocompatibility and osteogenesis of refractory metal implants, titanium, hafnium, niobium, tantalum and rhenium. *Biomaterials*, 22(11), pp.1253–1262.

McGinley, E.L., Fleming, G.J.P. & Moran, G.P., 2011. Development of a discriminatory biocompatibility testing model for non-precious dental casting alloys. *Dental Materials*, 27(12), pp.1295–1306.

McKee, G.K. & Watson-Farrar, J., 1966. Replacement of arthritic hips by the McKee-Farrar prosthesis. *The Journal of bone and joint surgery. British volume*, 48(2), pp.245–259.

Mendonça, D.B.S. et al., 2011. Titanium surface topography affects collagen biosynthesis of adherent cells. *Bone*, 49(3), pp.463–472.

Meng, S., Zhang, Z. & Rouabhia, M., 2011. Accelerated osteoblast mineralization on a conductive substrate by multiple electrical stimulation. *Journal of Bone and Mineral Metabolism*, 29(5), pp.535–544.

Minagar, S. et al., 2013. Cell response of anodized nanotubes on titanium and titanium alloys. *Journal of biomedical materials research. Part A*, 101(9), pp.2726–2739.

Mitra, S.K., Hanson, D.A. & Schlaepfer, D.D., 2005. Focal adhesion kinase: in command and control of cell motility. *Nature review of Molecular Cell Biology*, 6(1), pp.56–68.

N

Nakashima, Y. et al., 1999. Signaling pathways for tumor necrosis factor-alpha and interleukin-6 expression in human macrophages exposed to titanium-alloy particulate debris in vitro. *The Journal of bone and joint surgery. American volume*, 81(5), pp.603–15.

Navarro, M. et al., 2008. Biomaterials in orthopaedics. *Journal of the Royal Society, Interface / the Royal Society*, 5(October), pp.1137–1158.

Niinomi, M. & Boehlert, C.J., 2015. *Advances in Metallic Biomaterials*.

Novotna, K. et al., 2013. Adhesion and growth of vascular smooth muscle cells on nanostructured and biofunctionalized polyethylene. *Materials*, 6, pp.1632–1655.

O

Oak, J.-J. et al., 2009. Characterization of Surface Properties, Osteoblast Cell Culture in Vitro and Processing with Flow-Viscosity of Ni-Free Ti-Based Bulk Metallic Glass for Biomaterials. *Journal of Biomechanical Science and Engineering*, 4(3), pp.384–391.

Okazaki, Y. et al., 1998. Corrosion resistance, mechanical properties, corrosion fatigue strength and cytocompatibility of new Ti alloys without Al and V. *Biomaterials*, 19(13), pp.1197–1215.

Olivares-Navarrete, R. et al., 2014. Osteoblast lineage cells can discriminate microscale topographic features on titanium-aluminum-vanadium surfaces. *Annals of biomedical engineering*, 42(12), pp.2551–61.

Orthopedicimplants.wordpress.com, 2009. 05 February 2009. https://orthopedicimplants.wordpress.com/2009/02/05/.

Özkucur, N. et al., 2009. Local calcium elevation and cell elongation initiate guided motility in electrically stimulated osteoblast-like cells. *PLoS ONE*, 4(7), p.e6131.

P

Pan, H.-A. et al., 2012. Nanosurface design of dental implants for improved cell growth and function. *Nanotechnology*, 23(33), p.335703.

Park, J.K. et al., 2010. The topographic effect of zinc oxide nanoflowers on osteoblast growth and osseointegration. *Advanced Materials*, 22, pp.4857–4861.

Passeri, G. et al., 2010. Adhesion pattern and growth of primary human osteoblastic cells on five commercially available titanium surfaces. *Clinical oral implants research*, 21, pp.756–765.

Patel, S.B. et al., 2014. Enhancing surface characteristics of Ti–6Al–4V for bio-implants using integrated anodization and thermal oxidation. *Journal of Materials Chemistry B*, 2(23), p.3597.

Patrascu, I. et al., 2014. Corrosion of Biomaterials Used in Dental Reconstruction Dentistry. In *Developments in Corrosion Protection*. InTech.

Pellegrin, S. & Mellor, H., 2007. Actin stress fibres. *Journal of cell science*, 120, pp.3491–3499.

Pellicer, E. et al., 2013. On the biodegradability, mechanical behavior, and cytocompatibility of amorphous Mg72 Zn23 Ca5 and crystalline Mg70 Zn23 Ca5 Pd2 alloys as temporary implant materials. *Journal of biomedical materials research. Part A*, 101(2), pp.502–17.

Petrochenko, P.E. et al., 2014. Cytotoxic evaluation of nanostructured zinc oxide (ZnO) thin films and leachates. *Toxicology in vitro : an international journal published in association with BIBRA*, 28(6), pp.1144–52.

Petrochenko, P.E. et al., 2013. Cytotoxicity of cultured macrophages exposed to antimicrobial zinc oxide (ZnO) coatings on nanoporous aluminum oxide membranes. *Biomatter*, 3(3), p.e25528.

Pizzoferrato, A. et al., 2002. Inflammatory response to metals and ceramics. In R. Barbucci, ed. *Integrated Biomaterial Science*. New York: Kluwer Academic/plenum

Publishers, pp. 735–791.

Popp, J. et al., 2011. In vitro evaluation of osteoblastic differentiation on amorphous calcium phosphate-decorated poly(lactic-co-gylolic acid) scaffolds. *Journal of tissue engineering and regenerative medicine*, 5, pp.780–789.

Postiglione, L. et al., 2004. Different titanium surfaces modulate the bone phenotype of SaOS-2 osteoblast-like cells. , pp.213–222.

Prigent, H. et al., 1998. Evaluation of the biocompatibility of titanium-tantalum alloy versus titanium. *Journal of Biomedical Materials Research*, 39(2), pp.200–206.

R

Rajabi, A.H., Jaffe, M. & Arinzeh, T.L., 2015. Piezoelectric materials for tissue regeneration: A review. *Acta Biomaterialia*, 24, pp.12–23.

Rajzer, I. et al., 2010. In vitro and in vivo studies on biocompatibility of carbon fibres. *Journal of Materials Science: Materials in Medicine*, 21, pp.2611–2622.

Refai, A.K. et al., 2004. Effect of titanium surface topography on macrophage activation and secretion of proinflammatory cytokines and chemokines. *Journal of biomedical materials research. Part A*, 70, pp.194–205.

Ribeiro, C. et al., 2015. Piezoelectric polymers as biomaterials for tissue engineering applications. *Colloids and Surfaces B: Biointerfaces*, 136(SEPTEMBER), pp.46–55.

Rokkanen, P.U. et al., 2000. Bioabsorbable fixation in orthopaedic surgery and traumatology. *Biomaterials*, 21(24), pp.2607–2613.

Ross, M. & Pawlina, W., 2004. Histology: A Text and Atlas. In *Histology: A Text and Atlas*.

S

Sabbioni, E. et al., 1993. The intensity of vanadium(V)-induced cytotoxicity and morphological transformation in BALB/3T3 cells is dependent on glutathione-mediated bioreduction to vanadium(IV). *Carcinogenesis*, 14(12), pp.2565–2568.

Saha, N., Dubey, A.K. & Basu, B., 2012. Cellular proliferation, cellular viability, and biocompatibility of HA-ZnO composites. *Journal of Biomedical Materials Research Part B: Applied Biomaterials*, 100B(1), pp.256–264.

Saldaña, L. et al., 2011. In search of representative models of human bone-forming cells for cytocompatibility studies. *Acta Biomaterialia*, 7(12), pp.4210–4221.

Shafer, D.M. et al., 1995. The effect of electrical perturbation on osseointegration of titanium dental implants. *Journal of Oral and Maxillofacial Surgery*, 53(9), pp.1063–1068.

Sivakumar, M., Mudali, U.K. & Rajeswari, S., 1994. In vitro electrochemical investigations of advanced stainless steels for applications as orthopaedic implants. *Journal of Materials Engineering and Performance*, 3(6), pp.744–753.

St-Pierre, J.P. et al., 2005. Three-dimensional growth of differentiating MC3T3-E1 pre-osteoblasts on porous titanium scaffolds. *Biomaterials*, 26, pp.7319–7328.

Subramanian, B., 2015. In vitro corrosion and biocompatibility screening of sputtered Ti40Cu36Pd14Zr10 thin film metallic glasses on steels. *Materials Science and Engineering: C*, 47, pp.48–56.

T

Thyssen, J.P. & Menne, T., 2010. Metal Allergy s A Review on Exposures , Penetration , Genetics , Prevalence , and Clinical Implications. , pp.309–318.

Torricelli, P. et al., 2003. Comparative interspecies investigation on osteoblast cultures: Data on cell viability and synthetic activity. *Biomedicine and Pharmacotherapy*, 57, pp.57–62.

U

Ullm, S. et al., 2014. Biocompatibility and inflammatory response in vitro and in vivo to gelatin-based biomaterials with tailorable elastic properties. *Biomaterials*, 35, pp.9755–9766.

V

Vallés, G. et al., 2006. Differential inflammatory macrophage response to rutile and titanium particles. *Biomaterials*, 27(30), pp.5199–5211.

Vallés, G. et al., 2013. Simvastatin prevents the induction of interleukin-6 gene expression by titanium particles in human osteoblastic cells. *Acta Biomaterialia*, 9(1), pp.4916–4925.

Vandrovcova, M. et al., 2012. Effect of different surface nanoroughness of titanium dioxide films on the growth of human osteoblast-like MG63 cells. *Journal of biomedical materials research. Part A*, 100(4), pp.1016–32.

Vandrovcova, M. et al., 2014. Interaction of Human Osteoblast-Like Saos-2 and MG-63 Cells with Thermally Oxidized Surfaces of a Titanium-Niobium Alloy. *PLoS ONE*, 9(6), p.e100475.

Vandrovcová, M. & Bačáková, L., 2011. Adhesion, growth and differentiation of osteoblasts on surface-modified materials developed for bone implants. *Physiological Research*, 60(3), pp.403–417.

Visiongain, 2012. Global orthobiologics market will reach $15.3 bn by 2022. London 08 March 2012. https://www.visiongain.com/Press_Release/159/'Global-orthobiologics-market-will-reach-15-3bn-by-2022'-predicts-new-visiongain-report.

Viteri, V.S. De & Fuentes, E., 2013. Titanium and Titanium Alloys as Biomaterials Chapter. *Tribology - Fundamentals and Advancements*, pp.155–182.

W

Walia, H., Brantley, W.A. & Gerstein, H., 1988. An initial investigation of the bending and torsional properties of nitinol root canal files. *Journal of Endodontics*, 14(7), pp.346–351.

Wang, B.L., Li, L. & Zheng, Y.F., 2010. In vitro cytotoxicity and hemocompatibility studies of Ti-Nb, Ti-Nb-Zr and Ti-Nb-Hf biomedical shape memory alloys. *Biomedical materials (Bristol, England)*, 5(4), p.044102.

Wang, W. & Poh, C.K., 2013. Titanium Alloys in Orthopaedics. *Titanium Alloys - Advances in Properties Control*, pp.1–20.

Wataha, J.C., 2012. Predicting clinical biological responses to dental materials. *Dental Materials*, 28(1), pp.23–40.

Wataha, J.C. et al., 2004. Sublethal concentrations of Au (III), Pd (II), and Ni(II) differentially alter inflammatory cytokine secretion from activated monocytes. *Journal of biomedical materials research. Part B, Applied biomaterials*, 69(1), pp.11–17.

Wei, J. et al., 2009. Influence of surface wettability on competitive protein adsorption and initial attachment of osteoblasts. *Biomedical materials (Bristol, England)*, 4, p.045002.

Williams, D.F., 2008. On the mechanisms of biocompatibility. *Biomaterials*, 29(20), pp.2941–2953.

Wójciak-Stothard, B. et al., 1995. Activation of macrophage-like cells by multiple grooved substrata. Topographical control of cell behaviour. *Cell Biology International*, 19(6), pp.485–490.

Y

Yamamoto, A., Honma, R. & Sumita, M., 1998. Cytotoxicity evaluation of 43 metal salts using murine fibroblasts and osteoblastic cells. *Journal of Biomedical Materials Research*, 39(February), pp.331–340.

Yamazaki, T. et al., 2006. Biological impact of contact with metals on cells. *In Vivo*, 20, pp.605–612.

Yamazaki, T. et al., 2012. Protection against copper-induced cytotoxicity by inclusion of gold. *In Vivo*, 26(4), pp.651–656.

Yang, D. et al., 2013. The molecular mechanism of mediation of adsorbed serum proteins to endothelial cells adhesion and growth on biomaterials. *Biomaterials*, 34(23), pp.5747–5758.

Yang, W.E. & Huang, H.H., 2010. Improving the biocompatibility of titanium surface through formation of a TiO2 nano-mesh layer. *Thin Solid Films*, 518(24), pp.7545–7550.

Young, S.-H. et al., 2008. Performance evaluation of cytometric bead assays for the measurement of lung cytokines in two rodent models. *Journal of Immunological Methods*, 331(1-2), pp.59–68.

Yuan, H. et al., 2001. Bone induction by porous glass ceramic made from Bioglass® (45S5). *Journal of Biomedical Materials Research*, 58(3), pp.270–276.

Z

Zareidoost, A. et al., 2012. The relationship of surface roughness and cell response of chemical surface modification of titanium. *Journal of Materials Science: Materials in Medicine*, 23(6), pp.1479–1488.

Zaveri, T.D. et al., 2010. Contributions of surface topography and cytotoxicity to the macrophage response to zinc oxide nanorods. *Biomaterials*, 31(11), pp.2999–3007.

Zberg, B., Uggowitzer, P.J. & Löffler, J.F., 2009. MgZnCa glasses without clinically observable hydrogen evolution for biodegradable implants. *Nature materials*, 8(11), pp.887–891.

Zhang, E. et al., 2015. Influence of Cu content on the cell biocompatibility of Ti–Cu sintered alloys. *Materials Science and Engineering: C*, 46, pp.148–157.

Zhou, F. et al., 2009. Phenomenon of "contact guidance" on the surface with nano-micro-groove-like pattern and cell physiological effects. *Chinese Science Bulletin*, 54(18), pp.3200–3205.

Zok, F.W. & Miserez, A., 2007. Property maps for abrasion resistance of materials. *Acta Materialia*, 55(18), pp.6365–6371.

Annex

Related publications

González S, Pellicer E, Fornell J, **Blanquer A**, Barrios L, Ibáñez E, Solsona P, Suriñach S, Baró MD, Nogués C, Sort J. Improved mechanical performance and delayed corrosión phenomena in biodegradable Mg-Zn-Ca alloys through Pd-alloying. J. Mech. Behav. Biomed. 2012;6:53-62.

Pellicer E, González S, **Blanquer A**, Suriñach S, Baró MD, Barrios L, Ibáñez E, Nogués C, Sort J. On the biodegradability, mechanical behaviour and cytocompatibility of amorphous Mg72Zn23Ca5 and crystalline Mg70Zn23Ca5Pd2 alloys as temporary implant materials. J. Biomed. Mater. Res. A. 2013 Feb;101(2):502-17.

Hynowska A., **Blanquer A**., Pellicer E., Fornell J., Suriñach S., Baró M., González S., Ibáñez E., Barrios L., Nogués C., Sort J., 2013. Novel Ti–Zr–Hf–Fe Nanostructured Alloy for Biomedical Applications. Materials. 2013 Nov;6, 4930–4945.

Hynowska A., **Blanquer A.**, Pellicer E., Fornell J, Suriñach S., Baró M.D., Gebert A., Calin M., Eckert J., Nogués C., Ibáñez E., Barrios L., Sort J. Nanostructured Ti-Zr-Pd-Si-(Nb) bulk metallic composites: Novel biocompatible materials with superior mechanical strength and elastic recovery. J Biomed Mater Res Part B 2015:103B:1569–1579.